# MECHANISTIC STUDIES OF HETEROGENEOUSLY CATALYZED REACTIONS OF AMMONIA AND ACETIC ACID ON PLATINUM SURFACES

Thesis by

John J. Vajo

In Partial Fulfillment of the Requirements

for the Degree of

Doctor of Philosophy

California Institute of Technology

Pasadena, California

1987

(Submitted June 13, 1986)

*there will be no more I*
*he'll never say I any more*
*he'll never say anything any more*
*he won't talk to anyone*
*no one will talk to him*
*he won't talk to himself*
*he won't think any more*
*he'll go on*
*I'll be inside*
*he'll come to a place and drop*
*drop and sleep*
*badly because of me*
*he'll get up and go on*
*badly because of me*
*he can't stay still any more*
*because of me*
*he can't go on any more*
*because of me*
*there's nothing left in his head*
*I'll feed it all it needs*

S. Beckett

**Acknowledgments**

I would first like to express my appreciation to my thesis advisor, Henry Weinberg, for teaching me an exacting approach to scientific research. It has been a pleasure to work with all the members of the Weinberg group, especially Jenna, Wilman, and Yong-Kui, who were both collaborators and friends. I am also indebted to all the members of the staff at Caltech for their assistance, especially Chic and Tony for their expertise in machining, and Kathy for typing the many drafts of this thesis.

I would like to mention everyone from "the house", Betsey, Catface, Dick, Jen, Jim, Kathy, Mike, Neal, Nora, Paul H., Paul S., Pete, Rich, Steve, Stupid, and Sue, for many, many memorable times. Finally, I would like to acknowledge my friends Neal, Chris, Vic, Fran and Elyse, each of whom, in their own special and unique ways, has taught me a great deal about everything, including myself.

## Abstract

The design and operation of a versatile microreactor capable of studying the rates of both steady-state and batch heterogeneous reactions on a wire, a foil or a single crystalline surface at pressures between $10^{-7}$ and 1000 Torr are described. The residence time distribution of the microreactor was characterized in order to evaluate the validity of using the continuous stirred tank reactor approximation to calculate reaction rates.

Absolute reaction rates (i.e. the rate-per-unit catalyst surface area) have been measured for both the catalytic decomposition of $NH_3$ and $ND_3$ and the $NH_3 + D_2$ exchange reaction over a polycrystalline platinum wire. The pressure was varied between $5 \times 10^{-7}$ and 0.5 Torr, and the temperature ranged from 400 to 1200 K. At relatively low pressures and/or high temperatures, the order of the decomposition reaction is unity with respect to ammonia, and the reaction rate is dictated by a competition between the surface reaction and the desorption of molecularly adsorbed ammonia. Under these conditions a primary isotope effect was observed for the decomposition of $ND_3$. At relatively high pressures and/or low temperatures, the reaction rate is independent of ammonia pressure, and the recombinative desorption of nitrogen controls the rate of ammonia decomposition. The measured kinetics of the $NH_3 + D_2$ exchange reaction were employed together with adsorption-desorption parameters of $NH_3$, $N_2$ and $H_2$ to develop a mechanistic model that describes the reaction rate over the entire (wide) range of conditions studied.

Steady-state absolute reaction rates are reported also for the catalytic decomposition of $NH_3$ on the Pt(110)-(1x2) single crystalline surface at pressures between $1 \times 10^{-6}$ and $2.6 \times 10^{-6}$ Torr and at temperatures between 400 and 1000 K. Qualitatively, the kinetics is similar to those observed for ammonia

decomposition on the polycrystalline platinum surface. Thermal desorption measurements conducted *during* the steady-state decomposition reaction demonstrate directly that nitrogen adatoms are the predominant surface species, and that the recombinative desorption of nitrogen is the major elementary reaction that produces molecular nitrogen.

The decomposition of $CH_3^{13}COOH$ at 7 x $10^{-4}$ Torr on a polycrystalline platinum wire at temperatures between 300 and 900 K was examined in the microreactor. The major reaction products on the initially clean surface are $^{13}CO$, CO, $^{13}CO_2$, $H_2$ and adsorbed carbon-12. The adsorbed carbon accumulates on the surface until the reactions that produce these products are poisoned by the graphitic overlayer that is formed. On the graphitized platinum surface, acetic acid dehydrates catalytically to ketene and water. The relative quantities of $^{13}CO$ and $^{13}CO_2$ that are formed depend both on the surface temperature and on the surface carbon coverage.

The catalytic dehydration of acetic acid to ketene was investigated over a graphitized polycrystalline platinum surface at pressures between 8 x $10^{-7}$ and 7 x $10^{-4}$ Torr and temperatures between 500 and 800 K. Steady-state absolute reaction rates, thermal desorption measurements, and the reactivities of functionally related compounds suggest that the reaction proceeds via an irreversibly adsorbed intermediate, which is formed by dissociation of the oxygen-hydrogen bond of acetic acid. For temperatures below 540 K at pressures of 3.5 x $10^{-4}$ Torr and above, the rate of decomposition of the surface intermediate controls the overall rate of the reaction. At 675 K or above for the entire range of pressures studied, the rate of dehydration is determined by a competition between the rates of desorption and surface reaction of molecularly adsorbed acetic acid.

## Table of Contents

# Chapter 1.

# Introduction

Heterogeneous catalytic reactions are of major importance to almost all segments of the national economy. While heterogeneous catalysis has traditionally been considered an empirical science, recently detailed information concerning the elementary reactions that occur in a number of overall heterogeneous catalytic processes has become available including, for example, the oxidation of both carbon monoxide and hydrogen **(1)**, and the methanation reaction **(2)**. This information has been obtained through the utilization of a variety of modern surface-science techniques that permit the use of both well-defined catalytic surfaces and reaction conditions. Thus, for several technologically important catalytic systems, there is a substantial body of knowledge regarding the elementary processes of adsorption, surface reactions and desorption **(1)**. However, the vast majority of this information has been obtained under ultrahigh vacuum conditions, and often only a single step of an overall reaction is studied. The application of this extensive knowledge obtained at low pressures, $\lesssim 10^{-6}$ Torr, to the understanding of commercial catalytic reactions that occur at considerably higher pressures, $\gtrsim 1$ atm, would represent a significant step toward establishing heterogeneous catalysis as a fundamental science.

Utilizing data obtained at low pressures, a fundamental understanding has begun to emerge for both the oxidation of carbon monoxide over platinum surfaces **(1)** and the methanation reaction over nickel surfaces **(2)**. On the basis of coadsorption studies of carbon monoxide and oxygen adatoms, different kinetic regimes for the production of carbon dioxide have been identified. These regimes are related to the surface coverage of both carbon monoxide and oxygen adatoms. When the surface coverage of carbon monoxide is high, the overall rate of reaction is approximately proportional to the ratio, rather than the sum, of the partial pressures of oxygen and carbon monoxide. Under these conditions, therefore, the application of data obtained at low pressures to

considerably higher pressures is relatively straightforward. Indeed, similar absolute reaction rates have been measured over seven orders of magnitude of total pressure when the partial pressure ratio is maintained at a constant value. Similar results have been obtained for the oxidation of hydrogen on platinum surfaces **(1)**.

Measurements of the rates of methane formation from the hydrogenation of carbon monoxide over the Ni(100) surface have been analyzed together with the rate of surface carbide formation via the Boudart disproportionation reaction and the rate of carbide hydrogenation **(2)**. This analysis has led to the conclusion that the rate of methane formation from carbon monoxide and hydrogen is determined by a competition between carbide formation and hydrogenation. Consistent with this proposal, the rate of methanation has been demonstrated to be a monotonic function of the surface carbide concentration regardless of the total pressure or partial pressure ratio of hydrogen to carbon monoxide.

The reliable application of the knowledge obtained from surface-science measurements requires addressing several questions which accompany variations in pressure from ultrahigh vacuum to those employed commercially. For example, the elementary reactions of adsorption and desorption have been studied for many catalytically interesting systems **(1,2)**. The question arises, however, concerning the relevance of this information obtained at low pressures to a catalytic process occurring at much higher pressures. One approach that has been fruitful in answering this and similar questions is to obtain kinetic data over a wide range of conditions at pressures between ultrahigh vacuum and several atmospheres. These data illustrate what mechanistic changes occur as the pressure is varied and thereby reveal the applicability of data obtained independently to understand reaction mechanisms under conditions of commercial interest.

Several experimental systems have been designed to measure the kinetics of heterogeneous catalytic reactions at pressures between $10^{-8}$ Torr and several atmospheres **(3-6)**. In Chapter 2 of this thesis, a microreactor is described, which was designed specifically to measure both steady-state and batch reactions on a variety of catalytic surfaces at pressures between approximately $10^{-7}$ and 1000 Torr. This microreactor has been used to study the interaction of ammonia with a polycrystalline platinum wire, as described in Chapter 3, and to study the decomposition of acetic acid on both a clean and a graphitized platinum surface, as described in Chapters 5 and 6.

The approach outlined above has been implemented in Chapter 3 to develop a mechanistic model for both the decomposition of ammonia and the $NH_3 + D_2$ exchange reaction on platinum. Absolute reaction rates have been obtained for these reactions at total pressures from $5 \times 10^{-7}$ to 0.5 Torr and at temperatures between 400 and 1200 K. The absolute rates have been used together with independently measured data concerning the adsorption-desorption parameters of $NH_3$, $N_2$ and $H_2$ as well as reaction intermediates NH and $NH_2$ to develop a mechanistic model that describes the reaction rates over the complete range of conditions studied. The success of this model attests to the utility of the approach described above, namely, analyzing kinetic data obtained over a wide range of experimental conditions by using kinetic parameters determined independently from ultrahigh vacuum measurements.

The steady-state decomposition of ammonia has also been studied on the single crystalline Pt(110)-(1x2) surface, and this is described in Chapter 4. Although the accessible pressure range in these experiments was restricted to $\lesssim 5 \times 10^{-6}$ Torr, the composition of the surface and the rate parameters for the desorption of the product nitrogen have been determined *during the steady-state decomposition reaction.* Specifically, the rate parameters for the

desorption of nitrogen measured during the steady-state reaction agree well with the rate parameters for nitrogen desorption determined independently in the absence of the steady-state decomposition reaction. This result substantiates further the tenet that independently measured rate parameters may be used to understand an overall catalytic reaction.

The decomposition of $^{13}C$-labeled acetic acid ($CH_3{}^{13}COOH$) over a polycrystalline platinum wire has been examined in the microreactor and is described in Chapters 5 and 6. For an initially clean platinum surface, $^{13}CO$, CO, $^{13}CO_2$, $H_2$ and adsorbed carbon -12 are the major reaction products. The relative quantities of $^{13}CO$ and $^{13}CO_2$ produced depend on both the surface temperature and the fractional surface coverage of carbon. Eventually, the adsorbed carbon poisons completely the reactions that produce these products. At this time, approximately one monolayer of graphitic carbon is present on the platinum surface. On this graphitized surface, acetic acid is dehydrated catalytically at steady-state to ketene and water.

**References**

1. G. Ertl in "Catalysis Science and Technology", J. R. Anderson and M. Boudart, Eds., Vol. 4, Springer-Verlag New York, 1983 p. 209.

2. R. D. Kelly and D. W. Goodman in "The Chemical Physics of Solid Surfaces and Heterogeneous Catalysis", D. A. King and D. P. Woodruff, Eds., Vol. 4, Elsevier Amsterdam,1982,p. 427.

3. D. W. Goodman, R. D. Kelly, T. E. Madey and J. T. Yates, Jr., J. Catal. **63,** 226 (1980).

4. H. J. Krebs, H. P. Bonzel and G. Gafner, Surface Sci. **88,**269 (1979).

5. B. Kasemo, K. E. Keck and T. Högberg, J. Catal. **66,**441 (1980).

6. J. Goschnick and M. Grunze, J. Vac. Sci. Technol. **18,**561 (1981).

# Chapter 2.

# Versatile Microreactor for Studies of Gas-Surface Catalytic Reactions between $10^{-7}$ and 1000 Torr

[Chapter 2 consists of an article coauthored with W. Tsai and W. H. Weinberg, which appeared in the *Review of Scientific Instruments* **56**, 1439 (1985).]

# Versatile microreactor for studies of gas–surface catalytic reactions between $10^{-7}$ and 1000 Torr

J. J. Vajo, W. Tsai, and W. H. Weinberg

*Division of Chemistry and Chemical Engineering, California Institute of Technology, Pasadena, California 91125*

(Received 27 December 1984; accepted for publication 27 March 1985)

A microreactor system that is designed for studies of steady-state and batch heterogeneous reactions on a wire, foil, or single-crystal surface at pressures between $10^{-7}$ and 1000 Torr is described. The applicability of the continuous stirred tank reactor approximation that facilitates the calculation of absolute reaction rates is discussed. Results for the decomposition of ammonia on a polycrystalline platinum wire are used to illustrate the performance of the microreactor.

## INTRODUCTION

Modern surface–science techniques have increased tremendously our understanding of the elementary steps associated with adsorption, desorption, and catalytic reactions occurring at solid surfaces. It is obviously desirable to be able to apply this extensive knowledge obtained at low pressures, $10^{-10}$–$10^{-6}$ Torr, to clarify the kinetic and mechanistic details of commercial catalytic reactions that occur at considerably higher pressures, typically 1–100 atmospheres. To apply this knowledge reliably requires a delineation of the mechanistic changes that accompany variations in pressure from ultrahigh vacuum to those employed commercially. Moreover, increasing the accessible pressure regime for which accurate kinetic data may be obtained increases the likelihood of interpreting the measured rate data mechanistically in terms of elementary reactions.

Recently, there have been several investigations of catalytically important reactions at pressures between $10^{-8}$ Torr and several atmospheres.[1–11] Here, a microreactor is described that is capable of steady-state flow and batch heterogeneous reactions on a wire, foil, or single-crystal surface at pressures between $10^{-7}$ and 1000 Torr. In particular, the performance of this reactor is illustrated by considering the decomposition of ammonia over a polycrystalline platinum wire.[12]

## I. REACTOR DESIGN AND OPERATION

The reactor consists of a high-vacuum section, a small reaction volume, and a sample manipulator, which is used to position the catalyst either in the high-vacuum region or in the reactor volume for experiments in different pressure regimes. Adapted from a design of Auerbach *et al.*,[13] the manipulator is comprised of a doubly differentially pumped housing, a shaft, which supports the catalyst sample, and three spring-loaded Teflon O-rings, which allow the shaft to be translated and rotated. A schematic of the manipulator is shown in Fig. 1. The housing is a stainless-steel tube that contains the O-rings and is welded to a $2\frac{3}{4}$-in. flange for attachment to the reactor body. Two stainless-steel rings separate the O-rings and align them with two 0.46-cm pump-out ports. A removable top plate secures the O-rings in the housing. The first port is pumped by a mechanical pump, whereas the second port is pumped by a Varian 2-in. diffusion pump with a chilled water-cooled baffle.

A mini-feedthrough (Ceramaseal 807B9299-2) welded to a stainless-steel tube comprises the manipulator shaft. This shaft provides support for the crystal, wire, or foil via two 0.24-cm OFHC copper wires, which are also used to heat the sample. Cooling is achieved by filling the hollow shaft with liquid nitrogen. Temperatures are measured with a 0.0075-cm-diameter W-5% Re/W-26% Re thermocouple, which is spot welded to the sample. Spring-loaded Teflon O-rings (Accratronics AR10400-206AC) are used to form a seal between the shaft and the manipulator housing. The shaft can be translated and rotated while maintaining a seal. All sealing surfaces are machined to obtain an optimum metal-to-Teflon seal.

Leakage past the O-rings and the degree to which the base pressure in the system is limited by this leakage may be calculated as follows. The pressure before a seal, $P_a$, is related to the pressure after the seal, $P_b$, by

$$P_a L = SP_b, \tag{1}$$

where $L$ is the leak rate of the seal, and $S$ is the speed at which gases are pumped away. The leak rate of a 14-in.-diameter seal is stated by Auerbach *et al.*[13] to be $10^{-6}$ l/s. This corre-

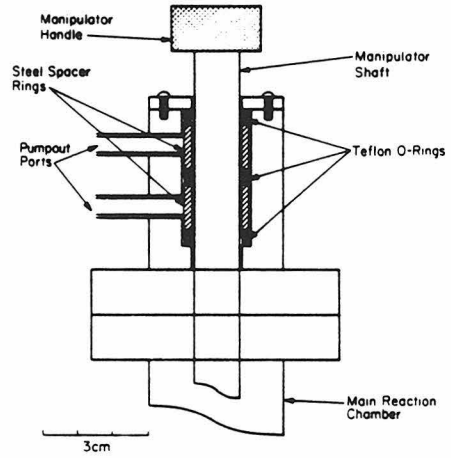


FIG. 1. Cross section of double differentially pumped sample manipulator.

 0034-6748/85/071439-04$01.30 

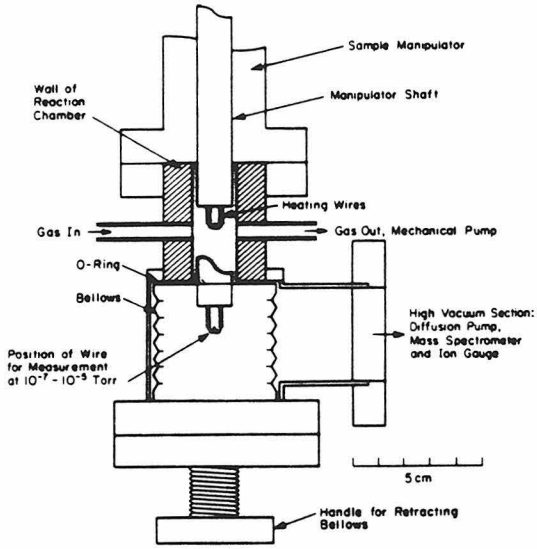


FIG. 2. Cross section of microreactor body, showing the wire in position for experiments at both $10^{-4}$–1000 Torr and $< 10^{-7}$–$10^{-4}$ Torr. Ports for pressure measurement and the leak to the high-vacuum section, which are orthogonal to the inlet and outlet flow ports, are not shown. The volume of the baratron and the access ports, together with the shaded region, is the reactor volume, 30 $cm^3$.

sponds to $3.6\times10^{-8}$ l/s for a $\frac{1}{4}$-in.-diameter seal. Assuming atmospheric pressure before the first seal and a pumping speed of $10^{-3}$ l/s (certainly a lower limit), the pressure in the first section should be $2.7\times10^{-2}$ Torr. Assuming the same pumping speeds in the second section and main reactor body results in a base pressure in the main chamber due to leakage that is below $3.5\times10^{-11}$ Torr. Since this is below current limitations due to other factors, seal leakage does not limit the base pressure of the microreactor.

The main chamber of the microreactor consists of a modified right-angle ultrahigh-vacuum valve linked to a high-vacuum pumping section, as shown in Fig. 2. To increase the ratio of the catalytic surface area to the total gas volume and, consequently, increase the sensitivity, the port opposite the bellows was replaced with a tube of 13/16-in. internal diameter. This diameter is sufficiently large to accommodate the manipulator shaft and results in a reactor volume of 10 $cm^3$. Surfaces that are exposed to high pressures are plated with $7.5\times10^{-5}$ in. of gold to suppress any reaction from occurring on the chamber walls.

Four ports of $\frac{13}{16}$-in. internal diameter, spaced 90° apart, provide for flow of reactant gases, pressure measurement, and detection of reaction products. The flow of gases is regulated by metering valves on the inlet and outlet flow lines. Flow rates can be varied from 0.1 to 100 $cm^3$/s by adjusting the calibrated inlet and outlet valves and the gas pressure behind the inlet valve. Mean residence times in the reactor under these conditions are adjustable between 0.1 and 10 s. Pressures are measured with MKS baratron gauges with sensitivities between either $10^{-4}$ and 1 Torr, $10^{-2}$ and 100 Torr, or $10^{-1}$ and 1000 Torr, depending on the pressure at which the experiments are conducted. The additional volume of the baratron, together with the access ports, increases the total reactor volume to 30 $cm^3$. Products are detected by a computer-interfaced EAI 1200 quadrupole mass spectrometer located in the high-vacuum section. Interchangeable pieces of Pyrex tubing with variable conductances provide a leak from the reactor to the high-vacuum section. The conductance of the Pyrex tubing is chosen to maintain a pressure of $\sim 10^{-6}$ Torr at the mass spectrometer during a reaction. Cajon Ultra-Torr fittings are used to facilitate exchange of the Pyrex tubes. The base pressure of the micro-reactor, as it is currently pumped by a liquid-nitrogen-trapped Varian 2-in. diffusion pump, is below $10^{-8}$ Torr.

An advantage of the compact design of this microreactor is the high sensitivity for reactions occurring over low area solids. A concomitant disadvantage, however, is that the surface cannot be examined spectroscopically either before, during, or after the catalytic reaction. Hence, a cleaning procedure for the particular surface under investigation must be formulated in a separate apparatus that does have such spectroscopic capabilities. An indication of the cleanliness of the surface may be ascertained *in situ* in the reactor via the thermal desorption spectra of probe molecules, e.g., hydrogen and carbon monoxide.

To conduct steady-state reactions between 0.01 and 1000 Torr, the sample is sealed in the reactor chamber, and the outflow of gases is pumped by a 75-l/min mechanical pump. A Pyrex tube provides the leak to the high-vacuum section. (For example, a 0.5-cm length of 0.0075-cm-i.d. tubing is used for reactions at 0.5 Torr.) For reactions at pressures between $10^{-4}$ and $10^{-2}$ Torr, the inlet metering valve is replaced by a 0.5-cm length, 0.008-cm-i.d. capillary tube to restrict inlet flow, and the outlet to the mechanical pump is sealed. The leak to the high-vacuum section is replaced with a tube of 0.46 cm i.d. which, in addition to providing a leak for product detection, provides for the outflow of gases pumped by the diffusion pump. Experiments at pressures between $10^{-7}$ and $10^{-5}$ Torr are conducted by opening the UHV right-angle valve and translating the catalyst directly into the high-vacuum section, as illustrated in Fig. 2. Batch reactions may also be performed by simply filling the reaction volume to the appropriate pressure and sealing the inlet and outlet flow lines. The leak to the mass spectrometer allows continuous monitoring of the accumulation of reaction products as a function of time.

To determine absolute reaction rates, the mass spectrometer is calibrated by flowing mixtures of products and reactants corresponding to different conversions through the reactor without a catalyst. Reaction rates are calculated under steady-state conditions at conversions below 10% using the continuous stirred tank reactor (CSTR) equation[14,15]

$$R = \frac{V}{\tau^{id} k_B T_g}(P_i - P_f), \tag{2}$$

where $R$ is the reaction rate (molecules/$cm^2$ s), $V$ is the reactor volume, $\tau^{id}$ is the average residence time assuming CSTR conditions, $k_B$ is the Boltzmann constant, $T_g$ is the gas temperature, and $P_i$ and $P_f$ are the partial pressures in the reactor associated with the feed and with the steady-state reaction mixture, respectively. Average residence times are

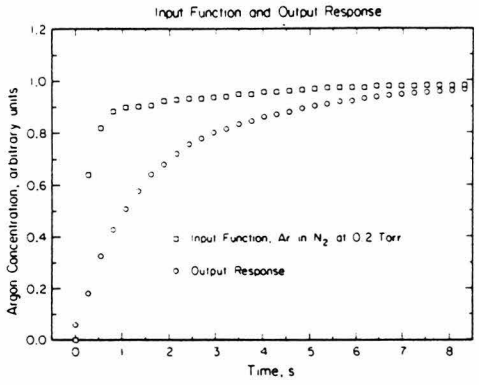


FIG. 3. Input function and output response for an approximate step function input of argon with nitrogen as a carrier gas at a pressure of 0.2 Torr. The average residence time for these conditions, determined using Eq. (4), is 1.42 s.

determined by filling the reactor with the outlet valve closed and monitoring the pressure rise as a function of time. Assuming that the gas obeys the ideal gas law and that at any time the pressure is constant throughout the reactor, the mass flow rate of gas into the reactor is given by

$$\frac{dn}{dt} = \frac{V}{k_B T_g}\frac{dP}{dt}, \tag{3}$$

where $n$ is the number of molecules and $P$ is the reactor pressure. The average residence time for steady-state flow under CSTR conditions at a pressure $P_0$ may be expressed as[15]

$$\tau^{id} \equiv \frac{n}{dn/dt} = \frac{P_0}{dP/dt_{P=P_0}}. \tag{4}$$

The validity of assuming a CSTR model for the reactor has been investigated by a series of step response experiments, which are described and discussed in the next section.

## II. CSTR APPROXIMATION

Although continuous stirred tank conditions are frequently assumed for experiments in steady-state flow reactors,[16–19] the validity of the CSTR approximation has not been examined directly in these studies. The CSTR assumption is inaccurate when the reactor has an appreciable volume, which allows back-mixing, and when there are dead volumes where mixing occurs inefficiently. The microreactor described here has been designed to minimize these undesirable effects. To examine the validity of the CSTR approximation, a series of experiments has been conducted to characterize the response of the microreactor. A computer-controlled solenoid valve was used to generate approximate step function inputs of argon into the reactor with nitrogen as a carrier gas. The response of the reactor was monitored as a function of time using the mass spectrometer. Typical input and response data are shown in Fig. 3 for a pressure of 0.2 Torr. The input function was measured directly at the inlet stream via a bypass from the microreactor.

Using the response data, the residence time distribution (RTD) $R(t)$ may be calculated. Here, $R(t)dt$ is the fraction of effluent with a residence time in the reactor that is between $t$ and $t+dt$. If the CSTR approximation is applicable, the experimentally determined RTD will resemble the RTD for a CSTR. The RTD for a CSTR may be written as[14]

$$R(t) = \frac{1}{\tau^{id}}\exp\left(\frac{-t}{\tau^{id}}\right), \tag{5}$$

where $\tau^{id}$ is calculated from Eq. (4). In general, the actual RTD may be obtained from experimental response data by deconvoluting the linear response equation[20]

$$C_{out}(t) = \int_0^\infty C_{in}(t-t')R(t')dt', \tag{6}$$

where $C_{in}(t)$ and $C_{out}(t)$ are the concentrations of species entering and leaving the reactor, respectively. Various methods, including numerical integration and Fourier transformation, were used to compute $R(t)$ from Eq. (6) for the data shown in Fig. 3. The result appears to be independent of the method employed, and the computed RTD is shown in Fig. 4. Also shown in Fig. 4 is the RTD for the CSTR model. Under these flow conditions, $\tau^{id} = 1.42$ s was calculated using Eq. (4).

The CSTR approximation may be evaluated quantitatively by comparing the predicted average conversions based on the CSTR model and the actual RTD. For an arbitrary RTD, the average conversion may be expressed as[14]

$$\hat{x} = \int_0^\infty x(t')R(t')dt', \tag{7}$$

where $x(t')$ is the integrated rate equation for a batch reaction. Assuming first-order kinetics, $x(t)$ may be written as

$$x(t) = 1 - \exp(-kt), \tag{8}$$

where $k$ is the reaction-rate coefficient. This expression simplifies at low conversions, where $kt \ll 1$, to

$$x(t) = kt. \tag{9}$$

Substituting Eq. (9) into Eq. (7) yields

$$\hat{x} = k\int_0^\infty t'R(t')dt'. \tag{10}$$

From Eq. (10) the average residence time may be defined as

$$\tau \equiv \int_0^\infty t'R(t')dt', \tag{11}$$

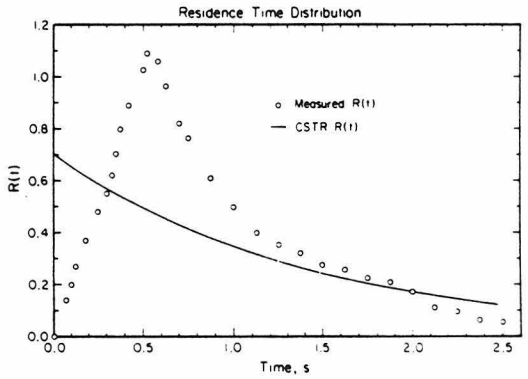


FIG. 4. Residence time distributions determined both experimentally from the data shown in Fig. 3 and computed assuming an ideal CSTR condition with $\tau^{id} = 1.42$ s.

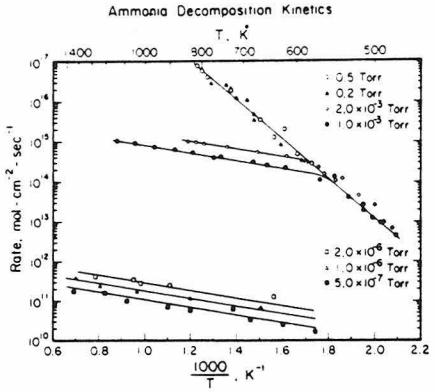


FIG. 5. Arrhenius plots of the rate of ammonia decomposition on platinum for ammonia pressures of 0.5, 0.2, $2\times10^{-3}$, $1\times10^{-3}$, $2\times10^{-6}$, $1\times10^{-6}$ and $5\times10^{-7}$ Torr. Lines have been drawn through the data points as a visual aid.

assuming that $R(t)$ is a normalized RTD. Thus, the average conversion for an arbitrary RTD and first-order kinetics at low conversions is

$$\hat{x} = k\tau. \tag{12}$$

Substituting Eq. (5) into Eq. (7) yields the following expression for the average conversion of a CSTR

$$\hat{x}^{id} = k\tau^{id}. \tag{13}$$

Consequently, comparing $\tau$ and $\tau^{id}$ determines quantitatively the error introduced by assuming ideal CSTR conditions. Using the RTD shown in Fig. 4, $\tau$ computed from Eq. (11) is 1.47 s. Comparing this value to $\tau^{id} = 1.42$ s indicates that under these conditions, the CSTR approximation is accurate to within 4% and hence may be used to compute absolute reaction rates. A similar result has been obtained for a range of flow rates at pressures between 0.1 and 10 Torr. For pressures below 0.1 Torr, the increased mean-free path of the gas molecules will improve agreement with the CSTR approximation, whereas for pressures above 10 Torr, further measurements would be necessary to examine the CSTR approximation.

## III. REACTOR PERFORMANCE

Absolute reaction rates determined for the decomposition of ammonia at steady state over a polycrystalline platinum wire are shown in Fig. 5. The production of nitrogen was monitored mass spectrometrically, and $P_{f,NH_3}$ in Eq. (2) was determined from the overall reaction stoichiometry. Residence times were $\sim$ 1.5 and 0.1 s for decomposition rates measured at pressures above $1\times10^{-3}$ Torr and below $2\times10^{-6}$ Torr, respectively. The range of observable rates, which already spans 7 orders of magnitude, may be extended further by increasing the residence time and by using a batch mode.[21] for the data of Fig. 5, average conversions were below 5%, except for temperatures above 800 K at pressures of $1\times10^{-3}$ and $2\times10^{-3}$ Torr, where average conversions were $\lesssim$15%. The observed kinetics suggest, however, that even for these rather high conversions, Eq. (9) remains applicable. This and other aspects of the decomposition kinetics displayed in Fig. 5 are discussed in detail elsewhere.[12]

## ACKNOWLEDGMENTS

This work was supported by the Army Research Office under Grant No. DAAG29-83-K-0094, and Central Research and Development Department of E. I. du Pont de Nemours and Company. The advice and assistance of Dr. Kurt Fickie, Dr. Charles Sobrero, and Dr. Jenna Zinck is very much appreciated.

[1] D. W. Goodman, R. D. Kelly, T. E. Madey, and J. T. Yates, Jr., J. Catal. **63**, 226 (1980).
[2] C. T. Campbell and D. W. Goodman, Surf. Sci. **123**, 413 (1982).
[3] D. E. Peebles, D. W. Goodman, and J. M. White, J. Phys. Chem. **87**, 4378 (1983).
[4] D. W. Goodman, Acc. Chem. Res. **17**, 94 (1984).
[5] M. J. Mummey and L. D. Schmidt, Surf. Sci. **91**, 301 (1980).
[6] M. J. Mummey and L. D. Schmidt, Surf. Sci. **109**, 29 (1981).
[7] H. J. Krebs, H. P. Bonzel, and G. Gafner, Surf. Sci. **88**, 269 (1979).
[8] B. Kasemo, K. E. Keck, and T. Högberg, J. Catal. **66**, 441 (1980).
[9] J. Goschnick and M. Grunze, J. Vac. Sci. Technol. **18**, 561 (1981).
[10] A. Vavere and R. S. Hansen, J. Catal. **69**, 158 (1981).
[11] N. D. Spencer, R. C. Schoonmaker, and G. A. Somorjai, J. Catal. **74**, 129 (1982).
[12] J. J. Vajo, W. Tsai, and W. H. Weinberg, J. Phys. Chem. (in press).
[13] D. J. Auerbach, C. A. Becker, J. P. Cowin, and L. Wharton, Rev. Sci. Instrum. **49**, 1518 (1978).
[14] J. M. Smith, *Chemical Engineering Kinetics*, 3rd ed. (McGraw-Hill, New York, 1981).
[15] J. J. Carberry, *Chemical and Catalytic Reaction Engineering* (McGraw-Hill, New York, 1976).
[16] D. G. Löffler and L. D. Schmidt, J. Catal. **41**, 440 (1976).
[17] C. G. Takoudis and L. D. Schmidt, J. Phys. Chem. **87**, 958 (1983).
[18] R. W. McCabe, J. Catal. **79**, 445 (1983).
[19] W. L. Holstein and M. Boudart, J. Catal. **72**, 328 (1981).
[20] O. Levenspiel, *Chemical Reaction Engineering*, 2nd ed. (Wiley, New York, 1972).
[21] We estimate that the minimum detectable rate, for all pressures may be lowered by 1–2 orders of magnitude using the reactor in the batch mode.

# Chapter 3.

# Mechanistic Details of the Heterogeneous Decomposition of Ammonia on Platinum

[Chapter 3 consists of an article coauthored with W. Tsai and W. H. Weinberg, which appeared in the *Journal of Physical Chemistry* **89**, 3243 (1985).]

Reprinted from The Journal of Physical Chemistry, 1985, 89, 3243.


# Mechanistic Details of the Heterogeneous Decomposition of Ammonia on Platinum

**J. J. Vajo, W. Tsai, and W. H. Weinberg***

*Division of Chemistry and Chemical Engineering, California Institute of Technology, Pasadena, California 91125* *(Received: December 26, 1984)*

Absolute reaction rates have been measured for the catalytic decomposition of $NH_3$ and $ND_3$ and for the $NH_3 + D_2$ exchange reaction over a polycrystalline platinum wire at pressures between $5 \times 10^{-7}$ and 0.5 torr and temperatures between 400 and 1200 K in a continuous flow microreactor. At relatively low pressures and/or high temperatures, a primary isotope effect was observed for the decomposition of $ND_3$, indicating that a surface reaction involving N–H bond cleavage is the rate-limiting step. Under these conditions, the order of the decomposition reaction is unity with respect to ammonia pressure with an apparent activation energy of 4.2 kcal/mol. As coverages increase, corresponding to relatively high pressures and/or low temperatures, the order of the decomposition reaction is zero with respect to ammonia, and the reaction rate becomes controlled by nitrogen desorption. In this case the apparent activation energy of the decomposition reaction is 22 kcal/mol. The kinetics of the $NH_3 + D_2$ exchange reaction have been used, together with data concerning the adsorption–desorption parameters of $NH_3$, $H_2$, and $N_2$ as well as the reaction intermediates NH and $NH_2$, to develop a mechanistic model which describes the reaction rate over a wide range of experimental conditions and which includes the energetics of each intermediate step in the decomposition reaction. This model is discussed in terms of a potential energy diagram for ammonia decomposition on platinum.

## 1. Introduction

Interest in the catalytic decomposition of ammonia on transition-metal surfaces has been motivated by its relative simplicity as a heterogeneous reaction and by its relationship, via microscopic reversibility, to the synthesis of ammonia from nitrogen and hydrogen. Although the decomposition reaction on platinum surfaces has been examined extensively,[1-7] a detailed mechanism which

(1) Löffler, D. G.; Schmidt, L. D. *J. Catal.* **1976**, *41*, 440.
(2) Löffler, D. G.; Schmidt, L. D. *Surf. Sci.* **1976**, *59*, 195.

0022-3654/85/2089-3243$01.50/0 

describes the reaction rate over a wide range of experimental conditions and which includes the energetics of individual reaction steps remains unformulated. Löffler and Schmidt have studied the decomposition kinetics on a platinum wire in a steady-state flow reactor with the ammonia pressure varying from 0.015 to 10.5 torr.[1] In the temperature range between 600 and 1700 K, they were able to fit their data accurately with a single Langmuir–Hinshelwood rate expression. However, the Langmuir–Hinshelwood rate expression provided no microscopic information concerning the individual, elementary reaction steps, and the lack of kinetic parameters for the adsorption and desorption of $NH_3$, $H_2$, and $N_2$ precluded a critical evaluation of particular kinetic models.

Recently, additional information has become available concerning the adsorption and desorption kinetics of $NH_3$, $H_2$, $N_2$, and probable reaction intermediates (NH and $NH_2$) on platinum surfaces. Thermal desorption mass spectrometry (TDS)[3,8] and electron energy loss spectroscopy[9] of ammonia chemisorbed on Pt(111) indicate the existence of two molecular states with desorption energies of 10–12 and 18–20 kcal/mol, respectively. The interaction of hydrogen with Pt(s)-9(111)×(111), i.e., the Pt(997) surface, has been elegantly studied by using helium beam scattering.[10,11] By monitoring the reduction in coherent helium scattering in the presence of disordered hydrogen adatoms, isosteric heats of adsorption of 22 and 19 kcal/mol were obtained for the step edges and the terraces, respectively. Since the activation energy for adsorption of hydrogen on platinum is known to be small,[11,12] at most 1 kcal/mol, the measured isosteric heats of adsorption are essentially equal to the activation energies of desorption. Moreover, "normal" values of the preexponential factor for a second-order desorption reaction of $10^{-3}$–$10^{-2}$ $cm^2/s$ were obtained.[11] The desorption of atomically adsorbed nitrogen as $N_2$ from a polycrystalline platinum ribbon has been investigated by using TDS.[13] Nitrogen desorption occurred with second-order kinetics, an activation energy of desorption of 19 kcal/mol, and a preexponential factor of the desorption rate coefficient of $4 \times 10^{-8}$ $cm^2/s$. Both of these rate parameters were found not to vary with the fractional surface coverage of nitrogen.[13] The activation energy for dissociative adsorption of nitrogen on iron surfaces has been estimated to be ≤20 kcal/mol depending on surface orientation and nitrogen coverage.[14] Although the adsorption kinetics of $N_2$ on platinum surfaces have not been investigated directly, threshold ionization measurements have established the desorption of $N_2^*$ from a platinum ribbon with 20 kcal/mol of vibrational excitation during ammonia decomposition at a pressure of 0.1–1.4 torr of ammonia and a temperature of 773–1373 K.[15] Laser-induced fluorescence has been used to determine an apparent activation energy of 63–69 kcal/mol for the desorption of NH radicals from a platinum wire in 0.1 torr of ammonia at 1200–1400 K.[16,17] The desorption of $NH_2$ radicals was not observed under similar conditions.

In the present work, we have measured absolute reaction rates for the catalytic decomposition of $NH_3$ and $ND_3$, and for the $NH_3$ + $D_2$ exchange reaction from $5 \times 10^{-7}$ to 0.5 torr in the temperature range between 400 and 1200 K. We have used these data, together with the aforementioned independently measured results, to clarify the detailed energetics of ammonia decomposition on platinum.

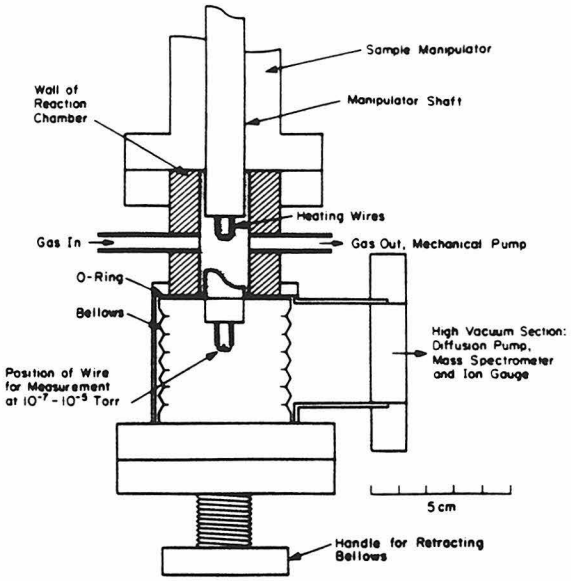


**Figure 1.** Cross section of microreactor body showing the wire in position for experiments at both $10^{-3}$–1 torr and $10^{-7}$–$10^{-5}$ torr. Ports for pressure measurement and the leak to the high vacuum section, which are orthogonal to the inlet and outlet flow ports, are not shown. The volume of the baratron and the access ports together with the shaded region is the reaction volume, 30 $cm^3$. The sample manipulator is described in detail elsewhere.[18]

The organization of this paper is the following. In section 2, the experimental details are described. In section 3, the experimental data are presented. A mechanistic model is developed in section 4 and discussed in section 5. Finally, the results are summarized in section 6.

## 2. Experimental Procedures

The experiments were performed in a microreactor capable of steady-state flow and batch heterogeneous reactions on a wire, foil, or single crystal surface. A detailed description of the experimental system is reported elsewhere.[18] The decomposition experiments were carried out over resistively heated platinum wires in flowing ammonia over a range of $P_{NH_3}$ from $5 \times 10^{-7}$ to 0.5 torr. A differentially pumped sample manipulator was used to translate and rotate the catalyst to different positions for experiments in various pressure regimes, as shown in Figure 1. Two 0.24-cm-diameter copper leads were used to support and heat the platinum, which was a 20-cm length of 0.0125-cm-diameter high purity (99.99%) polycrystalline wire wound into approximately 25 coils of 0.25-cm diameter. Temperatures were measured with a 0.0075-cm diameter W–5% Re/W–26% Re thermocouple, which was spot welded near the center of the wire.

The main chamber of the reactor, with a volume of 30 $cm^3$, consists of a right-angle ultrahigh vacuum valve which is linked to a high vacuum section through a retractable bellows connection, as shown in Figure 1. The pressure in the reactor was measured with an MKS Baratron gauge. A capillary leak to an EAI 1200 quadrupole mass spectrometer in the high vacuum section enabled the product signal to be monitored continuously by a CP/M Z-80 based microcomputer. The base pressure of the high vacuum section, which is pumped by a liquid nitrogen trapped Varian 2-in. diffusion pump, is approximately $10^{-6}$ torr.

(3) Gland, J. L.; Kollin, E. B. *Surf. Sci.* **1981**, *104*, 478.
(4) Guthrie, W.; Sokol, J.; Somorjai, G. A. *Surf. Sci.* **1981**, *109*, 390.
(5) Robertson, A. J. B.; Willhoft, E. M. A. *Trans. Faraday Soc.* **1967**, *63*, 476.
(6) Melton, C. E.; Emmett, P. H. *J. Phys. Chem.* **1964**, *68*, 3318.
(7) Logan, S. R.; Kemball, C. *Trans. Faraday Soc.* **1960**, *56*, 144.
(8) Gland, J. L. *Surf. Sci.* **1978**, *71*, 327.
(9) Sexton, B. A.; Mitchel, G. E. *Surf. Sci.* **1980**, *99*, 523.
(10) Poelsema, B.; Mechtersheimer, G.; Comsa, G. *Surf. Sci.* **1981**, *111*, 519.
(11) Poelsema, B.; Mechtersheimer, G.; Comsa, G. *Surf. Sci.* **1981**, *111*, L728.
(12) Christmann, K.; Ertl, G.; Pignet, T. *Surf. Sci.* **1976**, *54*, 365.
(13) Wilf, M.; Dawson, P. T. *Surf. Sci.* **1976**, *60*, 561.
(14) Grunze, M. In "The Chemical Physics of Solid Surfaces and Heterogeneous Catalysis"; King, D. A.; Woodruff, D. P., Eds.; Elsevier: Amsterdam, 1982; Vol. 4, p 150.
(15) Foner, S. N.; Hudson, R. L. *J. Chem. Phys.* **1984**, *80*, 518.
(16) Selwyn, G. S.; Lin, M. C. *Chem. Phys.* **1982**, *67*, 213.
(17) Selwyn, G. S.; Fujimoto, G. T.; Lin, M. C. *J. Phys. Chem.* **1982**, *86*, 760.
(18) Vajo, J. J.; Tsai, W.; Weinberg, W. H. *Rev. Sci. Instrum.*, in press.

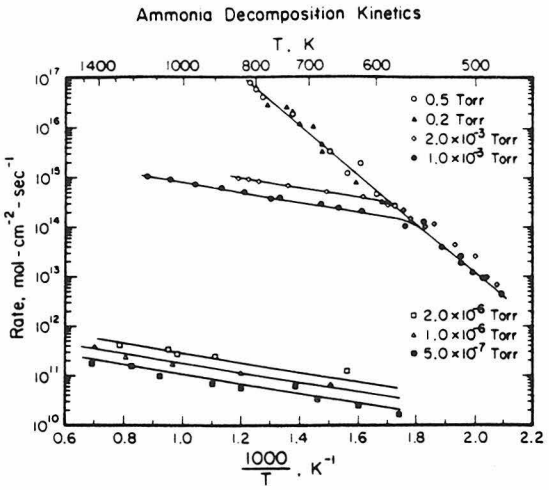


**Figure 2.** Arrhenius plots of the rate of ammonia decomposition on platinum for ammonia pressures of 0.5, 0.2, $2 \times 10^{-3}$, $1 \times 10^{-3}$, $2 \times 10^{-6}$, $1 \times 10^{-6}$, and $5 \times 10^{-7}$ torr. Lines have been drawn through the data points as a visual aid.

By manipulating the position of the wire, the flow rate of the gases, and the pumping speed, experiments were carried out at either $10^{-3}$–1 torr or $10^{-7}$–$10^{-5}$ torr. The flow rate could be varied from 0.1 to 100 cm³/s by adjusting the calibrated inlet and outlet valves. Mean residence times in the reactor under these conditions were adjustable between 0.1 and 10 s. Steady-state conversions were determined by monitoring the $N_2$ signal with the mass spectrometer. The mass spectrometer was calibrated by flowing stoichiometric mixtures of $NH_3$, $H_2$, and $N_2$, which corresponded to between 1% and 10% conversion, through the reactor over a room temperature platinum wire and monitoring the $m/e$ 28 signal with a total pressure of approximately $10^{-6}$ torr in the vacuum chamber.

Reaction rates were calculated under steady-state conditions at conversions below 10% with the continuous stirred tank reactor (CSTR) equation[19]

$$R = (V/\tau k T_g)(P_{NH_3,i} - P_{NH_3,f}) \qquad (1)$$

where $R$ is the reaction rate (molecules/(cm² s)), $V$ is the reactor volume, $\tau$ is the average residence time, $k$ is the Boltzmann constant, $T_g$ is the gas temperature, and $P_{NH_3,i}$ and $P_{NH_3,f}$ are the partial pressures of ammonia in the reactor associated with the feed and with the steady-state reaction mixture, respectively. The assumption of a CSTR model for the reactor was examined by a series of step-response experiments which indicated that the residence time distribution in the reactor was indeed approximated well by a CSTR.[18]

The ammonia used in this investigation was 99.99% anhydrous grade from Matheson and was purified further by freeze–thaw cycles in a dry ice/acetone bath. The deuterated ammonia was 99 atom % deuterium from Merck and was used without further purification.

Prior to the decomposition experiments, the platinum wire was heated in $10^{-7}$–0.1 torr of oxygen (99.99%) at 1100 K for 4 h and then reduced in $10^{-7}$–0.1 torr of hydrogen (99.99%) under the same conditions. (The actual pressures corresponded to the pressures at which the decomposition of ammonia was carried out subsequently.) This treatment led to reproducible decomposition rates of ammonia.

## 3. Experimental Results

*3.1. Decomposition of Pure $NH_3$.* Absolute rates for the decomposition of ammonia are shown in Figure 2 as a function of reciprocal temperature for ammonia pressures between 0.5 and $5 \times 10^{-7}$ torr. At lower temperatures and higher pressures, the reaction rate becomes independent of ammonia pressure. For example, below approximately 550 K the decomposition rates at pressures of 0.5 and $10^{-3}$ torr converge to a unique value, dependent only on the temperature, although the pressures differ by a factor of 500. Under these conditions the apparent activation energy is 22 ± 2 kcal/mol, with an extrapolated intercept at $1/T = 0$ of $(6.4 \pm 5) \times 10^{22}$ molecules/(cm² s).

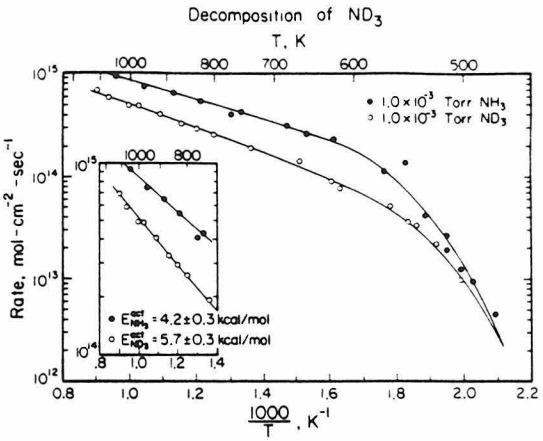


**Figure 3.** Comparison of the rate of decomposition of $ND_3$ and $NH_3$, both at $1 \times 10^{-3}$ torr. The inset shows the high-temperature region with an expanded scale illustrating the difference in activation energy for decomposition of $ND_3$ and $NH_3$. Lines have been drawn through the data points for clarity.

At higher temperatures and lower pressures, the data show a transition from a zero order to a first-order dependence of the rate on ammonia pressure. This transition is seen explicitly in Figure 2 for decomposition at $10^{-3}$ and $2 \times 10^{-3}$ torr. At higher and lower pressures only the zero-order and first-order kinetics are observed, respectively. When the data for the three lowest pressures shown in Figure 2 are used, the order with respect to ammonia pressure is 0.9 ± 0.05. Concurrent with the increased dependence of the rate on ammonia pressure, the apparent activation energy decreases from 22 kcal/mol to a high temperature limit of 4.2 ± 0.3 kcal/mol. The intercept at $1/T = 0$ for the high temperature rate is dependent on the pressure. Assuming a first-order dependence and normalizing with respect to ammonia pressure yields a value for the intercept of $(1.4 \pm 0.2) \times 10^{18}$ molecules/(cm² s torr). The activation energies and orders of reaction with respect to ammonia pressure agree well with earlier results of Löffler and Schmidt,[1] although our absolute rates are a factor of 2–5 lower.

*3.2. Decomposition of Pure $ND_3$.* Figure 3 shows the rate of decomposition of deuterated ammonia $ND_3$, together with the data for $NH_3$, both at $10^{-3}$ torr. At low temperatures the rates converge, and the kinetics for $ND_3$ decomposition appear almost identical with those for $NH_3$. However, at higher temperatures, as shown in the inset to Figure 3, the activation energy for decomposition of $ND_3$ is 5.7 ± 0.3 kcal/mol compared to 4.2 ± 0.3 kcal/mol for $NH_3$. This difference in the activation energies is indicative of a primary isotope effect. A simple calculation assuming a vibrational frequency of 3400 cm⁻¹ for the N–H bond predicts an increased activation energy of 1.3 kcal/mol. These results imply that, in the high-temperature (low activation energy) regime, a surface reaction involving the cleavage of at least one N–H bond is the rate-limiting step. Moreover, in regimes where the activation energy approaches 22 kcal/mol, the rate-limiting step apparently does not involve N–H bond cleavage.

*3.3. Isotope Exchange Reactions between $NH_3$ and Deuterium.* The results of isotopic exchange experiments, performed to investigate reactions of possible surface intermediates (for example, $NH_2$ and NH species, and N adatoms), are shown in Figure 4

(19) Smith, J. M. "Chemical Engineering Kinetics", 3rd ed.; McGraw-Hill: New York, 1981.

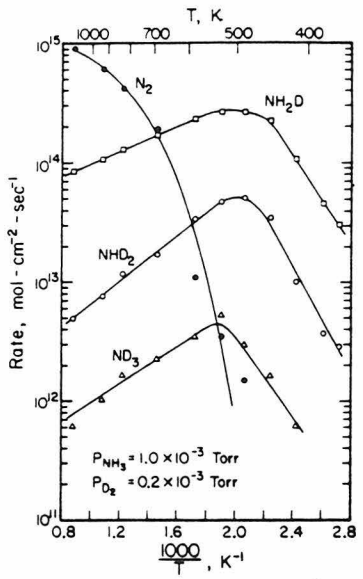


**Figure 4.** Rates of production of the products of the $NH_3 + D_2$ exchange reaction as a function of reciprocal temperature at a partial pressure ratio of $NH_3$ to $D_2$ of 5. Lines have been drawn through the data points for clarity.

for a partial pressure ratio of ammonia to deuterium of 5:1 with a total pressure of $1.2 \times 10^{-3}$ torr. Each of the three possible exchange products $NH_2D$, $NHD_2$, and $ND_3$ is observed. The ratio of the rates, calculated at the temperature corresponding to the maximum value of the rates, is 1.00:0.17:0.02 for $NH_2D$, $NHD_2$, and $ND_3$, respectively. The values of the absolute rates are approximate; they have been determined relative to the absolute rate of nitrogen production by comparing the mass spectrometer sensitivity for nitrogen and $NH_3$ and then using that value for the deuterated ammonia products. Hence the reaction rate for each of the exchange products was obtained by monitoring the parent ion peak intensity. On the basis of the measured fragmentation pattern of $NH_3$, the intensity of mass 18 was corrected for contributions due to cracking fragments of $ND_3$ and $NHD_2$. At high temperatures the apparent activation energy, determined by using a least-squares analysis, for production of $NH_2D$ is −2.3 ± 0.1 kcal/mol, while for $NHD_2$ and $ND_3$ the values are −4.4 ± 0.3 and −4.1 ± 0.4 kcal/mol, respectively. At lower temperatures the rate of production of all three species changes in a similar manner, and the apparent activation energies become 8.4 ± 0.4, 10.6 ± 0.6 and 8.7 ± 0.6 kcal/mol for $NH_2D$, $NHD_2$, and $ND_3$, respectively. The rate of ammonia decomposition, as determined from the rate of production of nitrogen, during the exchange reaction is also shown in Figure 4.

Similar experiments were conducted at partial pressure ratios of ammonia to deuterium of 2:1 and 1:1 with total pressures of $1.5 \times 10^{-3}$ and $2 \times 10^{-3}$ torr, respectively. The activation energies and position of the rate maxima are similar to those shown in Figure 4. The ratios of the rates, relative to $NH_2D$, were 1.00:0.28:0.04 and 1.00:0.50:0.07 for $NH_2D$, $NHD_2$, and $ND_3$ at pressure ratios of 2:1 and 1:1, respectively.

Steady-state rates for the decomposition of pure ammonia were, in all cases, achieved in a few seconds. In contrast, much longer times, often 5–10 min, were required for the exchange reactions. This observation may imply that ammonia and deuterium compete for the same adsorption sites on the platinum surface.[20]

## 4. Mechanistic Modeling

*4.1. Simple Model for Decomposition of Pure $NH_3$.* The similarity between the apparent activation energy of 22 kcal/mol determined at low temperatures and the nitrogen desorption energy of 19 kcal/mol,[13] together with the absence of an isotope effect at low temperatures, suggests that the rate-limiting step in the low-temperature, zero-order kinetic regime is the desorption of nitrogen. On the basis of this tenet, the decomposition reaction can be written mechanistically as

$$NH_3(g) \rightleftharpoons NH_3(a) \tag{2}$$

$$NH_3(a) \rightarrow N(a) + 3H(a) \tag{3}$$

$$2N(a) \rightarrow N_2(g) \tag{4}$$

$$2H(a) \rightarrow H_2(g) \tag{5}$$

The decomposition rate of ammonia is given by

$$R_{NH_3} = 2k^0_{d,N_2}(n_s\theta_N)^2 \exp(-E_{d,N_2}/kT) \tag{6}$$

where $k^0_{d,N_2}$ and $E_{d,N_2}$ are the preexponential factor and the activation energy of the desorption rate coefficient of nitrogen, respectively; $n_s$ is the number of surface sites per cm$^2$, and $\theta_N$ is the fractional surface coverage of nitrogen. This mechanism is expected to be valid far from overall equilibrium, under conditions where readsorption of hydrogen and nitrogen and the hydrogenation of surface nitrogen (the reverse of eq 3) can be neglected. The low conversion, <10%, maintained in our experiments satisfy these criteria.

To calculate reaction rates based on this mechanism, the following material balances for adsorbed ammonia and nitrogen were used

$$n_s(d\theta_{NH_3}/dt) = (1 - \theta_N - \theta_{NH_3})S^0_{NH_3}F_{NH_3} - k^0_{d,NH_3}n_s\theta_{NH_3}\exp(-E_{d,NH_3}/kT) - k^0_r\theta_{NH_3}n_s\exp(-E_r/kT) = 0 \tag{7}$$

$$n_s(d\theta_N/dt) = -2k^0_{d,N_2}(n_s\theta_N)^2\exp(-E_{d,N_2}/kT) + k^0_r n_s\theta_{NH_3}\exp(-E_r/kT) = 0 \tag{8}$$

where $S^0_{NH_3}$ is the zero coverage limit for the adsorption probability of ammonia; $F_{NH_3}$ is the molecular flux of ammonia to the surface; and $k^0_{d,NH_3}$, $k^0_r$, $E_{d,NH_3}$, and $E_r$ are preexponential factors and activation energies for ammonia desorption and surface reaction rate coefficients, respectively. In these calculations we have employed the following assumptions: (1) the adsorption of ammonia is governed by first-order Langmuir kinetics; (2) the preexponential factors and activation energies are independent of coverage; and (3) the steady-state hydrogen coverage is small. The assumption of first-order Langmuir kinetics is valid when the lifetime of any precursor state to adsorption is short compared to the time characteristic of significant surface diffusion. For the high temperatures, greater than 500 K, where ammonia decomposition occurs, we expect this condition to be fulfilled. For example, if the binding energy of the $NH_3$ precursor is on the order of 2 kcal/mol, then the surface residence time at 500 K implies a diffusion distance of only approximately 4 Å. The validity of the other two assumptions is discussed below.

Note that the steady states given in eq 7 and 8 are exact, since the data were obtained under steady-state flow conditions. When the values given in Table I are used, the calculated decomposition rates are in excellent agreement with the experimental values, as shown in Figure 5a–c. Although the desorption energy for nitrogen determined using TDS is 19 kcal/mol, to reproduce the observed activation energy at low temperatures it was necessary for $E_{d,N_2}$ to be 22 kcal/mol. The kinetics observed at high temperatures were described accurately only when $E_r$ and $k^0_r$ were 16 kcal/mol and $1.5 \times 10^{12}$ s$^{-1}$, respectively. Thus, employing independently determined values for desorption of ammonia and nitrogen results in only two adjustable parameters. The systematic deviation of the model predictions from the experimental data for ammonia pressures of $5 \times 10^{-7}$, $1 \times 10^{-6}$, and $2 \times 10^{-6}$ torr is accounted for at least partially by the difficulty in calibrating the reactor for absolute rates at these low pressures. The agreement between the experimental data and the model calculation is obviously very good indeed.

(20) Klein, R. L.; Schmidt, L. D. *J. Chem. Phys.* **1982**, *76*, 3823.

**TABLE I: Model Parameters for the Decomposition and Isotope Exchange Reactions of Ammonia on Platinum**

| | parameter | value | ref |
|---|---|---|---|
| $k^0_{d,NH_3}$ | ammonia desorption preexponential | $1 \times 10^{14}$ s$^{-1}$ | 3, 8 |
| $E_{d,NH_3}$ | ammonia desorption energy | 12 kcal/mol | 3, 8 |
| $S^0_{NH_3}$ | ammonia probability of adsorption | 1 | 3, 8 |
| $k^0_{d,N_2}$ | nitrogen desorption preexponential | $4 \times 10^{-6}$ cm$^2$ s$^{-1}$ | 13 |
| $E_{d,N_2}$ | nitrogen desorption energy | 22 kcal/mol | 13 |
| $k^0_{d,H_2}$, $k^0_{d,D_2}$ | hydrogen desorption preexponential | 0.01 cm$^2$ s$^{-1}$ | 10, 11 |
| $E_{d,H_2}$, $E_{d,D_2}$ | hydrogen desorption energy | 19 kcal/mol | 10, 11 |
| $S^0_{D_2}$ | deuterium probability of adsorption | 0.1 | 10, 11 |
| $k^0_r$, $k^0_1$, $k^0_2$ | surface reaction preexponentials | $1.5 \times 10^{12}$ s$^{-1}$ | |
| $E_r$, $E_1$ | surface reaction activation energies | 16 kcal/mol | |
| $E_{r,ND_3}$ | surface reaction energy for $ND_3$ | 17.2 kcal/mol | |
| $k^0_{-2}$ | hydrogenation reaction preexponential | $3 \times 10^{-17}$ cm$^4$ s$^{-1}$ | |
| $E_{-2}$ | surface hydrogenation activation energy | 28 kcal/mol | |
| $k^0_{-1}$ | exchange reaction preexponential | 0.05 cm$^2$ s$^{-1}$ | |
| $E_{eff}$ | $E_2 - E_{-1}$ | 4 kcal/mol | |
| $n_s$ | surface atom density | $1 \times 10^{15}$ cm$^{-2}$ | |

The mechanism given by eq 2–5 describes successfully the transition from the zero-order, high activation energy regime to the first-order, low activation energy regime. Consideration of the high- and low-temperature limits of eq 6–8 will elucidate the origins of this transition. Analysis of the model indicates that when the activation energy is $\gtrsim$15 kcal/mol, $\theta_N > 0.9$. Consequently, in this (low-temperature) case the surface is almost saturated with nitrogen. If we set $\theta_N$ to unity, eq 6 becomes

$$R_{NH_3} = 2k^0_{d,N_2} n_s^2 \exp(-E_{d,N_2}/kT) \qquad (9)$$

and the rate is independent of ammonia pressure. In addition, from eq 9 $k^0_{d,N_2}$, calculated from the extrapolated intercept at $1/T = 0$ of $(6.4 \pm 5) \times 10^{22}$ molecules/(cm$^2$ s), is $(3.2 \pm 2.5) \times 10^{-6}$ cm$^2$/s. The remarkable agreement of this value with the value of $4 \times 10^{-6}$ cm$^2$/s, determined by TDS,[13] substantiates further the fact that the desorption of nitrogen controls the rate of reaction at low temperatures.

For high temperatures and/or low ammonia pressures, eq 6–8 may be simplified, by assuming that $\theta_N$ and $\theta_{NH_3}$ are small, and combined to give the rate expression

$$R_{NH_3} = \frac{k^0_r S^0_{NH_3} F_{NH_3} \exp(-E_r/kT)}{k^0_{d,NH_3} \exp(-E_{d,NH_3}/kT) + k^0_r \exp(-E_r/kT)} \qquad (10)$$

from which the first-order dependence on ammonia pressure (flux) is established. Utilizing the values in Table I, we see that $k^0_{d,NH_3} \exp(-E_{d,NH_3}/kT) \gg k^0_r \exp(-E_r/kT)$. Thus, the apparent activation energy at high temperatures is given by $E_r - E_{d,NH_3}$. This expression illustrates clearly the origin of the isotope effect observed at high temperatures. Since the nonelementary surface reaction step, eq 3, involves dissociation of three N–H bonds, the activation energy for this step, $E_r$, should show an isotope effect. This is exactly what is observed. In order to model the data for $ND_3$ accurately, it is necessary that $E_{r,ND_3} = 17.2$ kcal/mol compared with 16 kcal/mol for $NH_3$. This increase of 1.2 kcal/mol compares well with the experimentally observed increase of 1.5 kcal/mol and with the theoretically predicted value of 1.3 kcal/mol; these three results are identical within experimental uncertainty.

Combining eq 7 with the relationship $k^0_{d,NH_3} \exp(-E_{d,NH_3}/kT) \gg k^0_r \exp(-E_r/kT)$ implies almost a complete adsorption–desorption equilibrium for ammonia. Thus, only a fraction, approximately $10^{-3}$ at 1000 K, of the adsorbed ammonia reacts; the remainder desorbs molecularly. In contrast, for ammonia decomposition on iron surfaces, it has been proposed that this equilibrium is not established.[21]

An analysis of the model indicates that any coverage dependence of the rate parameters describing eq 2–5, within reasonable limits, would not affect the calculated rates significantly. For low temperatures and/or high pressures, the rate is given by eq 6, where $\theta_N$ is approximately unity. Thus, a variation of $E_{d,N_2}$ with coverage would change the observed activation energy only slightly since

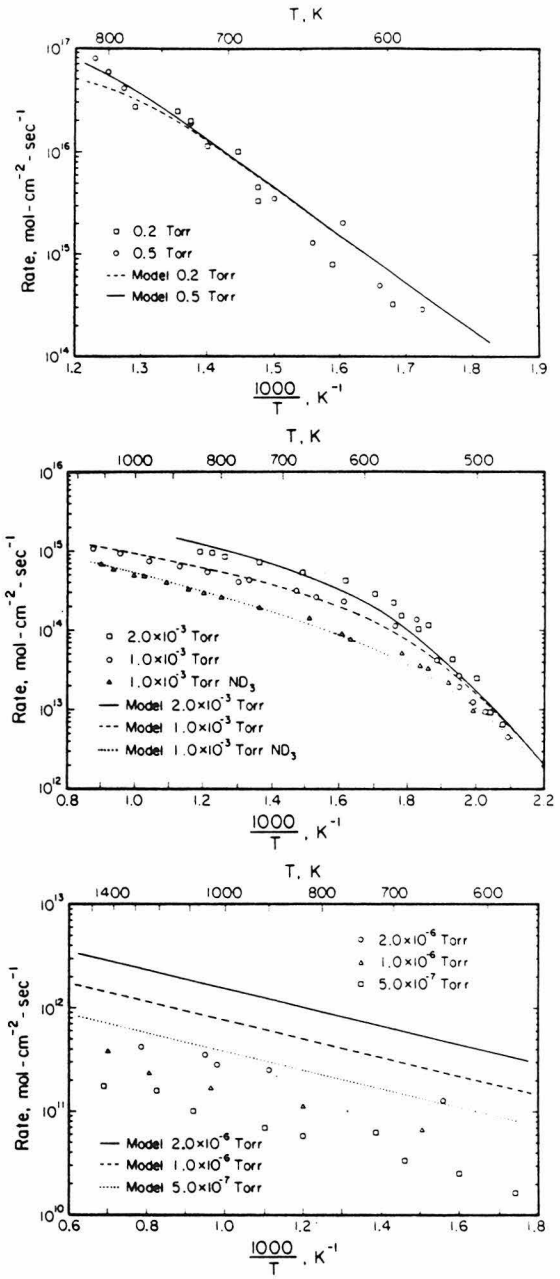


**Figure 5.** Comparison of calculations based on the mechanistic model described in the text with the experimental data for ammonia decomposition: (a) 0.5 and 0.2 torr; (b) $2 \times 10^{-3}$, $1 \times 10^{-3}$ torr, and $1 \times 10^{-3}$ torr of $ND_3$; (c) $2 \times 10^{-6}$, $1 \times 10^{-6}$, and $5 \times 10^{-7}$ torr.

(21) Ertl, G.; Huber, M. *J. Catal.* **1980**, *61*, 537.

$\theta_N$ varies only slightly. Furthermore, both the observed linearity of the Arrhenius plots at low temperature and TDS results for nitrogen desorption from platinum[13] mitigate against any significant variation of $E_{d,N_2}$ with coverage. Since the rate of ammonia decomposition under these conditions is given essentially by eq 9, the calculated decomposition rate is relatively insensitive to the rate parameters for eq 2 and 3, provided the rate of desorption and dissociation of ammonia does not become pathologically large or small, respectively. Therefore, a variation of $E_{d,NH_3}$ and/or $E_r$ with coverage would not change the calculated rates at low temperatures and/or high pressures.

For high temperatures and/or low pressures, a similar argument may be expounded. Under these conditions the total surface coverage is small, and any changes in $E_{d,NH_3}$ or $E_r$ would be expected to be small. Moreover, since the rate of decomposition, which is accurately given by eq 10, is relatively insensitive to the kinetic parameters for nitrogen desorption, any variation in $E_{d,N_2}$ which occurs at these low coverages would not affect the calculated values. Thus, the assumption of coverage independent kinetic parameters is valid insofar as it does not significantly affect the model results.

*4.1.1. Comparison of Simple Model with Langmuir–Hinshelwood Rate Expression.* As mentioned previously, earlier data for ammonia decomposition under conditions similar to those of the present study were fit with a Langmuir–Hinshelwood (L-H) rate expression.[1] While the use of the L-H expression provides a consistent framework for discussion of a heterogeneous reaction, the inherent assumption of a chemisorption equilibrium and the lack of information pertaining to individual elementary steps can lead to various misconceptions. For example, a L-H analysis of the data for ammonia decomposition in the first-order (high-temperature) regime yields the heat of adsorption for ammonia. For ammonia decomposition on platinum, where we have seen that the equilibrium assumption is justified, the calculated value is 16.7 kcal/mol,[1] compared to 12–18 kcal/mol determined by TDS.[3,8] However, a similar analysis for ammonia decomposition on iron, where an adsorption–desorption equilibrium is believed not to exist,[21] leads to a value of 39 kcal/mol,[22] which is too large by a factor of 3 compared to direct determinations.[23,24] Moreover, the reaction rate coefficient in the L-H expression has been interpreted as the rate coefficient for the desorption of nitrogen.[25] This implies that the apparent activation energy observed at high temperature is due to the difference of the desorption energies of nitrogen and ammonia, a conclusion which is inconsistent with the isotope effect observed at high temperatures. Compared to the L-H expression, the steady-state, nonequilibrium approach adopted in the current model is able to describe both situations where chemisorption equilibrium either is or is not attained. Moreover, the high-temperature limit of the current model is consistent with the observed isotope effect.

*4.2. Kinetic Model for Isotope Exchange Reactions.* Although eq 3 represents the decomposition of adsorbed ammonia as a single kinetic step, we expect that eq 3 is actually composed of three elementary steps involving the sequential loss of hydrogen from ammonia, with $NH_2(a)$ and NH(a) as intermediate species. Assuming that the formation of $NH_2D$, $NHD_2$, and $ND_3$ proceeds via the reverse of these three elementary dissociation reactions, the results of the isotope exchange reactions contain considerable information concerning the energetics of the intermediate species. It has been proposed that exchange of deuterium into ammonia on metal surfaces is a concerted reaction where N–H bond cleavage and N–D bond formation occur simultaneously.[3,26] On the basis of this idea, the exchange products would have evolved simply by sequential concerted reactions. In this case, the exchange kinetics would provide no information concerning the intermediate species of decomposition.

We believe, however, that the results shown in Figure 4 indicate a dissociative as opposed to a concerted reaction. Notice in Figure 4 that the energetics for production of all the exchange products are very similar. This implies that the mechanisms giving rise to the different exchange products have similar steps. These steps cannot be a series of concerted exchange reactions for the following reason. The maximum rate of production of $NH_2D$ is approximately equal to the rate of ammonia decomposition at high temperatures. Therefore, the probability for an adsorbed molecule of ammonia to exchange is approximately equal to the probability for decomposition, $10^{-3}$ at most. Neglecting the possibility that reaction of a singly deuterated ammonia could lead to no overall reaction, the probability for exchange of two deuterium atoms into ammonia is at most $10^{-6}$. Similarly, the probability for production of $ND_3$ is $10^{-9}$. For this mechanism, the ratio of the rates would be $1:10^{-3}:10^{-6}$ for $NH_2D$, $NHD_2$, and $ND_3$, respectively. Since this ratio is inconsistent with the experimentally observed ratios, we favor a dissociative mechanism.

Since $NH_2D$ is the major product of the exchange reaction, we have developed a model in which only the production of $NH_2D$ is considered. Completely deuterated ammonia, $ND_3$, will be included later (in section 4.2.2) as a perturbation to the present model. Written mechanistically, the reaction steps are the following:

$$NH_3(g) \rightleftarrows NH_3(a) \quad (2)$$

$$NH_3(a) \rightleftarrows NH_2(a) + H(a) \quad (11)$$

$$NH_2(a) \rightarrow N(a) + 2H(a) \quad (12)$$

$$D_2(g) \rightleftarrows 2D(a) \quad (13)$$

$$NH_2(a) + D(a) \rightleftarrows NH_2D(a) \quad (14)$$

$$NH_2D(a) \rightarrow NH_2D(g) \quad (15)$$

$$2H(a) \rightarrow H_2(g) \quad (5)$$

$$H(a) + D(a) \rightarrow HD(g) \quad (16)$$

$$2N(a) \rightarrow N_2(g) \quad (4)$$

Assuming that the activation energies of desorption and the preexponential factors of the desorption rate coefficients for $NH_2D$ and $D_2$ are the same as for $NH_3$ and $H_2$, respectively, the mass balance equations introduce six new parameters, namely, $k^0_1$, $k^0_2$, $k^0_{-1}$, $E_1$, $E_2$, and $E_{-1}$, which are the preexponential factors and activation energies for eq 11, 12, and 14, respectively. Furthermore, the kinetic parameters for the reverse of eq 11 are considered equal to those for eq 14, and vice versa. Consistent with the previous model, the adsorption of deuterium is assumed to be governed by second-order Langmuir kinetics, and the preexponential factors and activation energies are assumed to be independent of coverage. However, the fractional surface coverage of hydrogen is included in all calculations. The material balance equations indicate that the rates of reaction depend on $E_2 - E_{-1}$ only and, therefore, we define an effective activation energy, $E_{eff} \equiv E_2 - E_{-1}$. However, the fractional surface coverage of $NH_2$ depends on $E_2$ and $E_{-1}$ separately.

Rates of production of $NH_2D$ and decomposition of $NH_3$ (when the flux of deuterium is zero) were determined by solving iteratively the steady-state mass balance equations for $\theta_{NH_3}$, $\theta_D$, $\theta_H$, and $\theta_N$. To fit both the exchange data and the decomposition data for $NH_3$, the parameters $k^0_1$, $k^0_{-1}$, $E_1$, and $E_{eff}$ were varied. All of the parameters used are shown in Table I. As in the case of the previous model, the values of $k^0_1$ and $E_1$ given in Table I are required to fit the high-temperature data, while the kinetic parameters for the desorption of ammonia, nitrogen, and deuterium were obtained from direct independent measurements. The surface reaction preexponential factor $k^0_2$ was arbitrarily, although reasonably, set equal to $k^0_1$. The match between the experimental results and the model predictions was less sensitive to the two remaining parameters, $k^0_{-1}$ and $E_{eff}$. Their values were varied until the most accurate description of the data was obtained. Even in this (less sensitive) case, however, the permissible variation in

(22) Löffler, D. G.; Schmidt, L. D. *J. Catal.* **1976**, *44*, 244.
(23) Grunze, M.; Bozso, F.; Ertl, G.; Weiss, M. *Appl. Surf. Sci.* **1978**, *1*, 241.
(24) Weiss, M.; Ertl, G.; Nitschke, F. *Appl. Surf. Sci.* **1979**, *2*, 614.
(25) See ref 14, p 173.
(26) Kemball, C. *Proc. R. Soc., Ser. A* **1952**, *214*, 413.

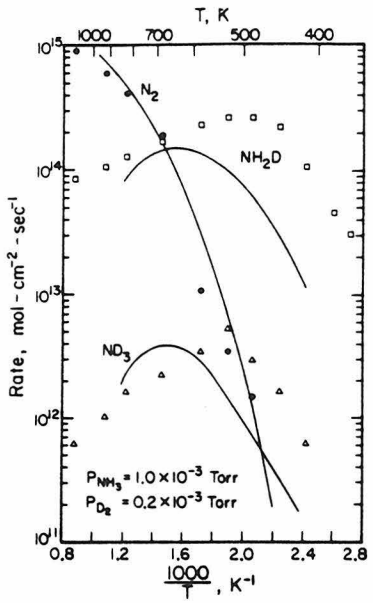


**Figure 6.** Comparison of model calculations with the experimental exchange data for $N_2$, $NH_2D$, and $ND_3$.

$E_{eff}$ is only approximately 1 kcal/mol.

In Figure 6 both the calculated and the experimentally determined rates of $NH_2D$ production are shown together with the rate of decomposition during the exchange reaction. Inspection of Figure 6 indicates that the energetics of the production of $NH_2D$ are reproduced reasonably well by the model. However, the calculated rates are shifted to higher temperatures with respect to the experimental data. This shift may indicate the limitations of assuming that the preexponential factors and activation energies are constant. Indeed, a coverage-dependent activation energy and preexponential factor for the desorption of hydrogen is necessary in order to describe accurately the inhibition of the decomposition of ammonia by hydrogen. This inhibition as well as the effect of varying the rate parameters for hydrogen desorption on the calculated rate of production of $NH_2D$ are discussed in detail elsewhere.[27] Also shown in Figure 6 is the rate of the decomposition of $NH_3$ at $1 \times 10^{-3}$ torr. Both the model predictions and the experimental data exhibit inhibition of the decomposition reaction in the presence of deuterium. Moreover, the model predicts accurately the observed inhibition. Inhibition of the decomposition of ammonia by a variety of partial pressures of deuterium and hydrogen has been investigated in detail and is reported elsewhere.[27]

When the mass balance equations for $NH_2(a)$ and $NH_2D(a)$ are used, the rate of production of $NH_2D$ may be written as

$$R_{NH_2D} = \frac{k_{eff}k_1\theta_{NH_3}\theta_D}{1 + k_{eff}(\theta_D + \theta_H)} \tag{17}$$

where $k_{eff} = k_{-1}/k_2$ and $k_1 = k^0{}_1 n_s \exp(-E_1/kT)$, with similar expressions for $k_2$ and $k_{-1}$. At high temperatures, $k_{eff}(\theta_D + \theta_H) \ll 1$, due to the low coverage of hydrogen and deuterium, $<10^{-3}$. (For example, $k_{eff}(\theta_D + \theta_H) = 0.15$ at $T = 833$ K.) Consequently, in this limit the rate expression becomes

$$R_{NH_2D} = k_{eff}k_1\theta_{NH_3}\theta_D \tag{18}$$

Analysis of the model results for $\theta_{NH_3}$ and $\theta_D$ shows that both ammonia and deuterium are within 0.1% of their respective adsorption–desorption equilibrium values. Therefore, the negative apparent activation energies observed at high temperatures result from decreasing equilibrium coverages of ammonia and deuterium as the temperature is increased.

For low temperatures, $1000/T > 2$, we find that $k_{eff}(\theta_D + \theta_H) \gg 1$ and $\theta_D > 10\,\theta_H$. In this limit, the rate expression becomes

$$R_{NH_2D} = k_1\theta_{NH_3} \tag{19}$$

This expression is similar to eq 10, which was derived for the decomposition reaction at high temperatures. However, in this case $\theta_{NH_3}$ is not simply an equilibrium value since $\theta_N$ in the ammonia mass balance, eq 7, is not negligible. On the basis of eq 19, the rate of exchange at low temperatures would be expected to show a primary isotope effect.

*4.2.1. Reduction of Exchange Model to Simple Decomposition.* By equating the flux of deuterium to zero, the above model reduces to a mechanistic model for the decomposition of pure $NH_3$. From the values given in Table I, the predicted rates are extremely close to those of the model discussed in section 4.1. The difference between the two models is approximately 5% at high and low temperatures, while the difference is largest, approximately 20%, at $1000/T = 1.8$ for $10^{-3}$ torr of ammonia.

Since hydrogen is explicitly included in the exchange model, we are able to evaluate our previous assumption of negligible hydrogen coverage. Analysis of the model indicates that the fractional coverage of hydrogen is at most 0.01. Therefore, $\theta_H$ can safely be neglected.

In order for the exchange model to describe accurately the decomposition of pure ammonia, it was necessary to have $E_1 = 16$ kcal/mol, which is equal to $E_r$ of the previous model that was described in section 4.1. This agreement between $E_1$ and $E_r$ suggests that the isotope effect, observed at high temperatures, involves cleavage of the first N–H bond.

*4.2.2. Production of $ND_3$.* Since the fraction of adsorbed ammonia which exchanges to form $NH_2D$ is less than $10^{-3}$, the same argument that mitigated against a concerted mechanism may be used to imply that consecutive dissociative exchanges would not lead to the observed rate of production of $ND_3$. A mechanism for the production of $ND_3$ which involves consecutive dissociative exchanges of $NH_2(a)$ to form $ND_2(a)$ (subsequently $ND_3$) with NH(a), NHD(a) and ND(a) as sequential intermediates cannot be ruled out on the basis of our experimental data. We cannot, however, assess critically this particular mechanism since imine species such as NH(a) and ND(a) have not been included in our mechanism. Therefore, we postulate that the formation of $ND_3$ proceeds by successive deuteration of nitrogen adatoms. The complicating possibility of hydrogenation can be neglected because $\theta_D > 10\theta_H$. This implies that the rate of addition of a hydrogen atom will be more than an order of magnitude lower than that for addition of a deuterium atom. Moreover, the rate of production of $NH_2D$ exceeds that of $ND_3$ by approximately a factor of 50. Hence the production of $ND_3$ via deuteration of nitrogen adatoms may be treated as a perturbation on the exchange mechanism, where the calculated values of $\theta_D$, $\theta_N$, and $\theta_{NH_3}$ will not be affected significantly by including the mechanistic steps for the production of $ND_3$. The mechanism may be written as

$$N(a) + 2D(a) \rightleftarrows ND_2(a) \tag{20}$$

$$ND_2(a) + D(a) \rightarrow ND_3(g) \tag{21}$$

where the (small) probability that adsorbed $ND_3$ will decompose has been neglected. From the material balance equation for $ND_2(a)$, the rate may be expressed as

$$R_{ND_3} = \frac{k_{eff}k_{-2}\theta_N\theta_D{}^3}{1 + k_{eff}\theta_D} \tag{22}$$

where $k_{-2} = k^0{}_{-2} n_s{}^3 \exp(-E_{-2}/kT)$ is the rate coefficient for eq 20. At high temperatures, eq 22 reduces to

$$R_{ND_3} = k_{eff}k_{-2}\theta_N\theta_D{}^3 \tag{23}$$

Differentiating the logarithm of $R_{ND_3}$ with respect to $\beta \equiv 1/kT$ yields the following expression

$$E_{-2} = -E_{eff} + \frac{\partial(\ln \theta_N)}{\partial\beta} + 3\frac{\partial(\ln \theta_D)}{\partial\beta} - \frac{\partial(\ln R_{ND_3})}{\partial\beta} \tag{24}$$

(27) Tsai, W.; Vajo, J. J.; Weinberg, W. H., in preparation.

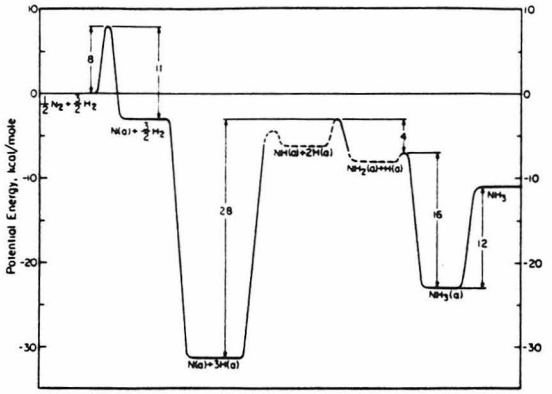


**Figure 7.** One-dimensional potential energy diagram illustrating from right to left the catalytic decomposition of $NH_3$ over Pt where $E_{d,NH_3}$ = 12 kcal/mol, $E_1$ = 16 kcal/mol, $E_{eff} = E_2 - E_{-1}$ = 4 kcal/mol, $E_{-2}$ = 28 kcal/mol, and $^1/_2E_{d,N_2}$ = 11 kcal/mol. Note that the catalytic synthesis of $NH_3$ from $N_2$ and $H_2$ is described by traversing this energy diagram from left to right. The model predicts an activation energy for adsorption of $N_2$ *molecules* of 16 kcal/mol.

Using the value for $E_{eff}$ from Table I, the experimental value for the term involving $R_{ND_3}$, and the model results for the terms involving $\theta_N$ and $\theta_D$, we find that $E_{-2}$ = 33 kcal/mol. A similar analysis for the low-temperature data gives $E_{-2}$ = 23 kcal/mol. The difference between the high-temperature and low-temperature values apparently suggests that $E_{-2}$ varies with coverage. Since the activation energies have been assumed to be constant, we use an average of the high- and low-temperature values, $E_{-2}$ = 28 ± 5 kcal/mol. Assuming the preexponential factor of the rate coefficient $k^0_{-2}$ to be $3 \times 10^{-17}$ cm$^4$ s$^{-1}$ and using the values for $\theta_N$ and $\theta_D$ determined from the exchange model, the curve shown in Figure 6 was calculated for the production of $ND_3$. The agreement that is achieved between the model prediction and the experimental data is further evidence that $ND_3$ is produced via deuteration of nitrogen adatoms.

## 5. Discussion

A one-dimensional potential energy diagram describing the decomposition (or synthesis) of ammonia on platinum is shown in Figure 7. This diagram was constructed from activation energies determined by using the kinetic models for the isotope exchange and decomposition reactions, and independently determined kinetic parameters for adsorption and desorption of nitrogen, hydrogen, and ammonia. An activation energy for desorption of ammonia of 12 kcal/mol was used for the model calculations. However, TDS indicates a second molecularly adsorbed state of ammonia with a desorption energy of 18 kcal/mol.[3,8] If 18 rather than 12 kcal/mol is used for the theoretical calculations, the value determined for $E_1$ changes from 16 to 22 kcal/mol. This result indicates that the absolute level, with respect to nitrogen and hydrogen in their standard states, for the activation barrier to dissociation of the first hydrogen from ammonia is −7 kcal/mol, as shown in Figure 7, independent of $E_{d,NH_3}$.

Also shown in Figure 7 is $E_{eff} = E_2 - E_{-1}$ which was found to be 4 kcal/mol. Since the calculated rates depend only on $E_2 - E_{-1}$, the potential energy level for $NH_2(a) + H(a)$, which is equal to $-E_{-1} - 7$ kcal/mol, cannot be determined from our kinetic model. This is indicated by a dashed curve in Figure 7. However, the desorption of $NH_2$ radicals during ammonia decomposition was not detected experimentally by laser-induced fluorescence (LIF).[16,17] Therefore, we expect that $E_{-1}$ is small, probably <5 kcal/mol; and consequently the fractional coverage of $NH_2$ is small, below the (unknown) limit of detection. With a value of 44 kcal/mol for the heat of formation of $NH_2$,[28] the potential energy level for $NH_2 + H(a)$ is 34.5 kcal/mol. The heat of adsorption of the $NH_2$ radical on the platinum surface is, therefore, $E_{-1}$ + 41.5 kcal/mol.

Although the rate of production of $NHD_2$ was not analyzed in detail, the identical argument that was articulated above indicates that only the difference in energy between the barriers on each side of the NH(a) + 2H(a) potential well would be obtained. The actual depth of the well cannot be determined. As mentioned previously, desorption of NH radicals during ammonia decomposition has been observed with an apparent activation energy of 63–69 kcal/mol.[16] To illustrate the relationship between the observed apparent activation energy and the actual activation energy for the desorption of NH radicals, consider the following argument. The rate of desorption of NH radicals may be written as

$$R_{d,NH} = k^0_{d,NH} n_s \theta_{NH} \exp(-E_{d,NH}/kT) \qquad (25)$$

where $k^0_{d,NH}$ and $E_{d,NH}$ are the preexponential factor and the activation energy of the desorption rate coefficient for NH radicals. Differentiating the logarithm of $R_{d,NH}$ with respect to $\beta$ yields the negative of the observed activation energy

$$\frac{\partial(\ln R_{d,NH})}{\partial \beta} = \frac{\partial(\ln \theta_{NH})}{\partial \beta} - E_{d,NH} = -66 \pm 3 \text{ kcal/mol} \qquad (26)$$

Thus only for the special case where $\partial(\ln \theta_{NH})/\partial\beta = 0$ is the observed activation energy equal to the desorption energy. Since the reaction is carried out at steady state and low conversions where the reaction between NH(a) and H(a) to form $NH_2(a)$ can be neglected, the rate of production of NH(a) is equal to the rate of decomposition of NH(a), and both these rates are equal to the rate of decomposition of ammonia. Therefore, at steady state

$$R_{NH_3} = k^0_{NH} n_s \theta_{NH} \exp(-E_{NH}/kT) \qquad (27)$$

where $k^0_{NH}$ and $E_{NH}$ are the preexponential factor and the activation energy of the rate coefficient for the decomposition of NH(a). For the reaction conditions employed in the LIF study, the activation energy for the decomposition of ammonia, determined from the model described in section 4.2, is approximately 5 kcal/mol. Thus from eq 27

$$\frac{\partial(\ln R_{NH_3})}{\partial \beta} = \frac{\partial(\ln \theta_{NH})}{\partial \beta} - E_{NH} = -5 \text{ kcal/mol} \qquad (28)$$

Combining eq 26 and 28, we obtain the activation energy for the desorption of NH radicals as 61 ± 3 + $E_{NH}$ kcal/mol. To compare this value with the energy determined in the present study, we require a value for the absolute potential energy level of the barrier leading to decomposition of NH(a) in order to express the desorption energy in terms of $E_{NH}$. Since the isotopic exchange data for the production of $NHD_2$ have not been analyzed, this energy level may not be obtained from our kinetic model. We adopt the simplifying assumption that the NH(a) + 2H(a) potential energy well is symmetrical. (Note that a more general case is shown in Figure 7.) As shown in Figure 7, the absolute potential energy level of the barrier for the *hydrogenation* of NH(a) to $NH_2(a)$ is −3 kcal/mol. Therefore, assuming a symmetrical well, the absolute level for NH(a) + 2H(a) is $-E_{NH}$ − 3 kcal/mol. Using a value of 85 kcal/mol for the heat of formation of NH,[29] the potential energy level for NH + 2H(a) is 66 kcal/mol, where we have used $E_{d,H_2}$ = 19 kcal/mol. Consequently, the activation energy for the desorption of NH radicals is 69 + $E_{NH}$ kcal/mol. This value agrees with the value determined via LIF within the experimental uncertainties.

The activation energy for hydrogenation of surface nitrogen, $E_{-2}$ = 28 kcal/mol, is shown also in Figure 7. Comparing this value with the activation energy for desorption of molecular nitrogen, 22 kcal/mol, shows that nitrogen desorption is favored energetically. Hydrogenation of surface nitrogen to form ammonia has been studied by Pirug and Bonzel on a polycrystalline platinum

(28) DeFrees, D. J.; Hehre, W. J.; McIver, R. T.; McDaniel, D. H. *J. Phys. Chem.* **1979**, *83*, 232.

(29) Graham, W. R. M.; Lew, H. *Can. J. Phys.* **1978**, *56*, 85.

foil by reaction of dissociatively adsorbed nitric oxide with hydrogen.[30] Although an activation energy for the hydrogenation reaction was not determined, an analysis of Pirug and Bonzel's data for the production of ammonia at a partial pressure ratio of hydrogen to nitric oxide of five (Figure 9 of ref 30) indicates almost quantitative agreement with our data for $ND_3$ production shown in Figure 4. The activation energy at high and low temperature as well as the temperature corresponding to the maximum rate are nearly identical. These results are consistent with a large energy barrier for the hydrogenation of nitrogen on platinum. Furthermore, since the ammonia produced in the NO + $H_2$ reaction necessarily results from hydrogenation of nitrogen adatoms, the agreement between the kinetics of ammonia production from NO + $H_2$ and the kinetics for $ND_3$ production from $NH_3$ + $D_2$ substantiates further the assertion that $ND_3$ results from deuteration of surface nitrogen.

Completion of the potential energy diagram using ${}^3/_2E_{d,H_2}$ = 28.5 kcal/mol and ${}^1/_2E_{d,N_2}$ = 11 kcal/mol results in an activation barrier for the dissociative adsorption of nitrogen of 8 kcal/mol on an atom basis or 16 kcal/mol for molecular nitrogen. The heat of adsorption of a nitrogen molecule adsorbed dissociatively on platinum is predicted to be exothermic by 6 kcal/mol. Evidently, the energetics for dissociative adsorption of nitrogen on platinum have not been examined directly. However, thermal desorption results have indicated an activated adsorption process.[13,31] Moreover, the probability of adsorption was observed to be independent of surface temperature over a range between 90 and 300 K.[13] This result indicates that in addition to being an activated process, the dissociative adsorption of nitrogen is apparently also a direct process,[31] in which *dissociation proceeds without prior thermal equilibration of the molecularly adsorbed species with the surface*. Direct dissociative adsorption of nitrogen on W(110) has been investigated by varying the incident translational energy of nitrogen with a helium-seeded molecular beam.[32] A simple analysis based on a one-dimensional potential energy barrier yielded a low coverage activation energy of 9.7 kcal/mol. Similar studies on platinum surfaces would be useful in elucidating the details of dissociative nitrogen adsorption.

Direct adsorption processes imply, through microscopic reversibility, direct desorption processes. Therefore it is energetically possible, during $NH_3$ decomposition, to desorb excited nitrogen molecules with excitation energies as large as the activation barrier for adsorption. The excitation energy may be translational and/or internal depending on the detailed shape of the potential energy surface. If only translational excitation is observed, the one-dimensional potential energy diagram shown in Figure 7 provides an adequate description of the process. If vibrational or rotational excitation is observed, the full potential energy surface must be taken into account. Vibrationally excited nitrogen with 20 kcal/mol of excess energy has been detected during ammonia decomposition on platinum.[15] The authors attribute this internal excitation to a recombination reaction involving adsorbed NH species. However, the observed vibrational energy may also be attributed to simple recombination of nitrogen adatoms, if the activation energy for adsorption is at least 20 kcal/mol. Considering the following argument, we believe that under the conditions where vibrational excitation was detected, the activation energy for adsorption may indeed be at least 20 kcal/mol. There are numerous examples where activation energies for adsorption increase sharply with coverage. For example, the activation energy for adsorption of nitrogen on Fe(100) has been shown to increase from an initial value of 2 to 11 kcal/mol at $\theta_N$ = 0.2.[33] We estimate that the fractional coverages of nitrogen were between 0.3 and 0.5 under conditions where vibrationally excited nitrogen was detected desorbing from platinum. Thus, postulating that the activation energy for dissociative adsorption of nitrogen has increased from an initial value of 16 to $\gtrsim$20 kcal/mol is not at all unreasonable.

Observation of vibrationally excited nitrogen implies that the transition state for desorption occurs early, close to the reactants (nitrogen adatoms) on the nitrogen–platinum potential energy surface. For an accurate description of this type of adsorption/desorption process, a multidimensional potential energy surface, as opposed to a simple one-dimensional description, must be employed. Measurements of the angular dependence of the adsorption probability have cast doubt upon the validity of the one-dimensional activation barrier for dissociative nitrogen adsorption on W(110).[32,34] Comparing this result for adsorption on W(110) with desorption results obtained on platinum suggests that the processes on both surfaces are similar. If the transition state for desorption of nitrogen from tungsten also occurs early, the transition state for the adsorption reaction will occur late, where the adsorbing nitrogen resembles two nitrogen adatoms. Described in terms of a potential energy surface for an atom–diatomic molecule collinear collision,[35] the hypothetical reactant particle must bend around into the product channel to reach the transition state. For nitrogen adsorption on tungsten, the incident translational energy must be converted into internal energy to bend around the potential surface and reach the transition state. Thus, the reaction probability as a function of incident translational energy does not have the simple step function form predicted by a one-dimensional model, and excitation of internal degrees of freedom near the transition state is important in surmounting the activation barrier for adsorption.

## 6. Synopsis

The results of this study may be summarized as follows:

1. For high temperatures and/or low pressures, a surface reaction involving the dissociation of the first N–H bond controls the rate of ammonia decomposition. The activation energy in this regime is 4.2 ± 0.3 kcal/mol, and the rate of decomposition exhibits a primary isotope effect.

2. For low temperatures and/or high pressures, the surface is nearly saturated with nitrogen, and the rate of nitrogen desorption controls the rate of reaction. Consequently, the reaction rate is independent of ammonia pressure, and the observed activation energy, 22 ± 2 kcal/mol, is equal to the activation energy for desorption of nitrogen.

3. The isotope exchange reaction, $NH_3$ + $D_2$, produces all three exchange products. The mechanism for exchange is dissociative. In particular, reasonable agreement with the experimental data has been obtained assuming that $ND_3$ results from deuteration of surface nitrogen adatoms.

4. The kinetics of ammonia decomposition on platinum for a wide range of temperatures and pressures can be described remarkably well by coverage independent kinetic parameters.

5. The dissociative adsorption of molecular nitrogen on platinum is an activated process with an activation energy predicted to be approximately 16 kcal/mol in the limit of zero surface coverage of nitrogen adatoms.

*Acknowledgment.* We gratefully acknowledge the financial support of the Army Research Office under Grant No. DAAG29-83-K-0094, and the Central Research and Development Department of E. I. du Pont de Nemours and Company.

**Registry No.** $NH_3$, 7664-41-7; Pt, 7440-06-4; D, 7782-39-0; H, 1333-74-0.

(30) Pirug, G.; Bonzel, H. P. *J. Catal.* **1977**, *50*, 64.

(31) For a recent review of activated adsorption, see: Morris, M. A.; Bowker, M.; King, D. A. In "Comprehensive Chemical Kinetics"; Bamford, C. H., Tipper, C. F. H., Compton, R. G. Eds.; Elsevier: Amsterdam, 1984; Vol. 19.

(32) Lee, J.; Madix, R. J.; Schlaegel, J. E.; Auerbach, D. J. *Surf. Sci.* **1984**, *143*, 626.

(33) Bozso, F.; Ertl, G.; Grunze, M.; Weiss, M. *J. Catal.* **1977**, *49*, 18.

(34) Auerbach, D. J.; Pfnür, H. E.; Rettner, C. T.; Schlaegel, J. E.; Lee, J.; Madix, R. J. *J. Chem. Phys.* **1984**, *81*, 2515.

(35) Polanyi, J. C. *Acc. Chem. Res.* **1972**, *5*, 161.

# Chapter 4.

## Steady-State Decomposition of Ammonia on the Pt(110)-(1x2) Surface

[Chapter 4 consists of an article coauthored with W. Tsai and W. H. Weinberg.]

**Abstract**

Steady-state absolute reaction rates are reported for the catalytic decomposition of ammonia on the Pt(110)-(1x2) single crystalline surface at pressures between 1 x $10^{-6}$ and 2.6 x $10^{-6}$ Torr and at temperatures between 400 and 1000 K. For temperatures below 475 K, the apparent activation energy is 24 ± 4 kcal/mole, and the reaction rates approach zero-order in ammonia pressure. At higher temperatures the activation energy decreases, becoming 1 ± 1 kcal/mole for temperatures above 550 K. Under these conditions the rate of decomposition is linearly dependent on ammonia pressure. The surface composition at 2 x $10^{-6}$ Torr and temperatures between 350 and 600 K was measured by thermal desorption experiments conducted *during* the steady-state decomposition of ammonia. The results indicate that nitrogen adatoms are the predominant surface species, and that the activation energy for nitrogen desorption is 24-26 kcal/mole, independent of the nitrogen coverage. A mechanistic model, developed previously, has been found to describe accurately the pressure and temperature dependence of both the decomposition kinetics and the measured steady-state coverage of nitrogen adatoms. Both the experimental measurements and the mechanistic model indicate that molecular nitrogen is produced by the recombinative desorption of nitrogen adatoms on the platinum surface.

## 1. Introduction

The decomposition of ammonia on platinum surfaces has been studied extensively using a variety of experimental techniques **(1-8)**. While the steady-state decomposition kinetics on polycrystalline platinum surfaces has been firmly established for a wide range of pressure and temperature **(1-4)**, the important surface intermediates and surface reactions, although suggested **(3,7,8)**, have not been determined unequivocally. Threshold ionization measurements have established the desorption of $N_2^*$ with 20 kcal/mole of vibrational excitation during ammonia decomposition at a pressure of 0.1-1.4 Torr on a platinum ribbon at temperatures between 773 and 1373 K **(7)**. Based on these results, the authors suggested that (at least under these conditions) the bimolecular reaction of two adsorbed NH species is the dominant reaction producing molecular nitrogen and controlling the rate of ammonia decomposition. Indeed, NH radials have been observed by laser-induced fluorescence (LIF) to desorb from a platinum wire in 0.1 Torr of ammonia at 1200-1400 K **(8)**. Although nitrogen adatoms were believed to be at least an order of magnitude more abundant for all the experimental conditions studied, the lack of an appropriate calibration precluded any estimate of the NH surface concentration.

In a recent study in our laboratory, absolute reaction rates were measured for ammonia decomposition by a polycrystalline platinum wire over a wide range of pressure and temperature **(3)**. The results were interpreted in terms of a steady-state, nonequilibrium mechanistic model embodied by elementary surface reactions. A quantitatively accurate description of the experimental data was obtained for the entire range of conditions studied ($5 \times 10^{-7} \leq p_{NH_3} \leq 0.5$ Torr and $400 \leq T \leq 1200$ K), using independently measured adsorption-desorption parameters for $NH_3$, $N_2$ and $H_2$. The model implies that at low tem-

peratures and/or high pressures, nitrogen adatoms are the dominant surface species, and that the recombinative desorption of nitrogen controls the observed rate of reaction. At high temperatures and/or low pressures, the surface coverage of all species is low, and a competition between the desorption of molecular ammonia and the cleavage of an N-H bond of adsorbed ammonia controls the rate of ammonia decomposition.

In the present study, absolute reaction rates have been measured for the steady-state decomposition of ammonia by a Pt(110)-(1x2) surface at pressures between 1 x $10^{-6}$ and 2.6 x $10^{-6}$ Torr and temperatures between 400 and 1000 K. Thermal desorption measurements, conducted *during* the steady-state decomposition, were used to determine the composition, coverage and kinetics of desorption of the adsorbed species during the ammonia decomposition. These results are used to evaluate our previously proposed mechanistic model **(3)** and to explore the surface structural dependence of the ammonia decomposition reaction on platinum.

## 2. Experimental Procedures

The measurements were performed in an ion-pumped, stainless steel belljar that has been described in detail previously **(9)**. The base pressure of the belljar was below 1 x $10^{-10}$ Torr of reactive gases. The Pt(110) crystal was oriented and cut from a single crystalline boule of platinum and was polished to within 1° of the (110) orientation using standard metallographic techniques. The crystal was etched in aqua regia and cleaned in situ by argon ion sputtering at 1200 K, heating in 5 x $10^{-7}$ Torr of oxygen at 800 K, and annealing to 1400 K. Auger electron spectroscopy was used to verify surface cleanliness. Special care was taken to reduce the bulk concentration of silicon impurity, since it has been shown that its presence is related to the formation of a "subsurface oxide" on Pt(111)

**(10)**. After cleaning and annealing, the (1x2) LEED pattern that is characteristic of the clean, reconstructed surface was observed.

Since decomposition of ammonia occurred readily on the hot filament of the mass spectrometer, the steady-state decomposition experiments were carried out with a directional beam doser consisting of a multichannel array of capillaries **(11)**. This provided a beam-pressure to background-pressure ratio of greater than 100:1 at the platinum surface. In addition, the crystal manipulator was cooled to approximately 100 K with liquid nitrogen, which further reduced the background ammonia pressure. Absolute "beam" fluxes were determined by measuring the rate of pressure decrease in the doser reservoir. Absolute reaction rates were determined by replacing the ammonia in the doser reservoir with nitrogen (the reaction product) and calibrating the mass spectrometer using the known flux from the capillary array.

Both $^{15}NH_3$ (99 atom % $^{15}N$) and $^{15}ND_3$ (99 atom % $^{15}N$, 99 atom % deuterium) were obtained from MSD Isotopes and were used without further purification. Their purities were verified in situ mass spectrometrically.

## 3. Experimental Results

### 3.1. Steady-State Decomposition of $^{15}NH_3$

Absolute reaction rates for the decomposition of $^{15}NH_3$ by the Pt(110)-(1x2) surface are shown in Fig. 1 as a function of temperature at an effective pressure of ammonia of $2 \times 10^{-6}$ Torr. These data were obtained by exposing the clean surface at 900 K to a continuous flux of $^{15}NH_3$. The surface was then cooled at a rate of 2-3 K/s while recording the $^{15}N_2$ mass spectrometric intensity **(12)**. Identical results were obtained by monitoring the $H_2$ product. The data displayed in Fig. 1 are shown as a function of reciprocal temperature in Fig. 2. In this representation, the two different kinetic regimes, which have been

observed previously for ammonia decomposition by platinum **(1-3)**, are quite evident. For temperatures below approximately 475 K, the apparent activation energy is 24 ± 4 kcal/mole; at higher temperatures, the activation energy decreases, becoming approximately 1 ± 1 kcal/mole for temperatures above 550 K.

The dependence of the reaction rate on ammonia pressure is shown in Fig. 3 for ammonia pressures of $1 \times 10^{-6}$, $1.7 \times 10^{-6}$ and $2.6 \times 10^{-6}$ Torr. For temperatures above approximately 550 K, the dependence of the reaction rate on ammonia pressure is nearly first-order, while for temperatures below 500 K the reaction rates begin to converge, approaching zero-order in ammonia pressure.

### 3.2 Surface Composition and Coverage During Ammonia Decomposition

The $^{15}N_2$ mass spectrometric intensity is shown as a function of temperature in Fig. 4 for several cooling and heating cycles during a continuous exposure of the Pt(110)-(1x2) surface to $^{15}NH_3$ at an effective pressure of $2 \times 10^{-6}$ Torr. For each cycle, the initial surface temperature was 900 K. The surface was then cooled at a rate of 2-3 K/s to a specified temperature, which was maintained for 30 s **(13)**. Thereafter, the surface temperature was increased at a rate of 5 K/s to 900 K. The cooling part of each cycle reflects the steady-state rate of decomposition of $^{15}NH_3$, as shown also in Fig. 1. Each heating curve reflects, however, both the steady-state rate of decomposition and the thermal desorption of nitrogen from the surface.

In addition to monitoring the production of $^{15}N_2$, as shown in Fig. 4, the $H_2$ (or $D_2$ during the decomposition of $^{15}ND_3$) mass spectrometric signal was also recorded. For each cycle, only the steady-state rate of decomposition was observed regardless of whether the surface was being heated or cooled; i.e. unlike the case of $N_2$ shown in Fig. 4, no hysteresis was observed for temperatures

above 350 K **(14)**. Since we estimate the mass spectrometric detection limit using this procedure to be approximately 0.05 monolayer, the ratio of the steady-state coverage of nitrogen atoms to that of hydrogen atoms on the surface at temperatures between 350 and 600 K is >20:1. This important result clearly establishes that during the steady-state decomposition of ammonia at 2 x $10^{-6}$ Torr and above 350 K, the most abundant intermediate on the Pt(110)-(1x2) surface is nitrogen adatoms.

Since these thermal desorption measurements, carried out during the steady-state ammonia decomposition reaction, showed only nitrogen desorption, the area between each heating and cooling curve (e.g. in Fig. 4) is a measure of the concentration of nitrogen adatoms present *during the steady-state decomposition of ammonia* at the particular temperature where the heating was begun. Steady-state fractional coverages of nitrogen for ammonia decomposition at 2 x $10^{-6}$ Torr and temperatures between 350 and 600 K were measured in this way and are shown in Fig. 5. In order to obtain these fractional coverages, the data were normalized to the saturation coverage of nitrogen adatoms, which was obtained at temperatures below 400 K. Although relative coverages are shown in Fig. 5, the absolute saturation coverage of nitrogen adatoms was determined to be 2.1 x $10^{15}$ $cm^{-2}$ by calibration against the known saturation coverage of carbon monoxide, as discussed in detail elsewhere **(15)**.

A comparison of the fractional coverages of nitrogen shown in Fig. 5 with the steady-state reaction rate shown in Fig. 2 reveals that the increase in the apparent activation energy observed below approximately 500 K is associated with the accumulation of surface nitrogen. Hence, as the fractional coverage of nitrogen approaches unity, the recombinative desorption of molecular nitrogen controls the rate of the ammonia decomposition reaction, and the observed

activation energy is the activation energy for the desorption of nitrogen.

By selecting an initial temperature at which the surface is saturated with nitrogen (i.e. below 400 K) and varying the heating rate from 3 to 25 K/s, the activation energy of the desorption rate coefficient of nitrogen may be evaluated as a function of fractional nitrogen coverage. For a rapidly pumped system (in which the rate of pumping is much greater than the rate of desorption), the desorption rate is proportional to the partial pressure (i.e. the ion current of the mass spectrometer), and the coverage at any point in a desorption spectrum may be obtained from the time-integrated product signal. By varying the heating rate with a constant initial coverage, i.e. a particular steady-state temperature, the spectra can be used to construct Arrhenius plots of the desorption rate at constant coverages of which the slope is $-E_{d,N_2}(\theta_N)/k_B$ **(16)**. Using this procedure, the activation energy for the desorption of nitrogen from the Pt(110)-(1x2) surface during the ammonia decomposition reaction has been measured and is shown as a function of fractional nitrogen coverage in Fig. 6. It is apparent that this activation energy is 24-26 kcal/mole and is independent of nitrogen coverage.

## 4. Discussion

### 4.1 Surface Composition during Ammonia Decomposition

The thermal desorption measurements conducted during the steady-state decomposition of ammonia on the Pt(110)-(1x2) surface at 2 x $10^{-6}$ Torr show clearly that over the entire range of temperatures studied nitrogen adatoms are the dominant surface species. For steady-state reaction temperatures below 400 K, the nitrogen overlayer corresponds to saturation coverage, approximately 2.1 x $10^{15}$ $cm^{-2}$ **(17)**. At higher reaction temperatures, the steady-state fractional coverage of nitrogen decreases, becoming <0.1 for temperatures

above 600 K. The steady-state concentrations of adsorbed species such as NH or $NH_2$ are at least a factor of 20 lower than that of nitrogen adatoms for temperatures above 350 K. This result is consistent with the LIF measurements described in Sect. 1 **(8)**. Although the desorption of NH radicals from a platinum wire was observed during the steady-state decomposition of ammonia at 1200-1400 K and 0.1 Torr, the concentration ratio of N(a) to NH(a) was estimated to be >10:1.

The activation energy for the recombinative desorption of molecular nitrogen from the Pt(110)-(1x2) surface during the steady-state decomposition of ammonia was found to be 24-26 kcal/mole, which agrees with the observed activation energy of 24 ± 4 kcal/mole for the steady-state decomposition of ammonia under conditions where the fractional surface coverage of nitrogen approaches unity (cf. Figs. 2 and 5). Moreover, both of these values agree with the activation energy of 24 ± 2 kcal/mole for the thermal desorption of nitrogen, determined independently, following the dissociative adsorption of ammonia at 400 K **(15)**. In these experiments, the surface was cooled to 300 K, and the system evacuated prior to the thermal desorption measurements. These results imply that when the surface concentration of nitrogen adatoms approaches saturation, the desorption of nitrogen controls the rate of ammonia decomposition.

### 4.2 Mechanistic Modeling

A microscopic description of the catalytic decomposition of ammonia has been presented and discussed in detail recently **(3)**. Briefly, this model is based on a series of elementary (or "almost elementary") reactions, namely,

$$NH_3(g) \underset{k_{d,NH_3}}{\overset{S_{NH_3}F_{NH_3}}{\rightleftarrows}} NH_3(a)\,, \qquad (1)$$

$$NH_3(a) \overset{k_r}{\rightarrow} N(a) + 3H(a)\,, \qquad (2)$$

$$2N(a) \overset{k_{d,N_2}}{\rightarrow} N_2(g)\,, \qquad (3)$$

and

$$2H(a) \overset{k_{d,H_2}}{\rightarrow} H_2(g)\,, \qquad (4)$$

where $S_{NH_3}$ is the probability of molecular adsorption of ammonia, $F_{NH_3}$ is the flux of ammonia to the surface, and $k_{d,NH_3}$, $k_r$, $k_{d,N_2}$ and $k_{d,H_2}$ are the rate coefficients of the four surface reactions. Each of these rate coefficients may be written as $k_i = k_i^{(0)}\exp[-E_i/k_BT]$ with (assumed) coverage-independent preexponential factors $k_i^{(0)}$ and activation energies $E_i$.

The steady-state rate of decomposition of ammonia is determined by solving the material balance equation for each adsorbed species. The model description of the measured rates of ammonia decomposition, utilizing the parameters listed in Table 1, are indicated by the continuous lines in Figs. 2 and 3. Obviously, the model accurately describes both the temperature and the pressure dependence of the reaction rate.

The model embodied by Eqs. (1)-(4) has been used successfully to describe the decomposition of ammonia by polycrystalline platinum at pressures between $5 \times 10^{-7}$ and 0.5 Torr and temperatures between 400 and 1200 K **(3)**. Independently measured values were used for the adsorption and desorption parameters of ammonia, nitrogen and hydrogen. To describe the decomposition of ammonia on the Pt(110)-(1x2) surface, the values of the initial

probability of adsorption of ammonia and the preexponential factors of the rate coefficients for the desorption of both ammonia and nitrogen were the same as those employed previously **(3)**. The desorption parameters for hydrogen on Pt(110)-(1x2) have been measured independently **(15)**. For the model results shown in Figs. 2 and 3, $E_{d,N_2}$ = 24.5 kcal/mole. However, essentially identical results were obtained with either $E_{d,N_2}$ = 24 kcal/mole and $k_{d,N_2}^{(0)}$ = 3 x $10^{-8}$ $cm^2/s$, or $E_{d,N_2}$ = 26 kcal/mole and $k_{d,N_2}^{(0)}$ = 2 x $10^{-7}$ $cm^2/s$. This range of $E_{d,N_2}$ was measured directly during ammonia decomposition on Pt(110)-(1x2), as shown in Fig. 6. Thus, the model contains two adjustable parameters, namely, $k_r^{(0)}$ and $E_r - E_{d,NH_3}$. The measured rates at high temperatures were described best by $E_r - E_{d,NH_3}$ = 0.5 kcal/mole. For comparison, $E_r - E_{d,NH_3}$ = 4 kcal/mole is required to describe the decomposition of ammonia on a polycrystalline platinum wire **(3)**. The difference in these values reflects the structural sensitivity of ammonia decomposition on platinum, an issue that is discussed in Sect. 4.3.

In addition to the absolute rate of ammonia decomposition, the model embodied by Eqs. (1)-(4) yields the steady-state coverage of each adsorbed species. As expected, the calculated steady-state coverages of both molecular ammonia and atomic hydrogen are small (<0.01) for all the conditions studied. The calculated fractional surface coverage of nitrogen adatoms as a function of reciprocal temperature is shown in Fig. 5, together with the measured coverage, each at an ammonia pressure of 2 x $10^{-6}$ Torr. The agreement between the calculated and the measured steady-state nitrogen coverages is excellent (using the same set of independently determined model parameters). The recombination of nitrogen adatoms is the only reaction which gives rise to molecular nitrogen in this mechanistic model. Therefore, the agreement between the calculated and the measured surface coverages of nitrogen implies that the recombinative

desorption of nitrogen is certainly the dominant (and arguably the only) mechanism of nitrogen production.

Vibrationally excited molecular nitrogen with 20 kcal/mole of excess energy has been detected during ammonia decomposition on polycrystalline platinum **(7)**. This internal excitation was attributed to a recombination reaction involving two adsorbed NH species. However, the observed vibrational energy may alternatively be attributed to the recombination of nitrogen adatoms, if the activation energy for the dissociative adsorption of molecular nitrogen is at least 20 kcal/mole. Based on a mechanistic model for the $NH_3 + D_2$ exchange reaction on a polycrystalline platinum wire, the dissociative adsorption of nitrogen is predicted to be an activated process, with an activation energy of approximately 16 kcal/mole in the limit of zero surface coverage **(3)**. Using model parameters appropriate for a polycrystalline surface, we estimate that the fractional coverage of nitrogen was between 0.3 and 0.5 under the experimental conditions where vibrationally excited nitrogen was detected desorbing from platinum. Postulating that the activation energy for the dissociative adsorption of nitrogen has increased from an initial (zero coverage) value of 16 kcal/mole to $\gtrsim$20 kcal/mole at these surface coverages is certainly not unreasonable.

### 4.3 Surface Structural Dependence of Ammonia Decomposition on Platinum

The decomposition of ammonia has been examined previously on a polycrystalline platinum wire that was cleaned by oxidation, reduction and annealing cycles at 1100 K **(3)**. Extensive annealing of a polycrystalline platinum ribbon at 1400 K for 12 hrs. has been shown to produce a surface with predominantly (111) orientation **(18)**. Assuming that the platinum wire consists of (111) oriented microcrystallites enables comparisons to be made with the Pt(110)-(1x2) surface used in the present study. However, the presence of a large

number of defect sites on the "oriented" polycrystalline surface must be considered in any comparison.

Under conditions where the surfaces are nearly saturated with nitrogen adatoms, the observed activation energies for the decomposition of ammonia on polycrystalline platinum and Pt(110)-(1x2) are 22±2 **(3)** and 24±4 kcal/mole, respectively. Although these values are identical within experimental uncertainties, the best model description of the measured rates was obtained with $E_{d,N_2}$ = 22 and 24.5 kcal/mole for the polycrystalline platinum and the Pt(110)-(1x2) surfaces, respectively. Since the recombinative desorption of nitrogen controls the rate of ammonia decomposition under these conditions, it follows that the desorption of nitrogen at high surface coverages of nitrogen adatoms is, at most, only slightly sensitive to the structure of the platinum surface. Similar results have been obtained for ammonia decomposition on a polycrystalline platinum disc and a Pt(210) surface **(2)**. The influence of defect sites, which should be less prevalent on the Pt(110)-(1x2) surface, is of minor importance during ammonia decomposition under these conditions of high surface coverage. Previously, the activation energy for the dissociative adsorption of nitrogen on a polycrystalline platinum surface was estimated to be 16 kcal/mole **(3)**. However, the similarity of $E_{d,N_2}$ for both the polycrystalline platinum surface and the Pt(110)-(1x2) surface certainly does not imply that the activation energies for the dissociative adsorption of nitrogen are similar on these two surfaces.

When the rate of ammonia decomposition is first-order in ammonia pressure, the observed activation energies are 4.2±0.3 and 1±1 kcal/mole for the polycrystalline platinum **(3)** and the Pt(110)-(1x2) surfaces, respectively. Using the measured range of 0-2 kcal/mole for the activation energy for ammonia decomposition on Pt(110)-(1x2) yields a reaction probability of (2-5.5)

x $10^{-3}$ at $1/T = 0$. The measured reaction probability at $1/T = 0$ for the polycrystalline platinum surface is (2.4-3.3) x $10^{-3}$ **(3)**. Based on the model embodied by Eqs. (1)-(4), the rate of ammonia decomposition in this regime is controlled by a competition between the rate of cleavage of an N-H bond and the rate of desorption of molecularly adsorbed ammonia. The observed activation energy is therefore given by $E_r - E_{d,NH_3}$ **(3)**. Values for $E_r$ and/or $E_{d,NH_3}$, individually accurate to within the measured difference in activation energy of approximately 3 kcal/mole, are not available. Thus a determination of the relative contributions from changes in $E_r$ and/or $E_{d,NH_3}$ is precluded. The observed difference in activation energies and the similarity of the reaction probabilities at $1/T = 0$ indicate that for finite temperatures, i.e. $1/T > 0$, where the rate of decomposition is linearly dependent on ammonia pressure, the reaction probability on the Pt(110)-(1x2) surface is greater than that on the polycrystalline surface. For example, at 2 x $10^{-6}$ Torr and 800 K, the reaction probabilities are 1.6 x $10^{-3}$ and 2.0 x $10^{-4}$ for the Pt(110)-(1x2) and the polycrystalline platinum surfaces, respectively.

## 5. Synopsis

The results of this study may be summarized as follows:

1. The steady-state decomposition kinetics of ammonia on Pt(110)-(1x2) is qualitatively similar to that observed on a polycrystalline platinum surface. Under conditions where the reaction rate is linearly dependent on ammonia pressure, the observed activation energy is 1± 1 kcal/mole. For conditions where the rate of decomposition becomes independent of ammonia pressure, the observed activation energy increases to 24±4 kcal/mole.

2. Nitrogen adatoms are the predominant surface species during ammonia decomposition at 2 x $10^{-6}$ Torr. For temperatures below 400 K, the

Pt(110)-(1x2) surface is saturated with nitrogen adatoms. At higher temperatures, the fractional coverage of nitrogen adatoms decreases, becoming <0.1 for temperatures above 600 K.

3. The mechanistic model developed previously for the decomposition of ammonia on a polycrystalline platinum wire describes accurately the pressure and temperature dependence of the reaction rate and the measured steady-state coverage of nitrogen adatoms on the Pt(110)-(1x2) surface.

4. The recombinative desorption of nitrogen is the major reaction mechanism producing molecular nitrogen during ammonia decomposition at $2 \times 10^{-6}$ Torr.

**Acknowledgment**

This research was supported by the National Science Foundation under Grant No. CHE-8516615.

**References**


1. D. G. Löffler and L. D. Schmidt, J. Catal. **41**, 440 (1976).

2. D. G. Löffler and L. D. Schmidt, Surface Sci. **59**, 195 (1976).

3. J. J. Vajo, W. Tsai and W. H. Weinberg, J. Phys. Chem. **89**, 3243 (1985).

4. W. Tsai, J. J. Vajo and W. H. Weinberg, J. Phys. Chem. **89**, 4926 (1985).

5. J. L. Gland and E. B. Kollin, Surface Sci. **104**, 478 (1981).

6. B. A. Sexton and G. E. Mitchell, Surface Sci. **99**, 523 (1980).

7. S. N. Foner and R. L. Hudson, J. Chem. Phys. **80**, 518 (1984).

8. G. S. Selwyn and M. C. Lin, Chem. Phys. **67**, 213 (1982).

9. J. L. Taylor, D. E. Ibbotson and W. H. Weinberg, J. Chem. Phys. **69**, 4298 (1978)

10. H. Niehus and G. Comsa, Surface Sci. **102**, L14 (1981).

11. D. E. Ibbotson, T. S. Wittrig and W. H. Weinberg, Surface Sci. **110**, 294 (1981)

12. The results presented in Fig. 1 are independent of cooling rate for rates less than 20 K/s, the highest rate used. This indicates that steady-state rates are established quickly compared to these rates of cooling.

13. The surface temperature was held constant to insure a steady-state rate of decomposition, although steady-states are almost certainly attained much more rapidly; see Ref. 12.

14. If the surface was cooled to below 300 K during exposure to $^{15}NH_3$ and subsequently heated, a small thermal desorption peak of $H_2$ was observed near 300 K. This is due entirely to hydrogen desorption from the Pt(110)-(1x2) surface and is unrelated to any adsorbed $NH_x$ species **(15)**.

15. W. Tsai, J. J. Vajo and W. H. Weinberg, in preparation.

16. J. L. Taylor and W. H. Weinberg, Surface Sci. **78**, 259 (1978).

17. The kinetic parameters for the desorption of molecular ammonia and hydrogen from the Pt(110)-(1x2) surface have been measured independently **(15)**. Based on these results, the steady-state fractional coverages of both molecular ammonia and hydrogen adatoms at temperatures above 400 K and an ammonia pressure of $2 \times 10^{-6}$ Torr are predicted to be $<10^{-3}$, i.e. approximately three orders of magnitude lower than the measured coverage of nitrogen.

18. R. M. Lambert and C. M. Comrie, Surface Sci. **46**, 61 (1974).

**Table 1.** Model Parameters for the Decomposition of Ammonia on Pt(110)-(1x2)

| | **Parameter** | **Value** | **Ref.** |
|---|---|---|---|
| $S^0_{NH_3}$ | Ammonia probability of adsorption | 1 | 3 |
| $k^{(0)}_{d,NH_3}$ | Ammonia desorption preexponential | $1 \times 10^{14}$ $s^{-1}$ | 3 |
| $k_r^{(0)}$ | Surface reaction preexponential | $1 \times 10^{11}$ $s^{-1}$ | |
| $E_r - E_{d,NH_3}$ | Difference between surface reaction and desorption activation energies | 0.5 kcal/mole | |
| $k^{(0)}_{d,N_2}$ | Nitrogen desorption preexponential | $4 \times 10^{-8}$ $cm^2/s$ | 3 |
| $E_{d,N_2}$ | Nitrogen desorption activation energy | 24.5 kcal/mole | |
| $k^{(0)}_{d,H_2}$ | Hydrogen desorption preexponential | $3 \times 10^{-4}$ $cm^2/s$ | 15 |
| $E_{d,H_2}$ | Hydrogen desorption activation energy | 19 kcal/mole | 15 |

**Figure Captions**

Fig. 1. Steady-state decomposition of $^{15}NH_3$ on Pt(110)-(1x2) at 2 x $10^{-6}$ Torr. The surface was exposed to a continuous flux of $^{15}NH_3$ at an initial temperature of 900 K and then cooled at a rate of 2-3 K/s while recording the $^{15}N_2$ mass spectrometric signal.

Fig. 2. Arrhenius plots of the data shown in Fig. 1. The continuous line represents the result of model calculations, as discussed in the text.

Fig. 3. Steady-state decomposition of ammonia on Pt(110)-(1x2). (A) 2.6 x $10^{-6}$ Torr, (B) 1.7 x $10^{-6}$ Torr; and (C) 1 x $10^{-6}$ Torr. The continuous lines represent the results of model calculations, as discussed in the text.

Fig. 4. Thermal desorption of $^{15}N_2$ from Pt(110)-(1x2) during the steady-state decomposition of $^{15}NH_3$ at 2 x $10^{-6}$ Torr. The temperatures indicated in the figure represent the temperatures at which the desorption was begun. The data have been smoothed as a visual aid.

Fig. 5. Steady-state fractional coverages of $^{15}N$ on Pt(110)-(1x2) during the decomposition of $^{15}NH_3$ at 2 x $10^{-6}$ Torr. The continuous line represents the results of model calculations, as discussed in the text.

Fig. 6. Activation energy as a function of coverage for the thermal desorption of $^{15}N_2$ from Pt(110)-(1x2), determined by varying the heating rate from 3 to 25 K/s at an initial temperature of 400 K during the steady-state decomposition of $^{15}NH_3$ at 2 x $10^{-6}$ Torr.

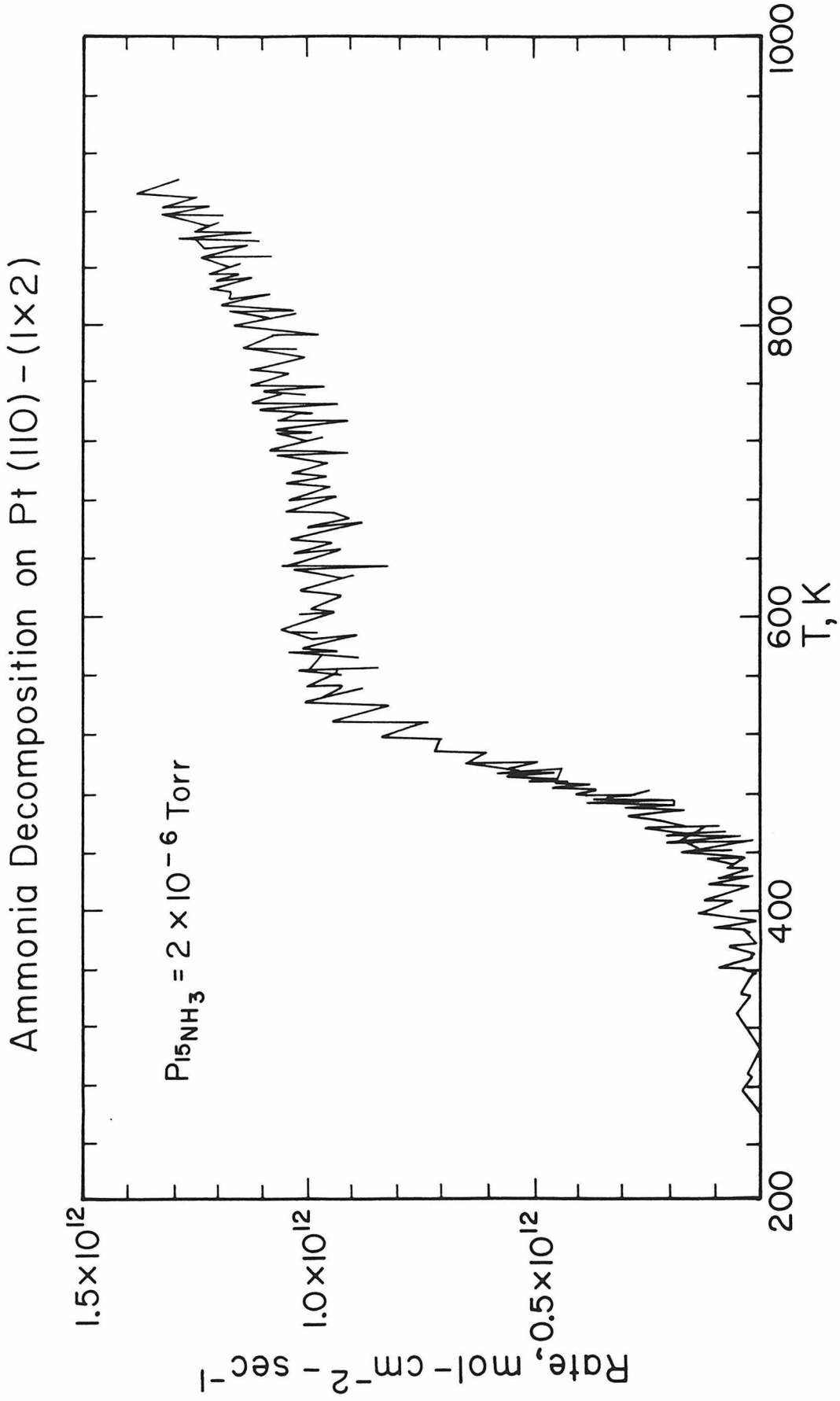
Ammonia Decomposition on Pt (110) - (1×2)
$P_{15_{NH_3}} = 2 \times 10^{-6}$ Torr
Rate, mol - cm$^{-2}$ - sec$^{-1}$
1.5×10$^{12}$
1.0×10$^{12}$
0.5×10$^{12}$
200
400
600
800
1000
T, K

Figure 1

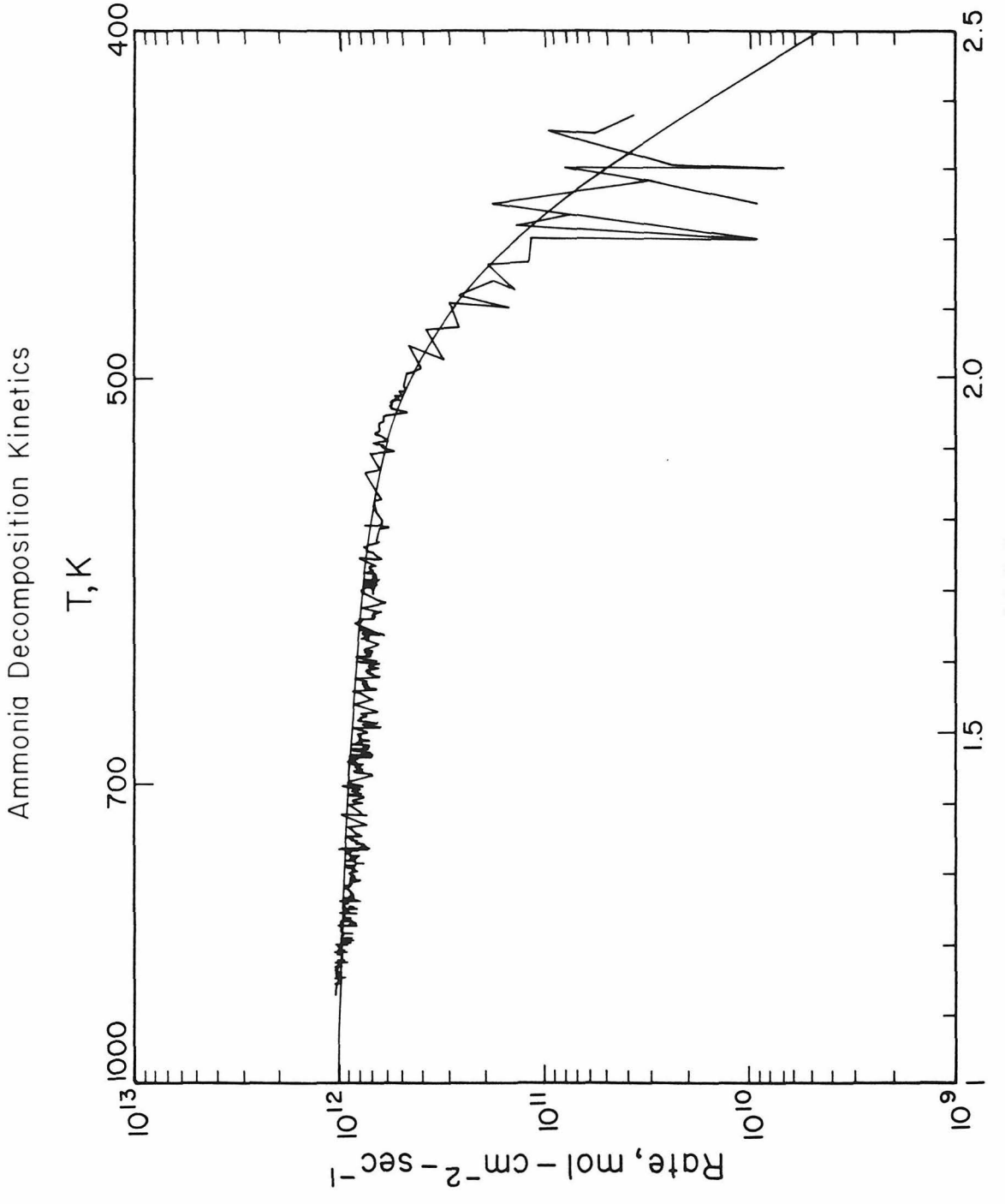
Ammonia Decomposition Kinetics
T, K
400
500
700
1000
Rate, mol – cm⁻² – sec⁻¹
10¹³
10¹²
10¹¹
10¹⁰
10⁹
1000/T, K⁻¹
2.5
2.0
1.5
1

Figure 2

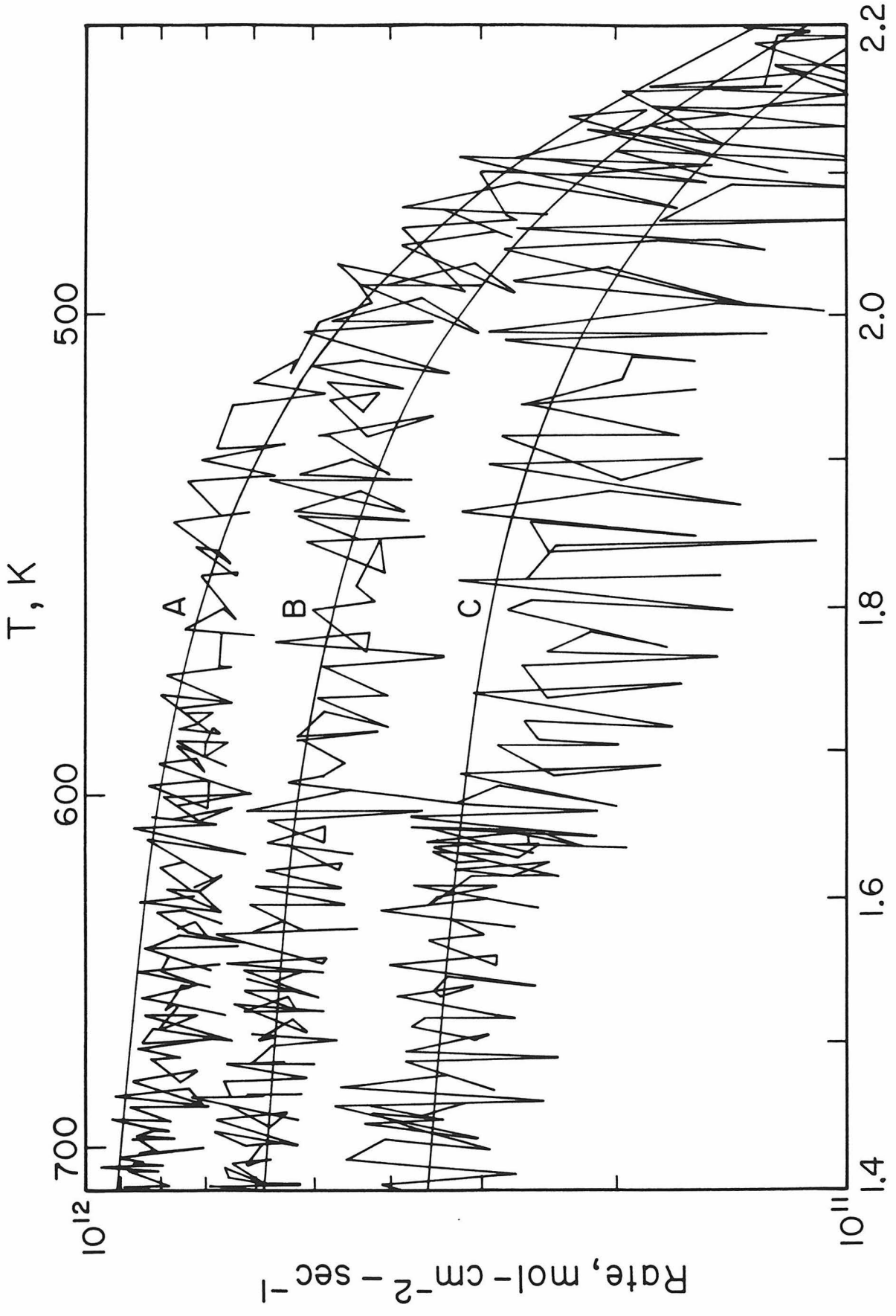
Rate, mol-cm$^{-2}$-sec$^{-1}$
$10^{12}$
$10^{11}$
T, K
700
600
500
A
B
C
$\frac{1000}{T}$, K$^{-1}$
1.4
1.6
1.8
2.0
2.2

Figure 3

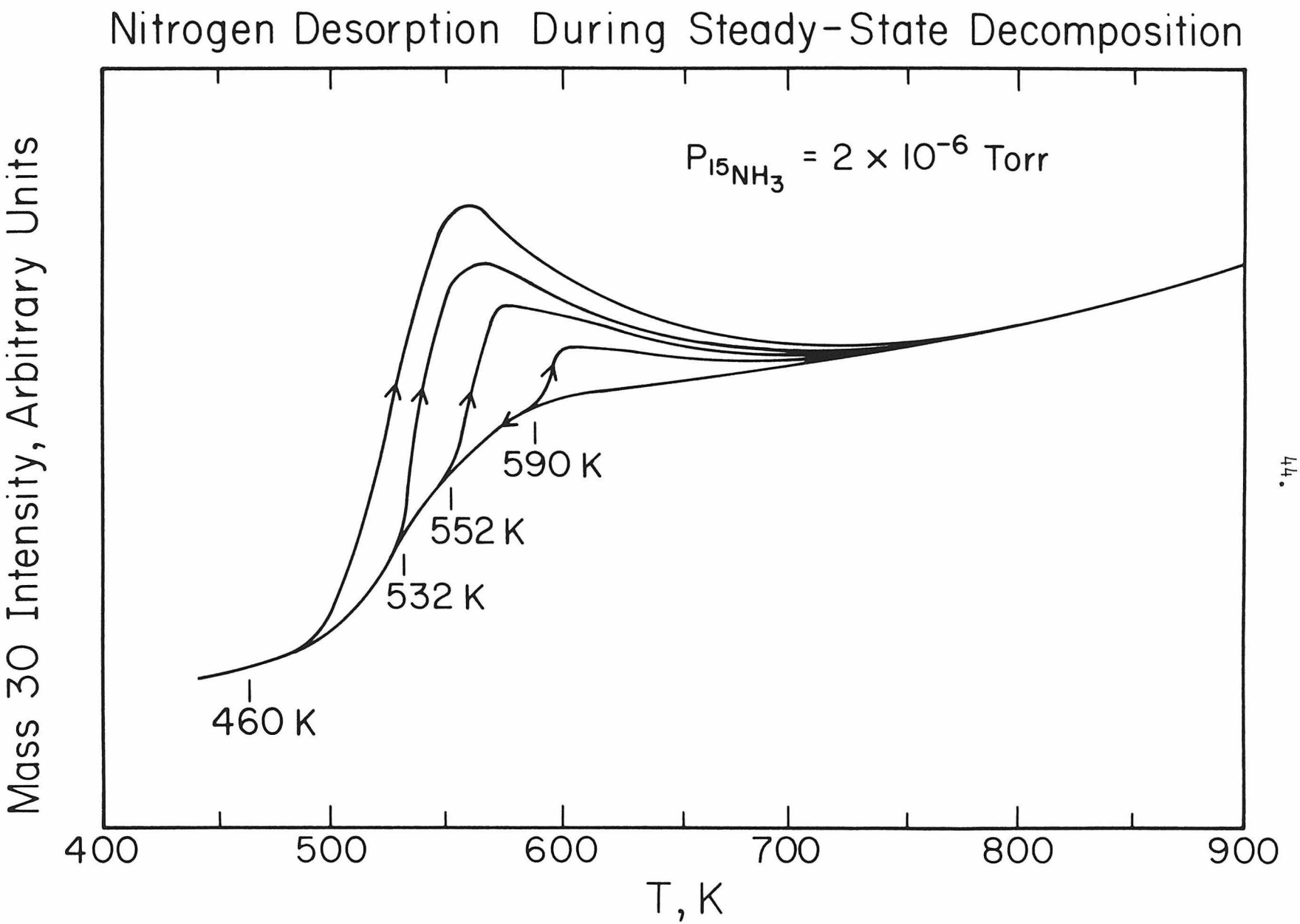
Nitrogen Desorption During Steady-State Decomposition
$P_{^{15}NH_3} = 2 \times 10^{-6}$ Torr
Mass 30 Intensity, Arbitrary Units
590 K
552 K
532 K
460 K
400
500
600
700
800
900
T, K

Figure 4

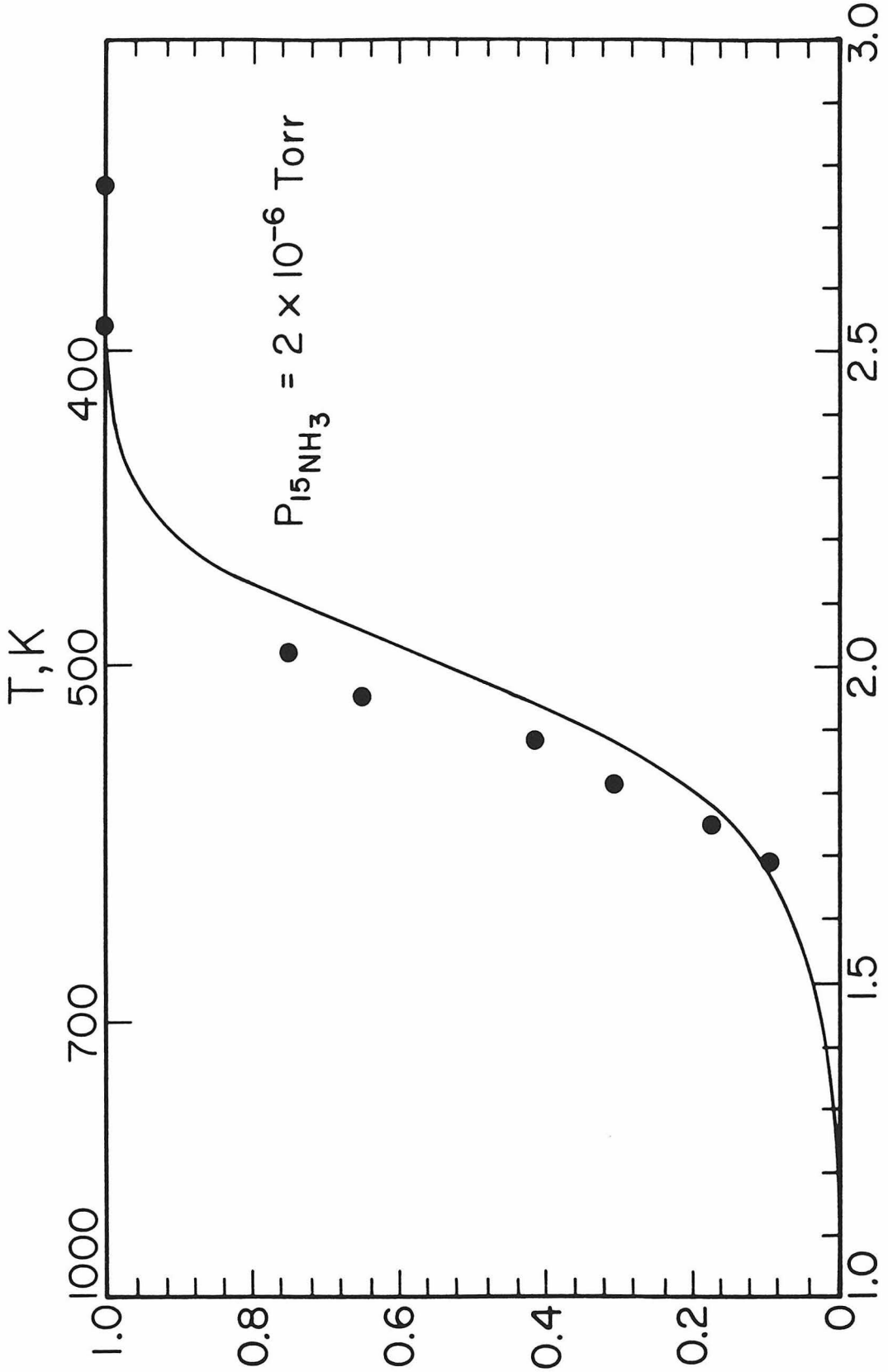
Fractional Coverage
1.0
0.8
0.6
0.4
0.2
0
T, K
1000
700
500
400
$P_{^{15}NH_3} = 2 \times 10^{-6}$ Torr
1.0
1.5
2.0
2.5
3.0
$\frac{1000}{T}$, $K^{-1}$

Figure 5

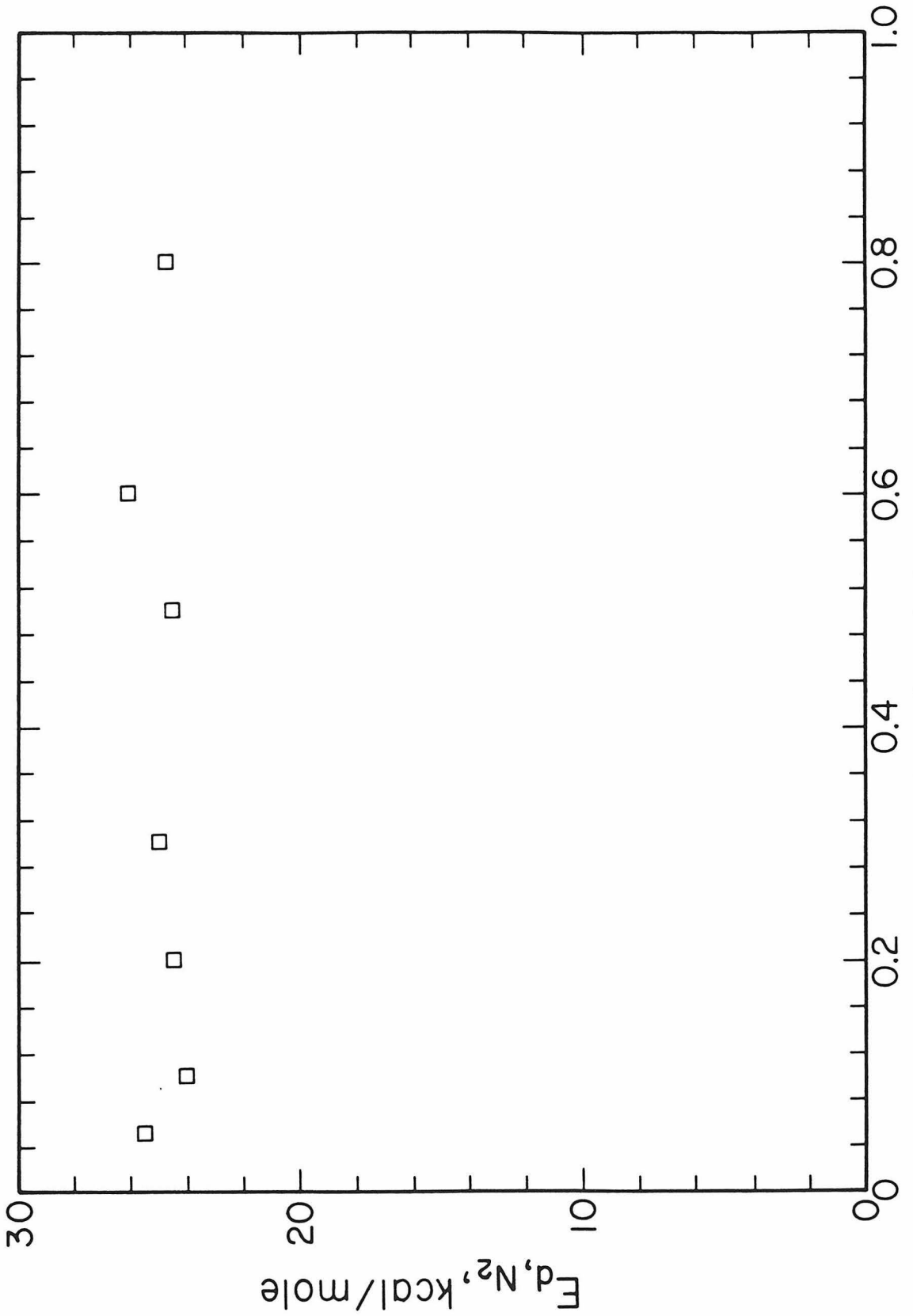


Figure 6

# Chapter 5.

## Acetic Acid Decomposition over a Polycrystalline Platinum Surface

[Chapter 5 consists of an article coauthored with Y.-K. Sun and W. H. Weinberg.]

**Abstract**

The decomposition of $CH_3\ ^{13}COOH$ on a polycrystalline platinum surface has been examined at temperatures between 300 and 900 K during continuous exposure to $CH_3\ ^{13}COOH$ at $7 \times 10^{-4}$ Torr. On an initially clean platinum surface $^{13}CO$, CO, $^{13}CO_2$, $H_2$ and adsorbed carbon-12 are the major reaction products. The adsorbed carbon eventually poisons completely the reactions that produce these products. For temperatures above approximately 800 K, the carbon overlayer that is formed is graphitic and saturates at carbon adatom concentration of $(2.6\text{-}3.5) \times 10^{15}$ $cm^{-2}$. The relative quantities of $^{13}CO$ and $^{13}CO_2$ that are produced depend both on the surface temperature and the carbon coverage. Lower temperatures and higher carbon coverages favor the production of $^{13}CO$. On the graphitized platinum surfaces, the catalytic dehydration of acetic acid to ketene and water proceeds at steady state.

**Introduction**

Although the catalytic decomposition of formic acid on transition metal surfaces has been studied extensively using both conventional catalytic measurements **(1-5)** and surface science techniques **(6-17)**, this is not the case for the decomposition of acetic acid **(18-20)**. Formic acid decomposition can produce CO, $CO_2$, $H_2$ and $H_2O$ with no self-poisoning of the surface. This reaction is therefore of interest as a prototypical branching surface reaction and as a measure of catalytic selectivity **(4)**. The investigation of acetic acid decomposition offers the possibility of clarifying the kinetic and mechanistic changes which occur upon introducing a carbon-carbon bond into the carboxylic acid. In addition, the decomposition of acetic acid may produce adsorbed carbon atoms which can chemically modify the catalytic surface and the mechanism of decomposition.

The decomposition of both acetic acid and formic acid has been investigated on the Ni(111) **(11,19)** and Ni(110) **(9,10,18)** surfaces, and the results of these studies may be used to compare the reactivities of acetic acid and formic acid. On the Ni(111) surface, acetic acid and formic acid decompose via their respective carboxylate intermediates **(11,19)**. However, thermal desorption measurements indicate that the surface formate is less stable than the surface acetate, the latter of which was observed to decompose to $CO_2$ with the simultaneous production of $H_2$ at 460 K when employing a linear heating rate $\beta$ of 7.1 K/s. For the surface formate, decomposition to $CO_2$ and $H_2$ occurred at 404 K with $\beta$ = 20 K/s. In each case, desorption of CO was observed near 450 K, which is typical of CO desorption following adsorption on a clean Ni(111) surface **(11)**. In addition to the differences in the stability of the adsorbed intermediates, the observed CO to $CO_2$ product ratios of 0.3 **(11)** and 1.6 **(19)** for formic acid and acetic acid decomposition on Ni(111) indicate considerably more CO production during the

decomposition of acetic acid. The preponderance of CO during the decomposition of acetic acid might be due partly to oxidation of the methyl carbon. Similar results have been obtained on Ni(110).

While the decomposition of acetic acid on platinum has not been investigated in detail, a similar sequence of stabilities was observed for formate and acetate on Pt(111) using electron energy loss spectroscopy (EELS) **(20)**. Formic acid decomposition on Pt(111) has been studied, however, using thermal desorption mass spectrometry **(14)**, modulated molecular beam scattering **(17)** and EELS **(15,16)**. In all cases it was found that formic acid decomposes almost completely to $CO_2$ and $H_2$ with only minor amounts of CO and $H_2O$ produced. The product ratio for acetic acid decomposition on any platinum surface has not been determined. Electron energy loss measurements following adsorption of acetic acid on Pt(111) at 100 K and annealing to 380 K revealed the presence of adsorbed CO **(20)**. However, $CO_2$ and $H_2$ were observed with reaction-limited kinetics near 450 K. Assuming surface acetate is the common intermediate, these results indicate that the reaction producing CO proceeds at a lower temperature (with a lower activation energy) than the reaction producing $CO_2$.

Similar results have been obtained for the decomposition of formic acid on the Ru(001) surface **(12,13)**. Chemisorbed carbon monoxide has been detected via EELS following the adsorption of formic acid with annealing to 200 K. Carbon dioxide is produced between 310 and 340 K, depending on the initial surface coverage, with a heating rate of 10 K/s. These results clearly imply that the reaction producing CO is favorable compared with the reaction producing $CO_2$,for the initial decomposition of chemisorbed formate on the Ru(001) surface.

In the present study, the decomposition of acetic acid on a polycrystalline

platinum surface has been examined at temperatures between 300 and 900 K during continuous exposure to acetic acid at $7 \times 10^{-4}$ Torr. The effects of temperature and of adsorbed carbon on the decomposition mechanism are discussed. Briefly, two disparate kinetic regimes are observed for the decomposition of acetic acid. Initially, CO, $CO_2$, $H_2$ and adsorbed carbon are the major reaction products. However, the adsorbed carbon eventually poisons completely the reactions that produce these products. On this graphitized platinum surface, the dehydration of acetic acid to ketene ($CH_2CO$) and water is the only reaction observed. Here we will focus on the transient decomposition reaction on the (initially) clean surface, whereas the steady-state dehydration reaction on the graphitized surface is discussed separately **(21)**.

## 2. Experimental Procedures

The experiments were performed in a continuous flow microreactor that has been described previously **(22,23)**. The catalyst was a 20 cm length of 0.0125 cm diameter high-purity (99.99%) polycrystalline platinum wire. Acetic acid (reagent grade, 99.7%) and $CH_3{}^{13}COOH$ (99 atom % $^{13}C$, MSD isotopes) were purified further by several freeze-thaw-pump cycles. Prior to each experiment, the surface was cleaned in oxygen and hydrogen, as described elsewhere **(21)**.

The reaction products, which were sampled via a capillary tube from the main chamber of the reactor, were monitored continuously by a microcomputer-interfaced EAI 1200 quadrupole mass spectrometer located in a high vacuum section of the reactor of which the base pressure is below $10^{-8}$ Torr. The absolute quantities of CO, $CO_2$ and $H_2$ produced during acetic acid decomposition (and of $CO_2$ and CO produced during oxygen titration measurements) were determined by calibrating the mass spectrometer using feeds with known concentrations of CO, $CO_2$ and $H_2$.

For the thermal desorption measurements, the bellows valve separating the main chamber of the reactor from the high vacuum section was opened, and the sample was translated into the high vacuum section (see Fig. 2 of Ref. 22). Heating was accomplished with a constant current power supply, which produced a nearly linear temperature ramp with a heating rate $\beta$ of 20 K/s. For the decomposition experiments, the same power supply was used to provide temperature ramps with $\beta$ between 2 and 54 K/s and final temperatures between 500 and 900 K. Temperatures were measured with a W-5%Re/W-26%Re thermocouple, which was spot-welded near the center of the wire.

## 3. Experimental Results

### 3.1 Decomposition of Acetic Acid

Relative reaction rates for the production of CO, $CO_2$, $H_2$, $CH_4$, $H_2O$ and ketene (uncorrected for mass spectrometric sensitivities) are shown in Fig. 1 as a function of time during a continuous flow of acetic acid at $7 \times 10^{-4}$ Torr. At t = 0, the temperature of the platinum surface is increased from 300 to 900 K with a heating rate of 50-54 K/s. As illustrated in Fig. 1, the rates of production of CO, $CO_2$, $H_2$ and $CH_4$ pass through maxima and then decline to their background values. Coincident with the decrease in the rate of production of CO, $CO_2$, $H_2$ and $CH_4$, the production of water and ketene is observed, which reaches a steady-state rate. When the platinum surface, treated as in Fig. 1, is cooled to 300 K and then reheated to 900 K, only water and ketene are produced with the same steady-state rate, as is shown in Fig. 2. The reactivities displayed in Figs. 1 and 2 indicate both that the surface has been altered chemically by the initial decomposition reaction and that a different surface is created that gives rise to a steady-state rate of dehydration of acetic acid.

Thermal desorption measurements from a platinum surface, exposed to acetic acid as in Fig. 1, show only ketene desorption. Although the desorption of water was not detected, adsorption on the walls of the vacuum system would have precluded its detection under these conditions. Furthermore, as described in detail in Sect. 3.4, the reaction with oxygen of a surface exposed to acetic acid at temperatures above 500 K produced $CO_2$ and CO with an approximate ratio of 5:1. This indicates that after the transient decomposition of acetic acid, the platinum surface contains substantial quantities of adsorbed carbon.

### 3.2 Decomposition of $CH_3{}^{13}COOH$

In order to investigate further the surface reactions of acetic acid which produce CO, $CO_2$, $H_2$ and adsorbed carbon, continuous flow decomposition measurements were made with $CH_3{}^{13}COOH$ employing a range of heating rates between 2 and 54 K/s with corresponding final surface temperatures between 500 and 900 K. Figures 3 and 4 show the rate of production of $^{13}CO$, CO, $^{13}CO_2$ and $H_2$ during exposure of the initially clean platinum surface at 300 K to $7 \times 10^{-4}$ Torr of $CH_3{}^{13}COOH$ with heating rates of 50-54 and 4-6 K/s, respectively. The results shown in Fig. 3, which are similar to those in Fig. 1, indicate that $^{13}CO_2$ and $H_2$ are the major decomposition products. In addition, both $^{13}CO$ and CO are produced, indicating the occurrence of oxidation of the carbon atom of the methyl group of acetic acid **(24)**. On the other hand, when the surface is heated at a rate of 4-6 K/s, CO, $^{13}CO$ and $H_2$ are the major reaction products, as may be seen in Fig. 4. Although the product signals shown in Fig. 4 have declined to their background values, additional CO, $CO_2$ and $H_2$ can be produced by increasing the surface temperature. However, surfaces heated to 800 K or higher are deactivated completely with respect to the formation of CO, $CO_2$ and $H_2$.

An absolute calibration of the areas under the $^{13}CO_2$ curves indicates the pro-

duction of increasing amounts of $^{13}CO_2$ with increasing final surface temperatures (for temperatures below 800 K). A maximum of (2.5-3.1) x $10^{15}$ molecules-$cm^{-2}$ is produced for surface temperatures above 800 K. Calibration of the quantities of $H_2$ and $^{13}CO$ that are produced indicates a molar ratio of $H_2$ to total $^{13}C$ (i.e. $^{13}CO_2$ + $^{13}CO$) of approximately two, independent of final temperature.

The fraction of acetic acid which decomposes to $^{13}CO$, determined by the ratio of the area of $^{13}CO$ to the total area of $^{13}CO$, is shown in Fig. 5 as a function of heating rate. Figure 5 quantifies the qualitative trend observed in Figs. 3 and 4. For low heating rates, $^{13}CO$ is the major product with respect to $^{13}CO_2$. As the heating rate increases, the fraction of acetic acid that decomposes to $^{13}CO$ decreases to a limiting value of 0.35 ± 0.05. The ratio of the amount of $^{13}CO$ produced to the total amount of carbon monoxide produced ($^{13}CO$ + CO) is independent of heating rate, as shown in Fig. 6. Moreover, this ratio is 0.5 ± 0.05, indicating that, independent of heating rate, equal quantities of CO and $^{13}CO$ are produced.

### 3.3 Thermal Desorption Mass Spectrometry

Thermal desorption spectra following large exposures (approximately 0.1 Torr-s) of unlabeled acetic acid on the initially clean platinum surface at 300 K were recorded by transferring the sample into the high vacuum section of the microreactor, as described in Sect. 2. Carbon monoxide desorbed in a single, broad peak with a maximum at 435-450 K. Similarly, $CO_2$ and $H_2$ desorbed with peak maxima at 425 and 440 K, respectively. No other products (e.g. acetic acid or water) were observed. However, since there was no line-of-sight between the mass spectrometer and the platinum surface, the sensitivity to small concentrations of acetic acid and water is poor. Calibrations of the thermal desorption

spectra for $CO_2$ and CO indicate the desorption of approximately 3 x $10^{13}$ and 4 x $10^{14}$ molecules-$cm^{-2}$, respectively.

### 3.4 Oxygen Titration Measurements

Carbon adatom concentrations, determined by the CO and $CO_2$ mass spectrometric intensities during reaction in 3 x $10^{-4}$ Torr of oxygen at 900 K, are shown in Table 1 (following 90 s exposures to acetic acid at pressures of $10^{-6}$, 7 x $10^{-4}$ and 0.1 Torr at 900 K). The concentrations of surface carbon from ethylene decomposition and both $^{13}C$ and $^{12}C$ from $CH_3{}^{13}COOH$ decomposition are also shown in Table 1. The concentrations of surface carbon vary only slightly with pressure and are nearly identical for acetic acid and ethylene. In addition, for the decomposition of acetic acid, more than 95% of the surface carbon originates from the methyl group. For comparison, the surface atom densities of Pt(111) and of the basal plane of graphite are 1.5 x $10^{15}$ $cm^{-2}$ and 3.8 x $10^{15}$ $cm^{-2}$, respectively.

### 3.5 Effects of Surface Carbon

The effects of adsorbed carbon on the decomposition of acetic acid were investigated by determining the fraction of acetic acid ($CH_3{}^{13}COOH$), which decomposes to $^{13}CO$ on surfaces with varying initial fractional coverages of $^{12}C$. In these measurements, a clean platinum surface was heated to various temperatures between 500 and 700 K during exposure to acetic acid to deposit a known concentration of carbon adatoms, and then cooled to 300 K. Subsequently, the surface was heated to 900 K ($\beta$ = 50-54 K/s), and the fraction of acetic acid which decomposes to $^{13}CO$ was determined. The initial concentration of carbon adatoms was determined from oxygen titration measurements, in which an identical exposure of acetic acid was used, followed by evacuation at 300 K and flashing for 30 s to 900 K to remove or decompose any adsorbed

acetic acid. The results, shown in Fig. 7, indicate that the fraction of acetic acid which decomposes to $^{13}CO$ increases with increasing initial carbon coverage. Note that the *final* carbon coverage in each case is identical, as verified by subsequent oxygen titration measurements. In addition, the temperature corresponding to the maximum rate of decomposition is shifted upward for both $^{13}CO$ and $^{13}CO_2$ on the carbon-covered surfaces, compared to the initially clean surface.

## 4. Discussion

### 4.1 Reaction Stoichiometry

The decomposition of $CH_3{}^{13}COOH$ on an initially clean polycrystalline platinum surface yields predominantly $^{13}CO$, CO, $^{13}CO_2$, $H_2$ and adsorbed carbon [C(a)]. Small quantities of $^{13}C(a)$ and $CH_4$ are also produced. Two *overall* reactions can account for the major products, namely,

$$CH_3{}^{13}COOH \rightarrow {}^{13}CO_2 + 2H_2 + C(a)\ , \qquad (1)$$

and

$$CH_3{}^{13}COOH \rightarrow {}^{13}CO + CO + 2H_2\ . \qquad (2)$$

The adsorbed carbon from reaction (1) poisons both of these reactions, as shown in Fig. 1, producing a surface on which the steady-state dehydration of acetic acid to ketene occurs.

Although water was not detected mass spectrometrically, adsorption on the walls of the vacuum chamber might have masked observation of the transient production of water. The following arguments, however, demonstrate clearly that water is not a major reaction product. As illustrated in Fig. 6, equal quantities of $^{13}CO$ and CO are produced, independent of surface temperature (and heating rate). If any acetic acid decomposed to form water via

$$CH_3{}^{13}COOH \rightarrow {}^{13}CO + H_2 + H_2O + C(a)\ , \qquad (3)$$

then more $^{13}CO$ than CO would necessarily have been produced. Furthermore, the saturation carbon adatom density of (2.6-3.5) x $10^{15}$ atoms–$cm^{-2}$, determined from oxygen titration measurements, is equal to the total number of $^{13}CO_2$ molecules that are produced, (2.5-3.1) x $10^{15}$ atoms–$cm^{-2}$. This confirms that reaction (1) is the only significant source of surface carbon and that no water is produced. Moreover, a material balance indicates a 2:1 molar ratio of $H_2$ to the total amount of $^{13}C$ that is produced, which is inconsistent with the stoichiometry of reaction (3). Furthermore, $CO_2$ is not a major reaction product. This conclusion follows from the observation that equal quantities of $^{13}CO$ and CO and negligible quantities of $^{13}C(a)$ are produced. The production of $CO_2$ is, therefore, inconsistent with the stoichiometries of reactions (1) and (2).

### 4.2 Production of Carbon Dioxide vs. Carbon Monoxide

Electron energy loss measurements have established that acetic acid dissociates upon adsorption on Pt(111) at 225 K to form a bidentate acetate species **(20)**. Moreover, a bidentate formate species has been identified using EELS on many transition metal surfaces, including the Pt(111) **(15,16)**, Ni(110) **(10)** and Ru(001) **(12,13)** surfaces. Since a similar species on the polycrystalline surface studied here is likely, the following discussion presumes that a bidentate acetate species is formed upon dissociative adsorption of $CH_3{}^{13}COOH$. The acetate may decompose by either C–$^{13}$C or $^{13}$C–O bond cleavage. Since surface reaction(s) of $^{13}CO_2(a)$ do not occur due to its short residence time **(25)**, C–$^{13}$C bond cleavage in the acetate leads directly to the desorption of $^{13}CO_2$ and the formation of $CH_{3-x}(a)$ + xH(a), where x can be 0, 1, 2 or 3, depending on the surface temperature. Ultimately, C(a) is formed, and the hydrogen desorbs as $H_2$. Decomposition of the adsorbed acetate via $^{13}$C–O bond cleavage followed by C–$^{13}$C bond

cleavage produces $^{13}CO(a)$, O(a) and $CH_{3-x}(a) + xH(a)$. Subsequent surface reactions of these species could lead to either $^{13}CO_2$ and C(a) or $^{13}CO$ and CO depending on the relative rates of oxidation of $^{13}CO(a)$ and C(a). However, as discusssed below, the oxidation of $^{13}CO(a)$ was found not to be a major reaction pathway. Since water is not a reaction product, all of the hydrogen desorbs as $H_2$.

The peak temperatures of 425 and 440 K, observed for the desorption of $CO_2$ and $H_2$ following adsorption of unlabeled acetic acid, are indicative of reaction-limited kinetics. The small difference in peak temperatures observed for $CO_2$ and $H_2$ is due to the decomposition of $CH_x$ species on this surface. In addition, $H_2$ production during the continuous flow transient decomposition experiments is coincident with the production of $^{13}CO_2$, as shown in Figs. 3 and 4. These results imply that the reaction step that controls the overall rate of production of $^{13}CO_2$ is the decomposition of the surface acetate. The desorption of CO, which occurs by oxidation of C(a), occurs earlier than the desorption of either $^{13}CO$ or $^{13}CO_2$, as may be seen in Fig. 4 **(26)**. Since $CO_2$ would desorb immediately upon formation at these temperatures, the C(a) which ultimately appears as CO is necessarily produced together with $^{13}CO(a)$ and O(a), i.e. via $^{13}C-O$ bond cleavage in the adsorbed acetate. Furthermore, CO(a) is produced on the surface before the desorption of carbon monoxide occurs. Both CO(a) and $^{13}CO(a)$ are present on the surface and, therefore, have equal probabilities of being oxidized to $CO_2$ and $^{13}CO_2$, respectively. Since $CO_2$ was shown not to be a reaction product, the oxidation of $^{13}CO(a)$ to $^{13}CO_2$ may also be excluded. Consistent with these results, the peak temperature observed for the desorption of carbon monoxide agrees with the results of carbon monoxide desorption from polycrystalline platinum **(27,28)**.

As the heating rate is increased from 2 to 54 K/s, the fraction of acetic acid which decomposes to $^{13}CO$ on the platinum wire declines, as shown in Fig. 5. This dependence implies that the reaction channels which produce $^{13}CO_2$ and $^{13}CO$ have different activation energies. For two competing reactions, the temperature dependence of the relative rates is given by $\exp[-(E_1 - E_2)/k_BT]$, where $E_1$ and $E_2$ are the activation energies for the two reactions. Thus, the fraction of the reactant that reacts via the lower activation energy pathway will decrease at higher temperatures (i.e. higher heating rates). Decomposition of acetic acid via $C-^{13}C$ bond cleavage produces $^{13}CO_2$, whereas initial $^{13}C-O$ bond cleavage leads to the production of $^{13}CO$. Therefore, the dependence shown in Fig. 5 indicates that the apparent activation energy for the formation of $^{13}CO_2$ larger than the apparent activation energy for the production of $^{13}CO$. As discussed in Sect. 1, similar behavior has been observed for acetic acid decomposition on the Pt(111) surface **(20)** and for formic acid decomposition on Ni(111), Ni(110) and Ru(001) surfaces **(9,11,13)**.

### 4.3 Effects of Surface Carbon

For carbon adatom concentrations of approximately $3 \times 10^{15}$ $cm^{-2}$, the reactions producing $^{13}CO$, $CO$, $^{13}CO_2$ and $H_2$ from $CH_3{}^{13}COOH$ are poisoned completely. However, for lower carbon coverages, these reactions are not poisoned totally, and the fraction of the $CH_3{}^{13}COOH$ which decomposes to $^{13}CO$ is shown as a function of the initial fractional carbon coverage in Fig. 7. As the initial carbon coverage increases, the fraction of acetic acid which decomposes to $^{13}CO$ increases. This result implies that while both reactions are ultimately poisoned by adsorbed carbon, the reaction producing $^{13}CO_2$ is poisoned selectively. Since the reaction pathways producing $^{13}CO_2$ also produce additional adsorbed carbon, unoccupied surface sites must be available for these reactions to occur. Thus, on a surface containing a partial overlayer of carbon adatoms, the selective

poisoning of reaction (1) with respect to reaction (2) is reasonable.

### 4.4 Nature of the Saturated Carbon Overlayer

The surface atom density of carbon produced by the decomposition of acetic acid, (2.6-3.5) x $10^{15}$ $cm^{-2}$, corresponds to approximately one monolayer of the basal plane of graphite, 3.8 x $10^{15}$ $cm^{-2}$. While the carbon overlayer could not be examined spectroscopically in the present work, other studies of carbon deposition on platinum **(29-33)** and nickel **(34,35)** surfaces strongly support the conclusion that the carbon overlayer produced from acetic acid decomposition at the elevated temperatures of interest here is graphitic. For example, exposure of the Ni(110) surface to ethylene at temperatures above 600 K led to the formation of an overlayer with a surface carbon atom concentration of 3.35 x $10^{15}$ $cm^{-2}$ and a carbon Auger peak with a graphitic shape **(35)**. A graphitic overlayer has also been prepared on Pt(111) by exposing the surface to ethylene at 300 K and annealing briefly to 873 K **(32)**. On the basis of these results and considering the reaction conditions of our experiments, it appears certain that the carbon overlayer formed both from acetic acid and from ethylene, which yield similar carbon adatom concentrations, is graphitic.

## 5. Synopsis

The results of this study may be summarized as follows:

1. On an initially clean polycrystalline platinum surface, $CH_3{}^{13}COOH$ at 7 x $10^{-4}$ Torr decomposes at temperatures above approximately 400 K to $^{13}CO$, CO, $^{13}CO_2$, $CH_4$, $H_2$ and adsorbed carbon. The adsorbed carbon eventually poisons the reactions that produce these products.

2. At temperatures above approximately 800 K, the carbon overlayer is graphitic with a carbon adatom concentration of (2.6-3.5) x $10^{15}$ $cm^{-2}$.

3. On the graphitized platinum surface, the steady-state dehydration of acetic acid to ketene is the only reaction that is observed.

4. The fraction of acetic acid that decomposes to $^{13}CO$ relative to $^{13}CO_2$ depends both on the surface temperature and the carbon adatom concentration. The production of $^{13}CO$ is favored at lower temperatures and higher carbon coverages.

**Acknowledgment**

This work was supported by the National Science Foundation under Grant No. DMR-8500789.

**References**


1. K. Fukuda, S. Nagashima, Y. Noto, T. Onishi and K. Tamaru, Faraday Soc. Trans. **64**, 522 (1968).
2. E. M. A. Willhoft and A. J. B. Robertson, J. Catal. **9**, 358 (1967).
3. G. M. Schwab and A. M. Watson, Faraday Soc. Trans. **60**, 1833 (1964).
4. P. Mars, J. Schloten and P. Zwietering, Advan. Catal. **14**, 35 (1963).
5. J. Block and J. Vogl, Z. Elektrochem. **63**, 3 (1959).
6. B. A. Sexton, Surface Sci. **88**, 319 (1979).
7. S. L. Miles, S. L. Bernasek and J. L. Gland, Surface Sci. **127**, 271 (1983).
8. M. Chtaib, P. A. Thirty, J. P. Delrue, J. J. Pireaux and R. Caudano, J. Electron Spect. **29**, 293 (1983).
9. R. J. Madix and J. L. Falconer, Surface Sci. **51**, 546 (1975).
10. R. J. Madix, J. L. Gland, G. E. Mitchell and B. A. Sexton, Surface Sci. **125**, 481 (1983).
11. J. B. Benziger and G. R. Schoofs, J. Phys. Chem. **88**, 4439 (1984).
12. B. H. Toby, N. R. Avery, A. B. Anton and W. H. Weinberg, J. Electron Spect. **29**, 318 (1983).
13. B. H. Toby, N. R. Avery, M. M. Hills and W. H. Weinberg, in preparation.
14. N. Abbas and R. J. Madix, Appl. Surface Sci. **16**, 424 (1983).
15. N. R. Avery, Appl. Surface Sci. **11/12**, 774 (1982).
16. N. R. Avery, Appl. Surface Sci. **14**, 149 (1982-83).
17. G. E. Gdowski, J. A. Fair and R. J. Madix, Surface Sci. **127**, 541 (1983).

18. R. J. Madix, J. L. Falconer and A. M. Suszko, Surface Sci. **54**, 6 (1976).

19. G. R. Schoofs and J. B. Benziger, Surface Sci. **143**, 359 (1984).

20. N. R. Avery, J. Vac. Sci. Technol. **20**, 592 (1982).

21. J. J. Vajo, Y.-K. Sun and W. H. Weinberg, in preparation.

22. J. J. Vajo, W. Tsai and W. H. Weinberg, Rev. Sci. Instrum. **56**, 1439 (1985).

23. J. J. Vajo, W. Tsai and W. H. Weinberg, J. Phys. Chem. **89**, 3243 (1985).

24. The complete oxidation of the methyl group carbon atom to $CO_2$ could not be monitored due to an overlap with a major fragmentation product of $CH_3^{13}COOH$ at 44 amu.

25. G. Ertl in "Catalysis Science and Technology", J. R. Anderson and M. Boudart, Eds., Vol. 4, Springer-Verlag: N.Y., 1983, p. 209.

26. This result indicates that CO is produced by the oxidation of C(a) at temperatures below the desorption temperature of carbon monoxide and that at least a fraction of this CO desorbs at a slightly lower temperature than would be expected for desorption of carbon monoxide. This may not be particularly surprising in view of the large carbon-oxygen bond energy in carbon monoxide, which renders the surface oxidation reaction highly exothermic leading to the production of "activated" CO(a).

27. R. A. Shigeishi and D. A. King, Surface Sci. **58**, 379 (1976).

28. Y. Nishiyama and H. Wise, J. Catal. **32**, 50 (1974).

29. D. L. Smith and R. P. Merrill, J. Chem. Phys. **52**, 5861 (1970).

30. W. H. Weinberg, H. A. Deans and R. P. Merrill, Surface Sci. **41**, 312 (1974).

31. B. Lang, Surface Sci. **53**, 317 (1975).

32. M. Abon, J. Billy, J. C. Bertolini and B. Tardy, Surface Sci. **167**, 1 (1986).

33. F. P. Netzer and R. A. Wille, J. Catal. **51**, 18 (1978).

34. R. Sau and J. B. Hudson, Surface Sci. **102**, 239 (1981).

35. R. Sau and J. B. Hudson, Surface Sci. **95**, 465 (1980).

**Table 1.** Surface Carbon Atom Concentrations $\rho_C$.

| Decomposed Species | Pressure, Torr[a] | $\rho_C$, $10^{15}$ cm$^{-2}$ |
|---|---|---|
| Acetic acid | $1 \times 10^{-6}$ | 1.5[b] |
| | $7 \times 10^{-4}$ | 2.6-3.5[c] |
| | 0.1 | 5.9[b] |
| Ethylene | $7 \times 10^{-4}$ | 2.4[b] |
| $CH_3{}^{13}COOH$ | $7 \times 10^{-4}$ | 3.0[b] ($^{12}$C) |
| | | 0.15[b] ($^{13}$C) |

[a]All exposures were for 90 s at 900 K.

[b]Value determined from a single measurement.

[c]Values indicate the range of six measurements.

**Figure Captions**

Figure 1. Time evolution curves for the production of CO, $CO_2$, $H_2$, $CH_4$, $H_2O$ and $CH_2CO$ (ketene) during constant exposure of an initially clean platinum surface to acetic acid at $7 \times 10^{-4}$ Torr. At t=0, the surface temperature was increased linearly at a rate of 50-54 K/s from 300 to 900 K, and thereafter held constant at 900 K. The data are uncorrected for relative mass spectrometric sensitivities and pumping speeds.

Figure 2. Time evolution curves for the production of CO, $CO_2$, $H_2$, $CH_4$, $H_2O$ and ketene during continuous exposure to acetic acid at $7 \times 10^{-4}$ Torr. The platinum surface was first exposed to acetic acid at 900 K, as in Fig. 1, and then cooled to 300 K. The final temperature was 900 K, and the linear heating rate was 50-54 K/s. The apparent increase in the CO signal is due entirely to a fragmentation product of the parent ketene.

Figure 3. Rates of production of $^{13}CO$, CO, $^{13}CO_2$ and $H_2$ during exposure of an initially clean platinum surface to $CH_3{}^{13}COOH$. At t=0, the temperature was increased from 300 to 900 K with a linear heating rate of 50-54 K/s.

Figure 4. As for Fig. 3, except that the heating rate is 4-6 K/s and the final surface temperature is 545 K.

Figure 5. Fraction of acetic acid that decomposes to $^{13}CO$ as a function of the heating rate. This fraction is defined as the ratio of the area under the $^{13}CO$ evolution curve to the total areas of the $^{13}CO$ and $^{13}CO_2$ curves. The areas were corrected for relative mass spectrometric

sensitivities and pumping speeds.

Figure 6. Fraction of the total number of carbon monoxide molecules produced during the decomposition of $CH_3{}^{13}COOH$ which is $^{13}CO$ as a function of the heating rate.

Figure 7. Fraction of the $CH_3{}^{13}COOH$ that decomposes to $^{13}CO$ relative to $^{13}CO + {}^{13}CO_2$ as a function of initial fractional carbon coverage. In each case the heating rate was 50-54 K/s, and the initial and final temperatures were 300 and 900 K. The surfaces were prepared by exposure to acetic acid, and the initial carbon coverages were determined by oxygen titration in separate measurements.

# Transient Decomposition of Acetic Acid on Clean Platinum

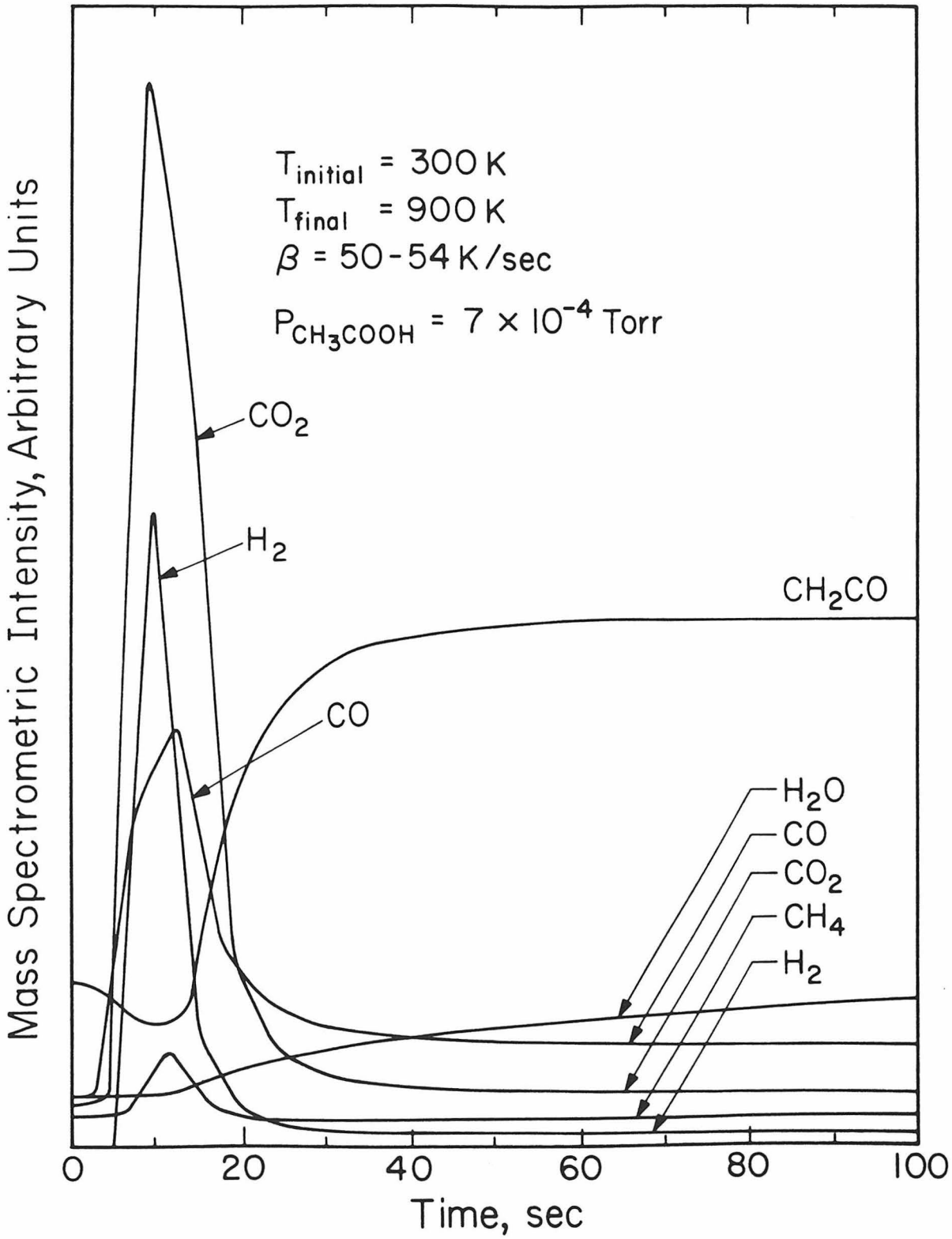


Figure 1

# Decomposition of Acetic Acid on Graphitized Platinum

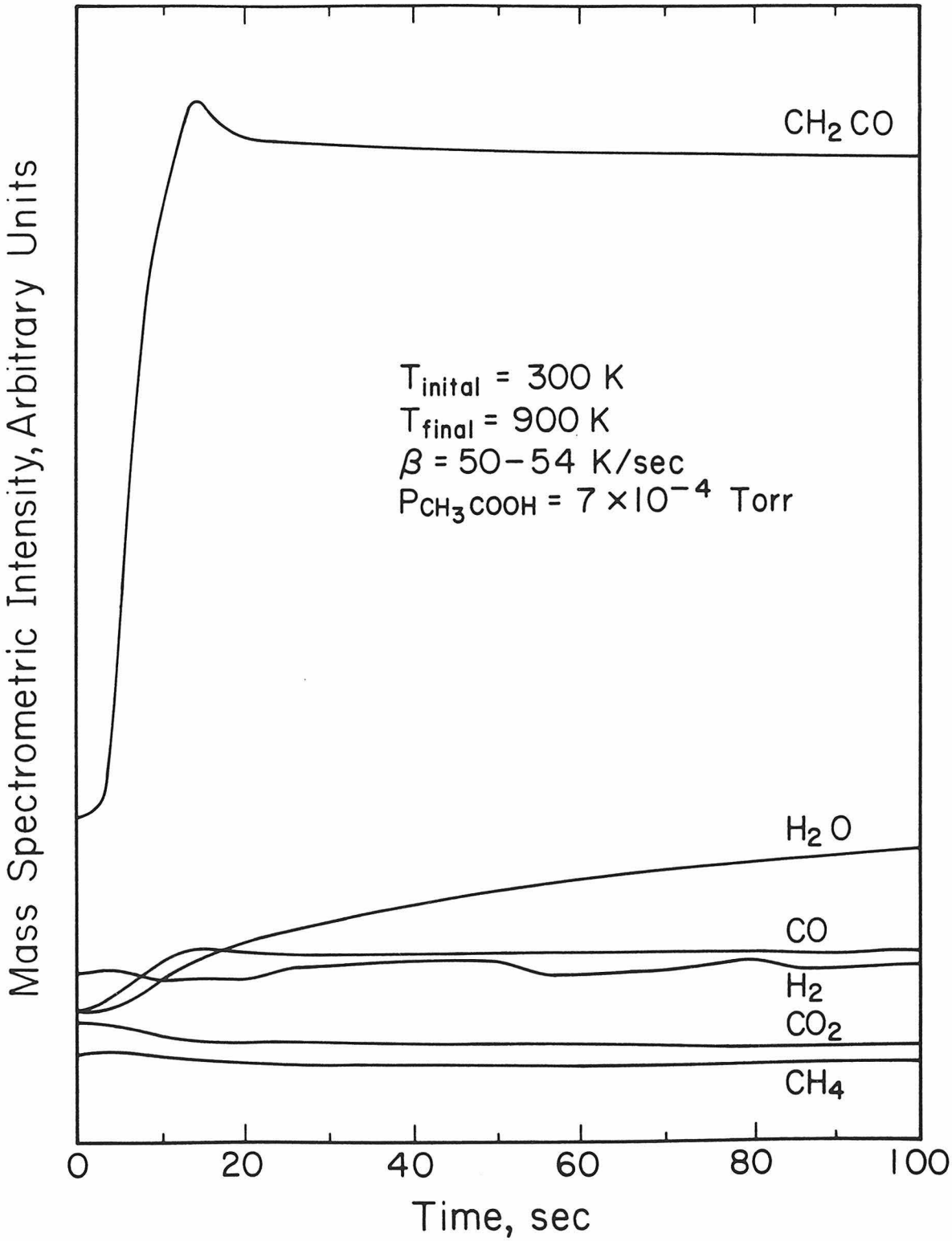


Figure 2

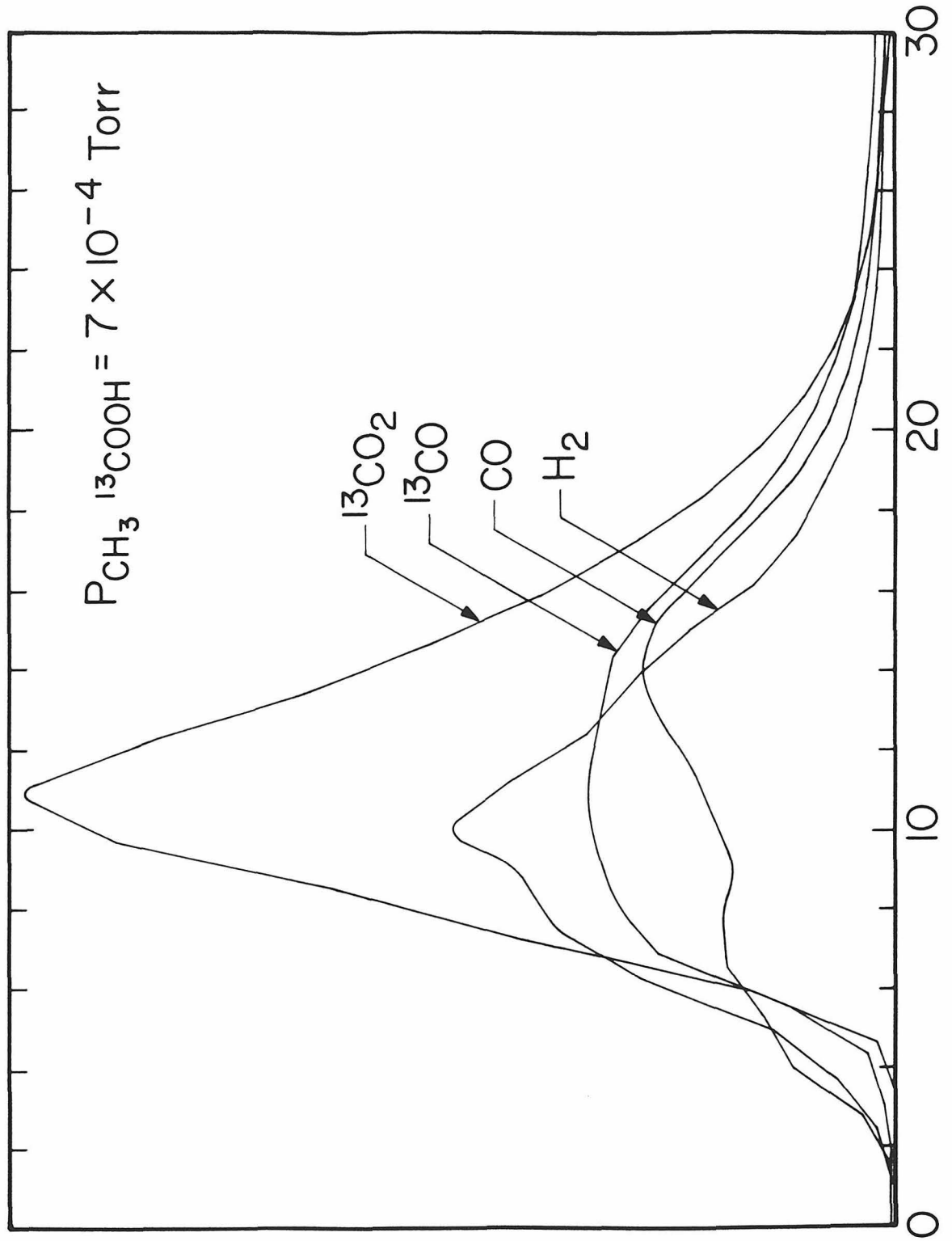
Mass Spectrometric Intensity,
Arbitrary Units
$P_{CH_3\ ^{13}COOH} = 7 \times 10^{-4}$ Torr
$^{13}CO_2$
$^{13}CO$
CO
$H_2$
0
10
20
30
Time, sec

Figure 3

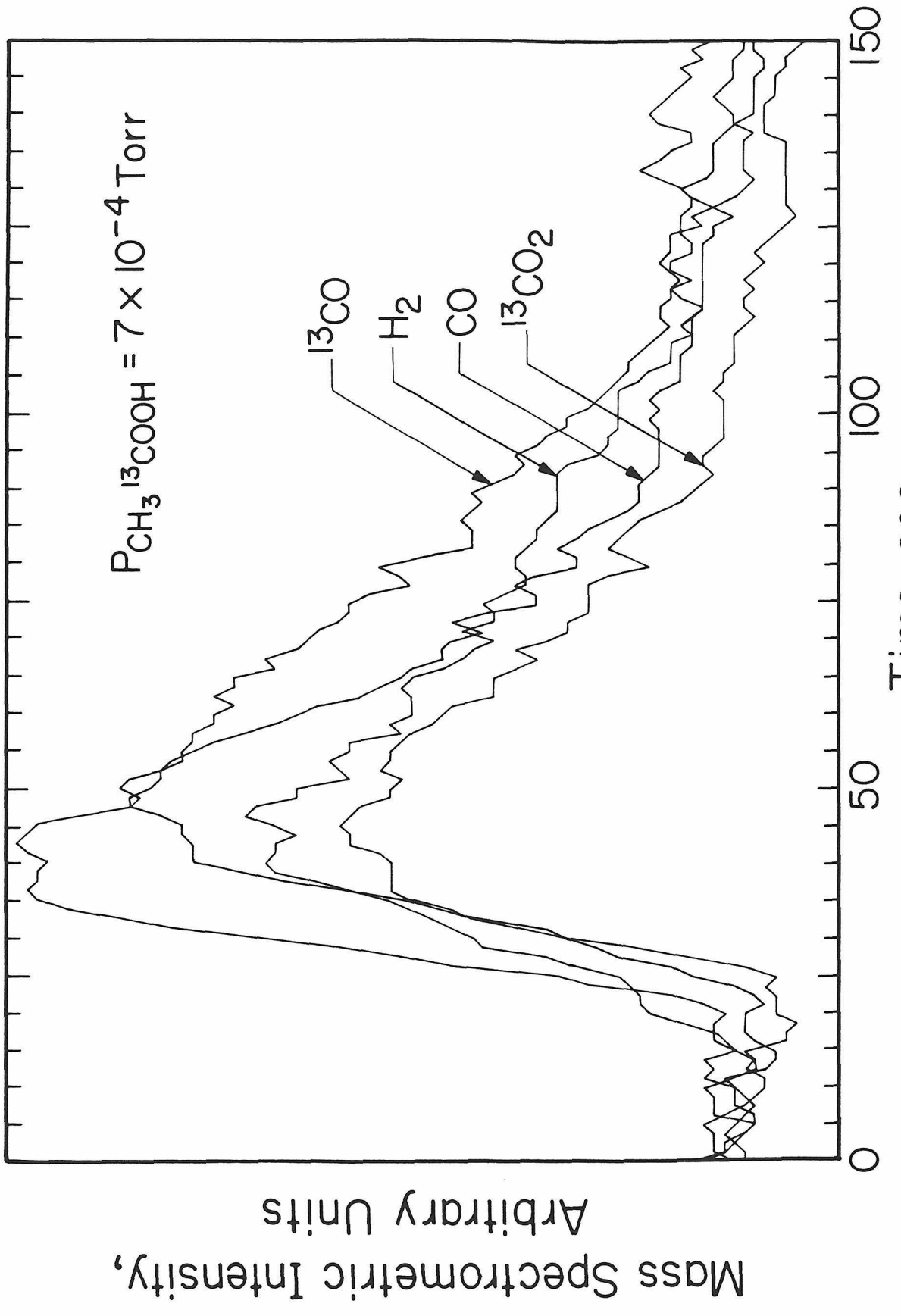
Mass Spectrometric Intensity,
Arbitrary Units
$P_{CH_3{}^{13}COOH} = 7 \times 10^{-4}$ Torr
$^{13}CO$
$H_2$
CO
$^{13}CO_2$
0
50
100
150
Time, sec

Figure 4

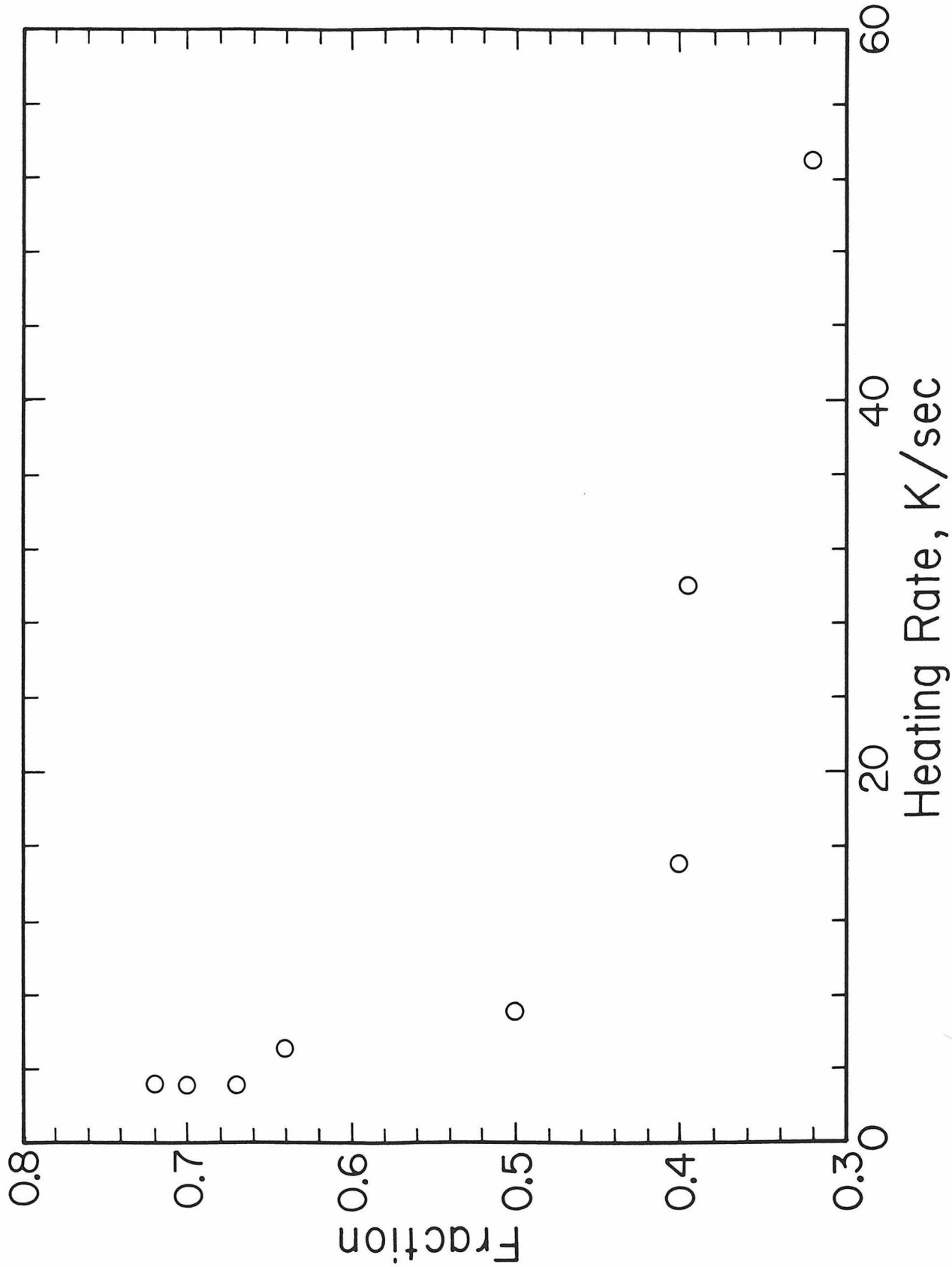


Figure 5

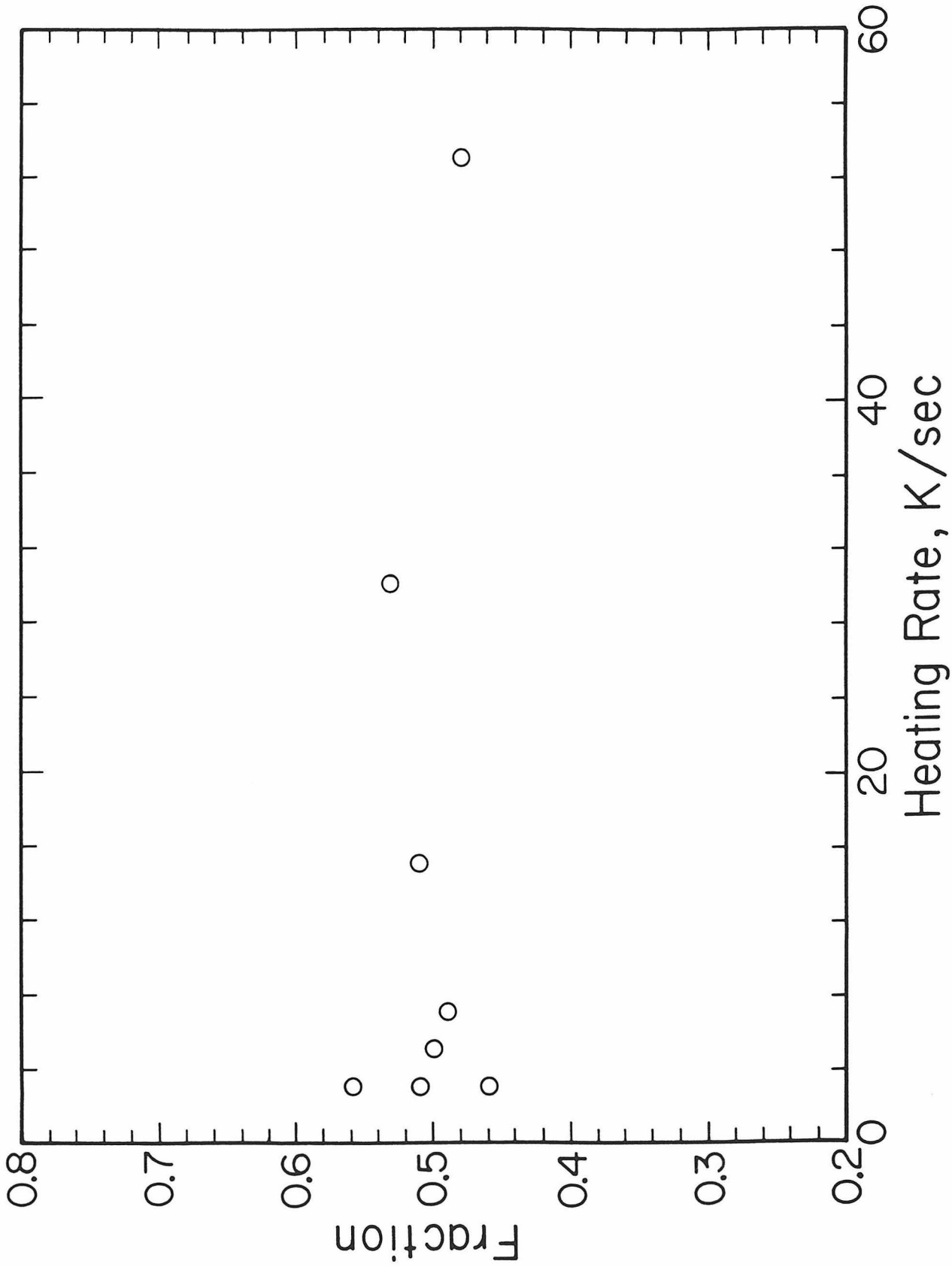


Figure 6

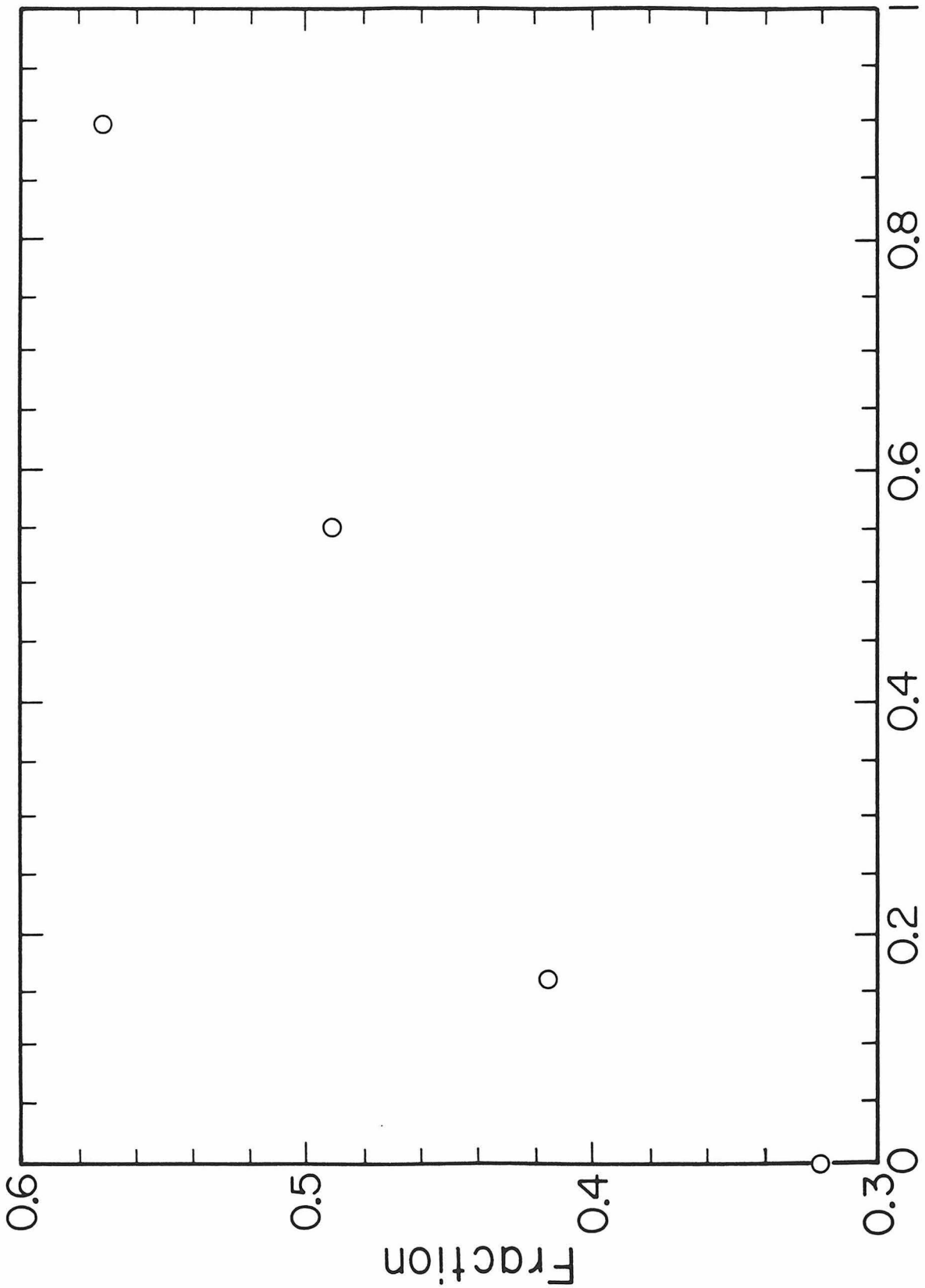
0.6
0.5
0.4
0.3
Fraction
0
0.2
0.4
0.6
0.8
1
Initial Fractional Carbon Coverage

Figure 7

# Chapter 6.

## Catalytic Dehydration of Acetic Acid on a Graphitized Platinum Surface

[Chapter 6 consists of an article coauthored with Y.-K. Sun and W. H. Weinberg.]

**Abstract**

Absolute reaction rates have been measured in a continuous flow microreactor for the steady-state, catalytic dehydration of acetic acid to ketene at pressures between $8 \times 10^{-7}$ and $7 \times 10^{-4}$ Torr and temperatures between 500 and 800 K. The catalyst was a polycrystalline platinum wire containing approximately a monolayer of graphitic carbon. At 675 K or above, for the entire range of pressures studied, the order of the dehydration reaction is unity with respect to acetic acid pressure. In this regime, the apparent activation energy is $1 \pm 1$ kcal/mole, and the extrapolated reaction probability at $1/T = 0$ is $(2.5\text{-}10) \times 10^{-4}$. Under these conditions, the rate of dehydration is determined by a competition between the rates of desorption and surface reaction of molecularly adsorbed acetic acid. For temperatures below 540 K and pressures of $3.5 \times 10^{-4}$ Torr and above, the reaction rate is independent of acetic acid pressure, and the apparent activation energy is $27 \pm 2$ kcal/mole. Under these conditions, the rate of decomposition of a surface intermediate controls the rate of reaction. A mechanistic model is developed and discussed, which describes accurately both the temperature and the pressure dependence of the rate of dehydration.

## I. Introduction

It is well-known that carbon overlayers on transition metal surfaces can affect both the reactivity and the selectivity of many heterogeneously catalyzed surface reactions **(1-11)**. These effects may have several origins. For example, carbon adatoms may physically occupy specific surface sites that are necessary for a particular reaction to occur, and they may chemically modify unoccupied sites by altering the electronic structure of the surface **(12-14)**. Both of these phenomena can change the reactivity and/or the selectivity of a heterogeneous catalyst.

The effect of adsorbed carbon on both the reactivity and the selectivity of a catalytic reaction may be illustrated by considering the decomposition of formic acid on the Ni(110) surface **(6)**. Since formic acid decomposition may produce either CO or $CO_2$, the relative rates of these competing reactions provide a measure of selectivity. On the clean Ni(110) surface, the $CO_2$ to CO product ratio observed upon heating a saturation coverage of formic acid at 315 K is 1:1. On a carbided Ni(110) surface, formed by the dissociative adsorption of ethylene at 600 K, the product ratio is 10±5:1, whereas the total quantity of formic acid which, decomposed, is unchanged compared to the clean surface. However, a shift in the temperature corresponding to the maximum rate of $CO_2$ production from 390 to 440 K indicates that the activation energy for $CO_2$ production is greater on the carbon-covered surface compared to the clean surface. Upon exposing the Ni(110) surface to ethylene at 800 K, a graphitic overlayer was formed. Decomposition of formic acid on this surface produced only 0.1 as much product as on the clean and carbided surfaces, and the product ratio was near unity.

Recently, the decomposition of acetic acid over a polycrystalline platinum

wire was studied in our laboratory at a pressure of $7 \times 10^{-4}$ Torr and at temperatures between 300 and 900 K **(11)**. Two disparate kinetic regimes were observed. On the initially clean platinum surface, acetic acid decomposed to yield CO, $CO_2$, $H_2$ and adsorbed carbon. No water was observed during this transient production of CO, $CO_2$ and $H_2$. The adsorbed carbon ultimately poisoned the reaction channels producing CO, $CO_2$ and $H_2$, while simultaneously initiating the steady-state, catalytic dehydration of acetic acid to ketene and water. Similar to the results described above for formic acid decomposition on nickel, both the reaction rate and the $CO_2$ to CO product ratio were found to be dependent on the carbon adatom concentration in the first regime. Since graphitic overlayers on platinum surfaces are formed readily from carbon adatoms at temperatures above 750 K **(15-17)**, the carbon-covered surface that dehydrates acetic acid and which is formed at 900 K is graphitic **(11)**. Moreover, the carbon adatom concentration, determined from oxygen titration measurements, corresponds to approximately one monolayer of the basal plane of graphite.

In the work described here, we shall focus on the steady-state dehydration of acetic acid to ketene and water, which occurs only on the graphitized platinum surface. Absolute reaction rates have been measured for reactant pressures between $8 \times 10^{-7}$ and $7 \times 10^{-4}$ Torr and at temperatures between 500 and 800 K. The steady-state reactivities of acetic anhydride, acetone, methyl acetate and isopropyl alcohol on the graphitized surface also have been investigated briefly. On the basis of these results, together with those of thermal desorption measurements, a consistent mechanism of the acetic acid dehydration reaction is developed. For completeness, the decomposition of acetic acid on the clean platinum surface is described briefly, whereas a detailed discussion of both this reaction and the nature of the carbon overlayer is presented elsewhere **(11)**.

The organization of this paper is as follows. In Sect. II the experimental details are described, and the experimental data are presented in Sect. III. The reaction mechanism is developed and discussed in Sect. IV. Finally, the major results of this work are summarized in Sect. V.

## II. Experimental Procedures

The experiments were performed over a range of pressures from 8 x $10^{-7}$ to 7 x $10^{-4}$ Torr in a steady-state flow microreactor that has been described previously **(18,19)**. The catalyst was a 20 cm length of 0.0125 cm diameter high purity (99.99%) polycrystalline platinum wire. All reagents were either reagent or research grade and were purified further by freeze-thaw-pump cycles in liquid nitrogen. Isotopically labeled ethylene, $^{13}C_2H_4$ (98 atom % $^{13}C$ from MSD Isotopes), was used without further purification.

The reaction products, which were sampled via a capillary tube from the main chamber of the reactor, were monitored continuously by a microcomputer-interfaced EAI 1200 quadrupole mass spectrometer, located in a high vacuum chamber of the reactor of which the base pressure is below $10^{-8}$ Torr. Absolute reaction rates for the steady-state dehydration of acetic acid were determined by monitoring the change in the parent ion signal at 60 amu and using the appropriate continuous stirred tank reactor (CSTR) formalism **(18,19)**. The reactor was well characterized as a CSTR by a series of step-response experiments **(18)**. Average conversions were below 5% except for temperatures above 600 K at 7 x $10^{-4}$ Torr, where average conversions were $\lesssim$20%. However, separate measurements in which the average conversions were below 8% for all conditions gave identical results **(20)**.

For thermal desorption measurements, the bellows value separating the main reaction chamber from the high vacuum section was opened, and the sample

was translated into the high vacuum section (see Fig. 2 of Ref. 18). Heating was accomplished with a constant current power supply that produced a nearly linear temperature ramp of 20 K/s over the temperature range 350-650 K. Temperatures were measured with a W-5%Re/W-26%Re thermocouple, which was spot welded near the center of the platinum wire.

Two different platinum wires were used in this study. Initially, each one was heated in 0.1 Torr of oxygen (99.99%) at 1000 K for three hours and then reduced in 0.1 Torr of hydrogen (99.995%) under the same conditions. Approximately ten cycles of this procedure led to reproducible, steady-state rates of acetic acid dehydration. A single oxidation-reduction cycle at $10^{-3}$ Torr and 1000 K for 30 minutes was conducted prior to each experiment to remove carbon that had been deposited during previous acetic acid decomposition. This treatment was found to produce a clean platinum surface, as judged by the reproducible rates of the acetic acid decomposition reactions that occur on the initially clean surface **(11)** and the steady-state rates of dehydration of acetic acid after formation of the graphitic overlayer. After the initial cleaning treatment at 0.1 Torr, longer oxidation-reduction cycles at $10^{-3}$ Torr did not change the measured rates.

## III. Experimental Results

### 1. Acetic Acid Decomposition

Relative rates of production of CO, $CO_2$, $H_2$, $H_2O$ and $CH_2CO$ (ketene), uncorrected for mass spectrometric sensitivities and pumping speeds, from an initially clean platinum surface are shown in Fig. 1 as a function of time during a constant flow (average residence time of 3.6 s) of acetic acid at a pressure of 7 x $10^{-4}$ Torr and a surface temperature of 900 K. It is apparent that the rates of production of CO, $CO_2$ and $H_2$ pass through a maximum and decline nearly to

their respective background values. Coincident with the decrease in the CO, $CO_2$ and $H_2$ signals, the rates of formation of both ketene and water rise to steady-state values **(21)**. These steady-state rates have been observed for more than two hours, corresponding to well over 100 catalytic "turnovers" per surface site, without significant change. Under these steady-state conditions, no reaction products were detected other than ketene and water. The minimum in the ketene signal, which coincides with the maximum for CO, $CO_2$ and $H_2$ in Fig. 1, is a consequence of the fact that mass 42 is also a fragmentation product of acetic acid. The minimum, therefore, is associated with the decomposition of acetic acid to CO, $CO_2$ and $H_2$, and it is unrelated to ketene.

The relatively slow rise in the water signal, compared with the ketene signal, is due to adsorption of water on the walls of the vacuum system. This has been confirmed by independent step-response experiments. After correction for mass spectrometric sensitivities and pumping speeds, the mass 42 and mass 18 steady-state signals shown in Fig. 1 correspond to a 1:1 molar ratio of ketene to water.

After exposure to acetic acid, the platinum surface contains a substantial concentration of carbon adatoms, as judged from oxygen titration experiments in which predominantly $CO_2$ is formed **(11)**. The concentration of surface carbon atoms following a 90 s exposure to acetic acid at $7 \times 10^{-4}$ Torr and a temperature of 900 K was $(2.6\text{-}3.5) \times 10^{15}$ $cm^{-2}$. Exposure of the platinum surface to acetic acid at 1000 K for five minutes did not alter the carbon adatom concentration. Although the surface that results from exposure to acetic acid at temperatures below 900 K was not examined extensively, it appears that for surface temperatures above 700 K an identical surface may be prepared with a sufficiently long exposure (annealing) time. The carbon adatom concentration produced from exposure to acetic acid at 0.1 Torr for 90 s at 900 K was 5.9 x

$10^{15}$ $cm^{-2}$. Other pressures were not investigated in detail. A similar concentration of carbon, 2.4 x $10^{15}$ $cm^{-2}$, was produced from a 90 s exposure of the surface at 900 K to 7 x $10^{-4}$ Torr of ethylene. For comparison, the surface atom densities of Pt(111) and of the basal plane of graphite are 1.5 x $10^{15}$ $cm^{-2}$ and 3.8 x $10^{15}$ $cm^{-2}$, respectively **(22)**.

To summarize, on an initially clean platinum surface, acetic acid decomposes to CO, $CO_2$ and $H_2$, and produces a graphitic overlayer. The surface becomes poisoned to these decomposition reactions, and subsequently, on the graphitic surface, acetic acid dehydrates catalytically to ketene and water.

**2. Steady-State Dehydration Kinetics**

Absolute steady-state reaction rates for the dehydration of acetic acid to ketene and water over the graphitized platinum surface are shown in Fig. 2 as a function of reciprocal temperature for pressures of 7 x $10^{-4}$ and 3.5 x $10^{-4}$ Torr. The kinetics displayed in Fig. 2 are essentially identical for all the methods that were used to prepare the graphitic overlayer, including graphite formation from ethylene (cf. Sect. III.1). In addition, annealing the graphitized surface in vacuum at 1000 K did not change the observed kinetics. For the data presented explicitly here, however, each of the graphitic overlayers was prepared by exposing the initially clean platinum surface to 7 x $10^{-4}$ Torr of acetic acid for 90 s at 900 K. At low temperatures ($\lesssim$540 K), the steady-state reaction rate is independent of acetic acid pressure. Under these conditions, the apparent activation energy is 27 $\pm$ 2 kcal/mole, with an extrapolated intercept at 1/T = 0 of (0.2-1.6) x $10^{24}$ molecules-$cm^{-2}$-$s^{-1}$. At higher temperatures ($\geq$675 K), the reaction rate scales linearly with the acetic acid pressure, and the activation energy decreases to 1 $\pm$ 1 kcal/mole. In this regime, the extrapolated intercept at high temperatures is (0.7-2.8) x $10^{17}$ molecules-$cm^{-2}$-$s^{-1}$-$Torr^{-1}$. This corresponds to a reac-

tion probability per surface collision of acetic acid of (2.5-10) x $10^{-4}$. The error bar at $10^3/T$ = 1.4 in Fig. 2 indicates the variation in the measured rate after repeatedly cleaning the surface and redepositing the graphitic overlayer. The dehydration of perdeutero acetic acid showed no detectable isotope effect under any conditions, although the uncertainty in the measured activation energy would have obscured any change in the activation energy that is less than 1-2 kcal/mole. Thus, a primary isotope effect involving cleavage of a C-H bond with a vibrational frequency of 3000 $cm^{-1}$ would not be observed, since the expected increase in the activation energy is only 1.1 kcal/mole for C-D bond cleavage.

At the lowest temperatures studied (≤540 K), the steady-state CO signal, which is a fragmentation product of ketene, increased relative to the ketene mass spectrometric intensity. Since the mass spectrometric intensities at these low temperatures are approaching our detection limit, it was not possible to quantify this behavior. However, this may represent another steady-state decomposition mechanism that competes with dehydration to ketene at low temperatures where the overall rate of decomposition is very small (e.g. the reaction probability at 540 K and 7 x $10^{-4}$ Torr is approximately $10^{-5}$).

Figure 3 shows the steady-state rate of dehydration of acetic acid as a function of pressure from 8 x $10^{-7}$ to 7 x $10^{-4}$ Torr at 675 K. The reaction order with respect to acetic acid pressure, measured from the data that were recorded below $10^{-5}$ Torr, is 0.95 ± 0.05. While the *relative* rates determined at these low pressures are quite accurate, the calibration that is necessary to calculate absolute rates is difficult at low pressures. The error bar at 3 x $10^{-6}$ Torr indicates the absolute error present in all the data at pressures below $10^{-5}$ Torr. Considering this rather large absolute error and the much smaller uncertainties for measurements at higher pressures, a first-order dependence of the rate on pressure is suggested at 675 K over the entire range of pressures studied, i.e. for

pressures below $10^{-3}$ Torr.

Steady-state dehydration of acetic acid was also conducted on a graphitic surface composed of $^{13}C$ to ascertain the stability of the graphitic overlayer. The $^{13}C$ labeled surface was prepared by exposing the clean platinum surface to 7 x $10^{-4}$ Torr of $^{13}C_2H_4$ for 90 s at 900 K. Comparison of the $^{13}C$ surface concentration, determined by oxygen titration, following dehydration of acetic acid at 7 x $10^{-4}$ Torr and 675 K for 20 min with the $^{13}C$ surface concentration measured without reaction, revealed that the $^{13}C$ atoms remain on the surface during the dehydration of acetic acid. Hence, the dehydration of acetic acid over graphitized platinum is a "catalytic" reaction in the strictest sense, i.e. no component of the "catalyst" is incorporated into the reaction product.

### 3. Thermal Desorption Measurements

A thermal desorption spectrum of ketene following exposure of the graphitized platinum surface to 7 x $10^{-4}$ Torr of acetic acid for 240 s at 300 K is shown in Fig. 4. A single peak occurs at a temperature of 520 K. The desorption spectrum is independent of the delay time associated with transferring the sample from the reaction chamber to the high vacuum chamber. Moreover, the desorption spectrum is independent of exposure time (>4 min) and surface temperature (between 300 and 700 K), provided the surface is cooled to 300 K before the acetic acid is evacuated. Exposures at pressures below 7 x $10^{-4}$ Torr were not investigated. An approximate calibration using the mass spectrometric sensitivity and the pumping speed for $CO_2$ indicates the desorption of (0.1-5) x $10^{13}$ molecules-$cm^{-2}$ of ketene. Although the desorption of neither acetic acid nor $H_2O$ was observed, these species would not be detected for surface concentrations below approximately 5 x $10^{13}$ $cm^{-2}$ due to the adsorption of acetic acid and $H_2O$ on the system walls.

Carbon monoxide was also observed to desorb from the graphitized platinum surface following exposure to acetic acid. The peak temperature was approximately 540 K and showed the same independence of surface temperature and delay time in transfer as ketene. The amount of CO that desorbed corresponded to approximately half the amount of ketene that desorbed and (as verified by independent measurements) was not due to adsorption from the background. This desorption of CO may be related to the increase in the mass 28 : mass 42 ratio observed at low temperatures during the steady-state reaction (cf. Sect III.2). Due to the lack of quantitative steady-state data concerning this reaction pathway, however, the origin of the CO was not investigated further.

**4. Steady-State Reaction of Related Compounds**

To gain further insight into the mechanism of the steady-state dehydration of acetic acid, the reactions of four functionally related model compounds, namely, acetic anhydride, isopropyl alcohol, acetone and methyl acetate, were investigated briefly. In each case, the graphitic overlayer was prepared in a manner identical to that used for the steady-state measurements of acetic acid dehydration, i.e. an exposure of $7 \times 10^{-4}$ Torr of acetic acid for 90 s at 900 K. The rates of decomposition of each compound were measured at a pressure of $7 \times 10^{-4}$ Torr. Acetic anhydride decomposed predominantly to ketene and acetic acid, with an activation energy of 12-15 kcal/mole which was constant over the temperature range 420-650 K. A minor amount of water, <1% of the acetic acid signal, was observed above 535 K. Isopropyl alcohol dehydrated to propylene and water, with an activation energy decreasing from approximately 16 kcal/mole at temperatures between 450 and 500 K to approximately 3 kcal/mole at 625 K. Qualitatively, the observed steady-state kinetics for the dehydration of isopropyl alcohol are similar to those for acetic acid dehydration. Acetone and methyl acetate showed no reaction at any temperature studied ($\leq$700 K).

## IV. Discussion

### 1. Reaction Kinetics and Adsorbed Intermediates

For temperatures below approximately 570 K and pressures between $10^{-3}$ and $10^{-4}$ Torr, the steady-state rate of dehydration of acetic acid to ketene on graphitized platinum exhibits a linear Arrhenius behavior and a diminishing dependence on acetic acid pressure as the temperature decreases (cf. Fig. 2). These observations suggest that under these conditions the catalytic surface is nearly saturated with either acetic acid, a reaction intermediate or a reaction product. Since the heat of adsorption of acetic acid, water and ketene on graphitized platinum is expected to be $\lesssim$5 kcal/mole **(23)**, a mechanism in which the surface is saturated with an intermediate in the dehydration reaction species is implicated. For example, the intramolecular elimination of water from molecularly adsorbed acetic acid is not a viable mechanism of dehydration, since *molecular* acetic acid would be adsorbed reversibly at 300 K. Moreover, the thermal desorption of ketene at 520 K following both exposure of the surface to acetic acid at 300 K and the reaction of acetic acid at elevated temperatures are identical, provided the surface is cooled in the presence of acetic acid. This result implies that the adsorbed intermediate in the reaction is stable and readily formed at 300 K.

Information concerning the reaction intermediate is provided by the observed reactivities of methyl acetate, acetone and isopropyl alcohol. On the basis of both these results and those pertaining to acetic acid, we suggest that the physically most reasonable intermediate that leads to ketene from acetic acid dehydration is a monodentate acetate, designated $\eta^1$–$CH_3COO$(a), formed by the dissociation of the oxygen-hydrogen bond of acetic acid. As discussed below, this intermediate is consistent with the observed reactivity (or lack

thereof) of methyl acetate, acetone and isopropyl alcohol, as well as that of acetic acid on the graphitized platinum surface. The observed lack of reactivity of methyl acetate in which the hydroxyl hydrogen of acetic acid is replaced with a methyl group indicates the importance of the acidic hydrogen. Since the oxygen-carbon bond is substantially more difficult to cleave than the oxygen-hydrogen bond, dissociation of the acidic hydrogen is implicated in the formation of the surface intermediate. Note that since the heats of reaction for both the dehydration of acetic acid and the elimination of methanol from methyl acetate are approximately 34 kcal/mole **(24)**, arguments based solely on thermochemistry cannot account for the observed differences in reactivity. Similarly, acetone, in which the hydroxyl group is replaced with a methyl group, is unreactive.

The relative importance of the acidic hydrogen is also illustrated by the dehydration of isopropyl alcohol, which exhibits kinetics that are qualitatively similar to those of acetic acid. Although much less acidic than that of acetic acid, the hydroxyl hydrogen of isopropanol can dissociate, forming an alkoxy intermediate. This alkoxy intermediate that is formed by cleavage of the oxygen-hydrogen bond of isopropanol is analogous to the monodentate acetate intermediate that is formed from cleavage of the acidic hydrogen from acetic acid. Since the intermediates are analogous, similar kinetics may be expected. In addition, the measured apparent activation energies at low temperatures of 27 and 16 kcal/mole for the dehydration of acetic acid and isopropanol vary consistently with the C-OH bond energies of 107 and 92 kcal/mole for acetic acid and isopropyl alcohol, respectively **(25)**. Assuming the same relative C-O bond energies in the adsorbed intermediates, the observed activation energies indicate that the cleavage of the C-O bond can be important in controlling the rate of decomposition of the surface intermediate.

In contrast to the kinetics observed at low temperatures ($\lesssim$570 K), at high temperatures ($\geq$675 K) the rate of dehydration of acetic acid is first-order in acetic acid pressure, and the reaction probability approaches (2.5-10) x $10^{-4}$. This low reaction probability indicates that the vast majority of acetic acid molecules which adsorb (weakly) on the surface subsequently desorb without reacting. Hence, the steady-state surface coverage of acetic acid is essentially equal to the equilibrium value in the absence of any decomposition. A low reaction probability of acetic acid is also consistent with our measurements of the decomposition of acetic anhydride. Although acetic anhydride decomposes readily to ketene and acetic acid, only a small fraction (<1%) of the acetic acid that is formed on the surface reacts further via dehydration.

**2. Mechanistic Modeling**

The steady-state reaction kinetics and the thermal desorption measurements, taken together, imply that the dehydration of acetic acid proceeds via an irreversibly adsorbed intermediate. Although the mechanistic model described below postulates that this adsorbed intermediate is a monodentate acetate, *the numerical results are insensitive to the structure of the intermediate provided it is readily formed at 300 K and stable upon heating to approximately 520 K.*

Assuming a monodentate acetate intermediate, the dehydration of acetic acid may be written mechanistically as follows:

$$CH_3COOH(g) \underset{k_d}{\overset{S(\theta)F}{\rightleftarrows}} CH_3COOH(a)\,, \qquad (1)$$

$$CH_3COOH(a) \overset{k_1}{\rightarrow} \eta^1\text{–}CH_3COO(a) + H(a)\,, \qquad (2)$$

$$\eta^1\text{–}CH_3COO(a) \xrightarrow{k_2} CH_2CO(g) + OH(a)\ , \tag{3}$$

and

$$OH(a) + H(a) \xrightarrow{k_3} H_2O(g)\ , \tag{4}$$

where $S(\theta)$ represents the functional dependence of the probability of adsorption of acetic acid on the fractional coverage of each surface species; F is the molecular flux of acetic acid to the surface; and $k_d$, $k_1$, $k_2$ and $k_3$ are the reaction rate coefficients for the desorption of acetic acid and the three surface reactions. The probability of adsorption of acetic acid may be written as

$$S(\theta) = S^0(1 - \sum_i \theta_i)\ , \tag{5}$$

where $S^0$ is the probability of adsorption on the graphitized platinum surface in the limit of zero adsorbate coverage, $\theta_i$ is the fractional surface coverage of species i, and the sum is over all surface species. Each of the reaction rate coefficients may be written as $k_i = k_i^{(0)}\exp(-E_i/k_BT)$ with (assumed) coverage-independent preexponential factors $k_i^{(0)}$ and activation energies $E_i$.

To calculate the steady-state rate of acetic acid dehydration via this mechanism, the steady-state material balance equations for each surface species were solved. Since only three of the mass balance equations are linearly independent, the additional assumption that $\theta_{\eta^1\text{–}CH_3COO}$ is equal to $\theta_H$ was invoked. As discussed below, the rate of reaction (4) is rapid compared to that of reaction (3), validating this assumption. The probability of molecular adsorption of acetic acid on the clean graphitic surface $S^0$ was taken to be unity, and the surface site density $n_s$, which is necessary to calculate absolute rates, was taken to be $10^{14}$ $cm^{-2}$ **(26)**. For the recombinative desorption of water, reaction (4), the preexponential factor and the activation energy have been determined from a

molecular beam investigation of the $H_2O + D_2O$ exchange reaction on pyrolytic graphite **(27,28)**. Thus, the model described by the elementary reactions (1)-(4) contains four parameters, namely, $k_2^{(0)}$ and $E_2$, and the composite quantities $E_1 - E_d$ and $k_f^{(0)}/k_d^{(0)}$. These parameters were adjusted until the best description of the experimental data was obtained. The values for each of the variables used in the model calculations are given in Table 1, and the model results for the dehydration of acetic acid at $7 \times 10^{-4}$ and $3.5 \times 10^{-4}$ Torr are compared with the experimental data in Fig. 2. Obviously, the model accurately describes both the temperature and the pressure dependence of the reaction rate.

Although the model contains four adjustable parameters, a consideration of the analytic form of the reaction rate in the limits of high and low temperature illustrates that the values of these "adjustable" parameters are actually quite severely constrained by the data. In the limit of high temperature, where the coverage of all surface species approaches zero, the reaction rate becomes

$$R = \frac{S^0 F k_f^{(0)}}{k_d^{(0)}} \exp[-(E_1 - E_d)/k_B T] . \qquad (7)$$

Thus, the activation energy observed at high temperature, $1 \pm 1$ kcal/mole, is equal to $E_1 - E_d$, and the reaction probability at $1/T = 0$ is $S^0 k_f^{(0)}/k_d^{(0)}$. At low temperature, the surface becomes saturated with the reaction intermediates $\eta^1$–$CH_3COO$(a) and H(a). Since for all the reaction conditions studied, the fractional surface coverages of molecular acetic acid, ketene and water are negligible, $\theta_{\eta^1\text{-}CH_3COO} = \theta_H = 0.5$, and the reaction rate at low temperature may be written as

$$R = 0.5 n_s k_2^{(0)} \exp(-E_2/k_B T) . \qquad (8)$$

The observed activation energy, $27 \pm 2$ kcal/mole, is therefore equal to $E_2$, and the extrapolated intercept at $1/T = 0$, (0.2-1.6) $\times 10^{24}$ molecules-cm$^{-2}$–s$^{-1}$, is

equal to 0.5 $n_s k_2^{(0)}$.

An analysis of the thermal desorption measurements provides *independent* determinations of $k_2^{(0)}$ and $E_2$. Calibration of the ketene thermal desorption spectrum indicates the desorption of (0.1-5) x $10^{13}$ molecules-$cm^{-2}$, 0.5 $n_s$, of ketene. Using this range of values together with the measured result $n_s k_2^{(0)}$ = (0.4-3.2) x $10^{24}$ molecules-$cm^{-2}$ $-s^{-1}$ yields $k_2^{(0)}$ = (0.04-16) x $10^{11}$ $s^{-1}$. Since we are postulating that ketene originates from the unimolecular decomposition of an adsorbed intermediate, a first-order Redhead analysis **(29)** applied to the thermal desorption spectrum of ketene using $T_p$ = 520 K and $k_2^{(0)}$ = 0.04-16 x $10^{11}$ $s^{-1}$ is appropriate. This gives $E_2$ = 23-29 kcal/mole, which agrees well with the value of $E_2$ determined independently from the steady-state kinetics.

In order for the mechanism embodied by reactions (1)-(4) to describe the experimental data correctly, the rate coefficient for the recombinative desorption of molecular hydrogen must be small compared to that for the production of water. The desorption of molecular hydrogen following both the adsorption of atomic hydrogen and the dissociative adsorption of water has been studied on pyrolytic graphite **(27,28)**. These results indicate that hydrogen is produced from dissociatively adsorbed water only at temperatures above 2000 K, and even under these conditions, the rate of production of water is an order of magnitude larger than that of hydrogen desorption **(27)**. An analysis of our model indicates that $k_3 n_s^2 \gg k_2 n_s$ for all conditions studied, e.g. a "worst" case occurs at 800 K for which $k_3 n_s^2 > 100\ k_2 n_s$. Consequently, the steady-state coverages of $\eta^1$–$CH_3COO$(a) and H(a) are equal, since water is produced rapidly after the decomposition of $\eta^1$–$CH_3COO$(a) into ketene and OH(a).

### 3. Potential Energy Diagram for Acetic Acid Dehydration

A mechanistic model was developed in Sect. IV.2, which describes the observed

kinetics for the dehydration of acetic acid to ketene over a graphitized platinum surface. The energetics of this reaction implied by this model is shown in Fig. 5 in the form of a potential energy diagram along the "reaction coordinate". The reference energy level of acetic acid in the gas phase is defined as zero.

To evaluate the energy levels for each of the other points along the reaction coordinate, the bond energies tabulated in Table 2 were utilized. Note that the predicted energy levels are consistent with the known endothermicity of the overall reaction, namely, 34 kcal/mole **(24)**. In addition, for temperatures above 675 K, the observed activation energy is 1 ± 1 kcal/mole, which is consistent with the potential energy level for $\eta^1$–$CH_3COO(a)$ + H(a). The measured value for $E_2$ is 27 ± 2 kcal/mole, which is in good agreement with the predicted value of $E_2 \gtrsim 29$ kcal/mole.

Although carbon-hydrogen bond energies in hydrocarbons are typically 100 kcal/mole, following Balooch and Olander **(28)**, a hydrogen-surface bond energy of 61 kcal/mole was used to construct the potential energy diagram shown in Fig. 5. However, identical energy levels would be calculated by assuming that the hydrogen-surface bond energy is 100 kcal/mole with a concurrent reduction of approximately 80 kcal/mole in the carbon-carbon bond energy of the graphite overlayer for each dissociatively adsorbed acetic acid molecule. In this case, the HO-S and $\eta^1$–$CH_3COO$-S bond energies would become approximately 90 and 80 kcal/mole, respectively. This alternate formulation is equally consistent with the measured activation energies for both the desorption of hydrogen and the recombinative desorption of water from the basal plane of graphite **(27,28)**.

## V. Synopsis

The results of this study may be summarized as follows:

1. On a polycrystalline platinum surface containing approximately a monolayer of graphitic carbon, the catalytic dehydration of acetic acid to ketene and water proceeds at steady-state.

2. For reactant pressures above $3.5 \times 10^{-4}$ Torr and temperatures below 540 K, the reaction rate is independent of acetic acid pressure, and the apparent activation energy is $27 \pm 2$ kcal/mole. Under these conditions the rate of decomposition of an irreversibly adsorbed intermediate controls the rate of reaction.

3. The reaction intermediate is formed from acetic acid on the graphitized platinum surface at 300 K and, upon heating, decomposes at 520 K with the accompanying desorption of ketene. Dissociation of the acidic hydrogen of acetic acid appears to be important in the formation of the intermediate.

4. For reactant pressures below $7 \times 10^{-4}$ Torr and at temperatures above 675 K, the reaction rate is linearly dependent on acetic acid pressure, and the apparent activation energy is $1 \pm 1$ kcal/mole. In this regime, the reaction rate is determined by a competition between the rates of desorption and surface reaction of molecularly adsorbed acetic acid.

**Acknowledgment:**

This work was supported by the National Science Foundation under Grant No. 8500789.

**References**


1. D. F. Ollis and M. Boudart, Surface Sci. **23**, 320 (1970).
2. S. D. Worley and J. T. Yates, Jr., J. Catal. **48**, 385 (1977).
3. E. I. Ko, J. B. Benziger and R. J. Madix, J. Catal. **62**, 264 (1980).
4. M. A. Barteau and R. J. Madix, J. Catal. **62**, 329 (1980).
5. S. M. Davis, F. Zaera and G.A. Somorjai, J. Catal. **77**, 439 (1982).
6. J. G. McCarty and R. J. Madix, J. Catal. **38**, 402 (1975).
7. J. G. McCarty and R. J. Madix, J. Catal. **54**, 210 (1976).
8. T. S. Wittrig, P. D. Szuromi and W. H. Weinberg, J. Chem. Phys. **76**, 3305 (1982).
9. P. D. Szuromi, J. R. Engstrom and W. H. Weinberg, J. Chem. Phys. **80**, 508 (1984).
10. P. D. Szuromi, J. R. Engstrom and W. H. Weinberg, J. Chem. Phys. **89**, 2497 (1984).
11. J. J. Vajo, Y.-K. Sun and W. H. Weinberg, in preparation.
12. M. Kiskinova and D. W. Goodman, Surface Sci. **108**, 64 (1981).
13. N. D. Lang, S. Holloway and J. K. Norskov, Surface Sci. **150**, 24 (1985).
14. P. J. Feibelman and D. R. Hamann, Phys. Rev. Letters **52**, 61 (1984).
15. F. P. Netzer and R. A. Wille, J. Catal. **51**, 18 (1978).
16. D. L. Smith and R. P. Merrill, J. Chem. Phys. **52**, 5861 (1970).
17. M. Abon, J. Billy, J. C. Bertulini and B. Tardy, Surface Sci. **167**, 1 (1986).
18. J. J. Vajo, W. Tsai and W. H. Weinberg, Rev. Sci. Instrum **56**, 1439 (1985).

19. J. J. Vajo, W. Tsai and W. H. Weinberg, J. Phys. Chem. **89**, 3243 (1985).

20. For these experiments, the conversion was lowered by placing an additional pump on the outlet of the reactor, thereby decreasing the residence time of the acetic acid.

21. The existence of ketene was confirmed by monitoring the parent ion signal at 42 amu and the fragmentation products at 41, 28 and 14 amu. Water was monitored at 18 amu. For the fragmentation intensities of ketene, see A. Cornu and R. Masut,"Compilation of Mass Spectral Data", 2nd ed., Vol. 1, Heydon and Son, N.Y., 1975.

22. These values result from assuming a hexagonally close-packed surface and an atom-atom distance of 2.746 Å and 1.42 Å for platinum and graphite, respectively.

23. A. V. Kouznetzov and K. D. Shcherbakova, J. Chromatog. **49**, 21 (1970).

24. This result is based on the following values for the various heats of formation: $\Delta H_f$ (acetic acid) = -106.7, $\Delta H_f$ (methyl acetate) = -98, $\Delta H_f$ (ketene) = -14.6, $\Delta H_f$ (water) = -57.8, and $\Delta H_f$ (methyl alcohol) = -48.1. All quantities are in kcal/mole for the gas phase at 298 K.

25. "Handbook of Chemistry and Physics", 51st ed., R. C. Weast Ed., Chemical Rubber Co., Cleveland, 1970, p. F-166.

26. Based on the excluded area of an acetic acid molecule, the saturation surface density is approximately $10^{14}$ $cm^{-2}$.

27. D. R. Olander, T. R. Acharya and A. Z. Ullman, J. Chem. Phys. **67**, 3549 (1977).

28. M. Balooch and D. R. Olander, J. Chem. Phys. **63**, 4772 (1975).

29. P. A. Redhead, Vacuum **12**, 203 (1962).

30. D. F. McMillen and D. M. Golden, Ann. Rev. Phys. Chem. **33**, 493 (1982).

**Table 1:** Model Parameters for the Dehydration of Acetic Acid on a Graphitized Platinum Surface.

| | **Parameter** | **Value** | **Ref.** |
|---|---|---|---|
| $S^0$ | Probability of adsorption of acetic acid | 1 | |
| $k_2^{(0)}$ | Preexponential factor for decomposition of surface intermediate | $1x10^{10}$ $s^{-1}$ | |
| $E_2$ | Activation energy for decomposition of surface intermediate | 27.5 kcal/mole | |
| $k_3^{(0)}$ | Preexponential factor for recombinative desorption of water | $7x10^{-10}$ $cm^2$–$s^{-1}$ | **27** |
| $E_3$ | Activation energy for recombinative desorption of water | 0 kcal/mole | **27** |
| $E_1 - E_d$ | Difference between surface reaction and desorption activation energies | 2 kcal/mole | |
| $k_1^{(0)}/ k_d^{(0)}$ | Ratio of surface reaction and desorption preexponential factors | $10^{-3}$ | |
| $n_s$ | Surface site density | $10^{14}$ $cm^{-2}$ | **26** |

**Table 2:** Bond Energies for the Dehydration of Acetic Acid on a Graphitized Platinum Surface.

| Bond | Bond Energy, kcal/mole | Note |
|---|---|---|
| $CH_3COO$-H | 107 | (a) |
| $CH_3CO$-OH | 107 | (b) |
| $CH_3COOH$-S | 5 | (c,d) |
| $CH_2CO$-S | 5 | (d) |
| $H_2O$-S | 5 | (d) |
| H-S | 61 | (e) |
| HO-S | 58 | (f) |
| $\eta^1$–$CH_3COO$-S | 52 | (g) |
| $\eta^1$–$CH_3CO$-O(a) | 101 | (g) |

(a) See Ref. 30.

(b) See Ref. 25.

(c) "S" denotes bonding to the graphitized platinum surface.

(d) The adsorbate-surface bond energy for each physically adsorbed species is *estimated* to be 5 kcal/mole.

(e) The activation energy for the recombinative desorption of hydrogen from the basal plane of graphite is 18 kcal/mole **(28)**, which implies a bond energy of 61 kcal/mole.

(f) The activation energy for the recombinative desorption of water from the basal plane of graphite is 0 kcal/mole **(27)**. Given an H-S bond energy of 61 kcal/mole, this implies an HO-S bond energy of 58 kcal/mole.

(g) Typically, substitution of the hydrogen in an alcohol or a carboxylic acid with an alkyl group reduces the C-O bond energy by 10 kcal/mole, from approximately 90 to 80 kcal/mole **(25)**. Using the reduced HO-S (carbon) bond energy of 58 kcal/mole, linear scaling implies that the reduction here is approximately 6 kcal/mole.

**Figure Captions**

Figure 1. Time evolution curves for the production of CO, $CO_2$, $H_2$, $H_2O$ and $CH_2CO$ (42 amu) during the constant exposure of an initially clean platinum surface to acetic acid at $7 \times 10^{-4}$ Torr. At t=0, the surface temperature was increased at a rate of 50-54 K/s from 300 to 900 K and thereafter held constant at 900 K. The data are uncorrected for fragmentation, mass spectrometric sensitivities and pumping speeds.

Figure 2. Arrhenius plots of the rate of dehydration of acetic acid at $7 \times 10^{-4}$ and $3.5 \times 10^{-4}$ Torr. For each pressure, a graphitic overlayer was first prepared by exposing a clean platinum surface to $7 \times 10^{-4}$ Torr of acetic acid at 900 K for 90 s. The error bar at $10^3/T = 1.4$ indicates the variation in the rate observed by repeatedly removing and depositing the graphitic overlayer. The lines are the results of model calculations which are described in the text.

Figure 3. Absolute reaction rates for the dehydration of acetic acid at 675 K as a function of acetic acid pressure. The error bar at $3 \times 10^{-6}$ Torr indicates the systematic error in calibration of the rates for all pressures below $10^{-5}$ Torr.

Figure 4. Thermal desorption spectrum of ketene following either reaction at evaluated temperatures (500-700 K) and cooling to 300 K in the presence of acetic acid, or exposure of the graphitic overlayer to acetic acid at 300 K. The heating rate is 20 K/s, and the maximum desorption rate occurs at 520 K.

Figure 5. One-dimensional potential energy diagram illustrating the catalytic dehydration of acetic acid to ketene over a graphitized platinum surface. The energy levels have been calculated by choosing acetic acid in the gas phase as the reference level and using the bond energies listed in Table 2.

# Transient Decomposition of Acetic Acid on Clean Platinum

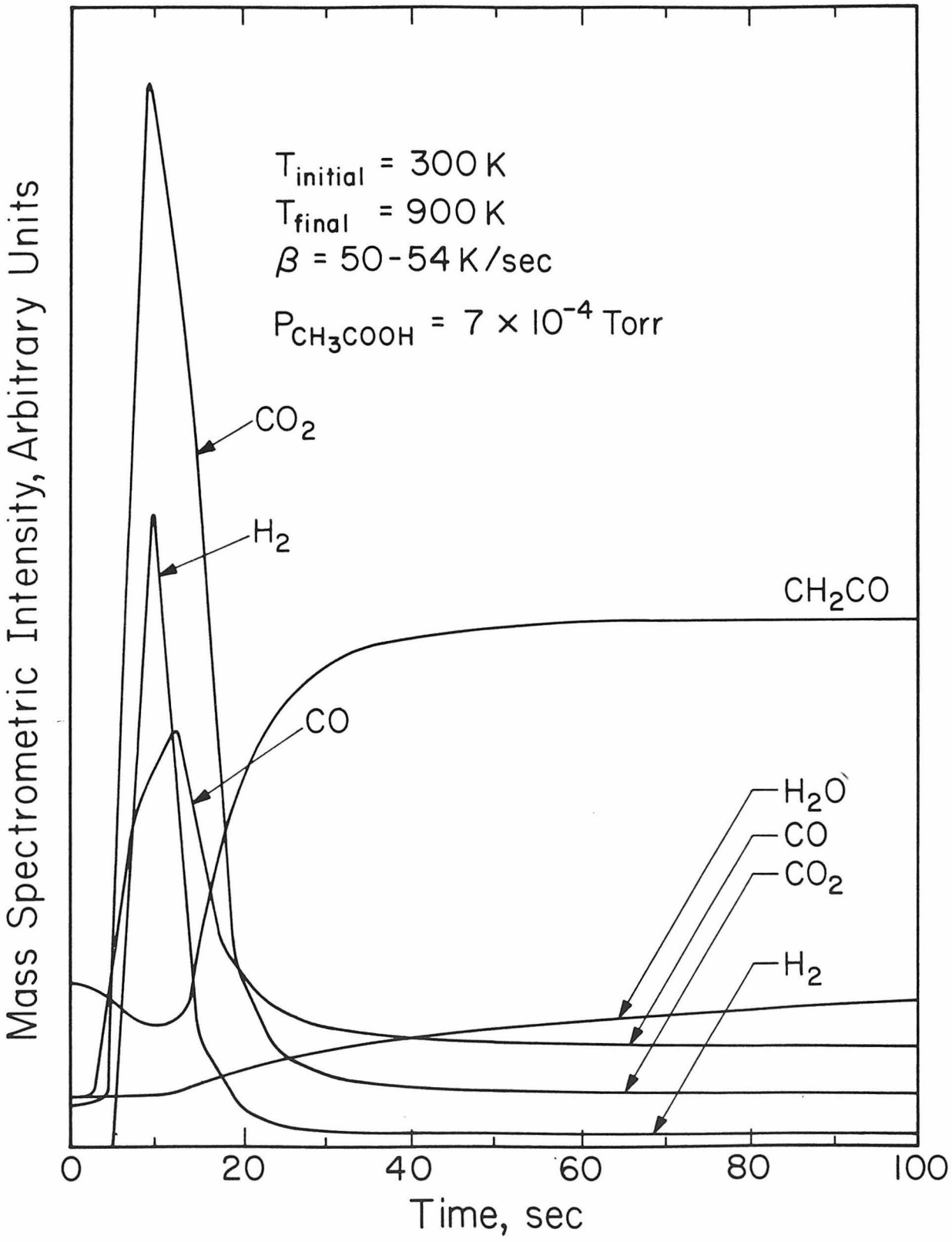


Figure 1

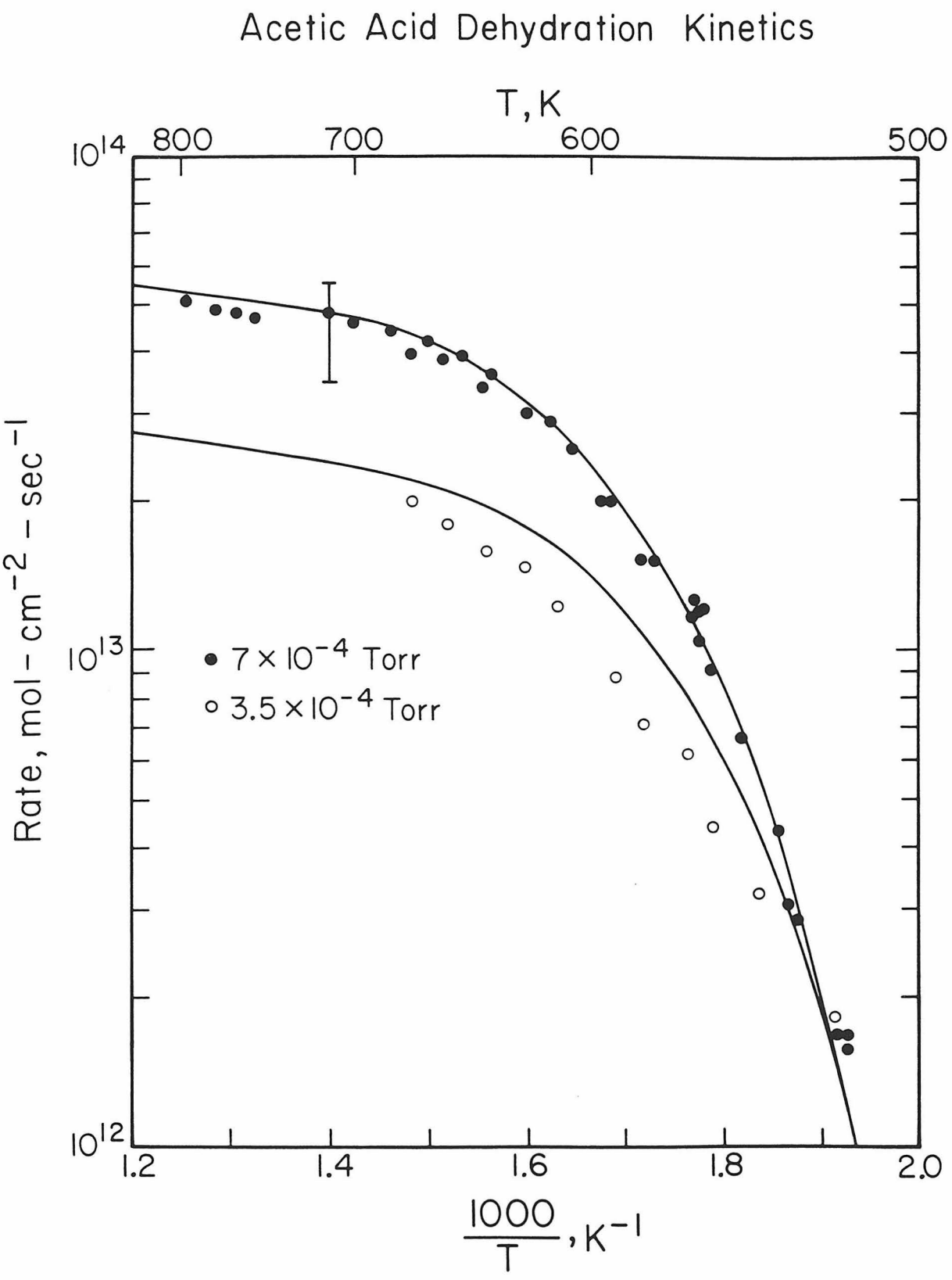
Acetic Acid Dehydration Kinetics
T, K
800
700
600
500
$10^{14}$
$10^{13}$
$10^{12}$
Rate, mol - cm$^{-2}$ - sec$^{-1}$
• 7 × 10$^{-4}$ Torr
○ 3.5 × 10$^{-4}$ Torr
1.2
1.4
1.6
1.8
2.0
$\frac{1000}{T}$, K$^{-1}$

Figure 2

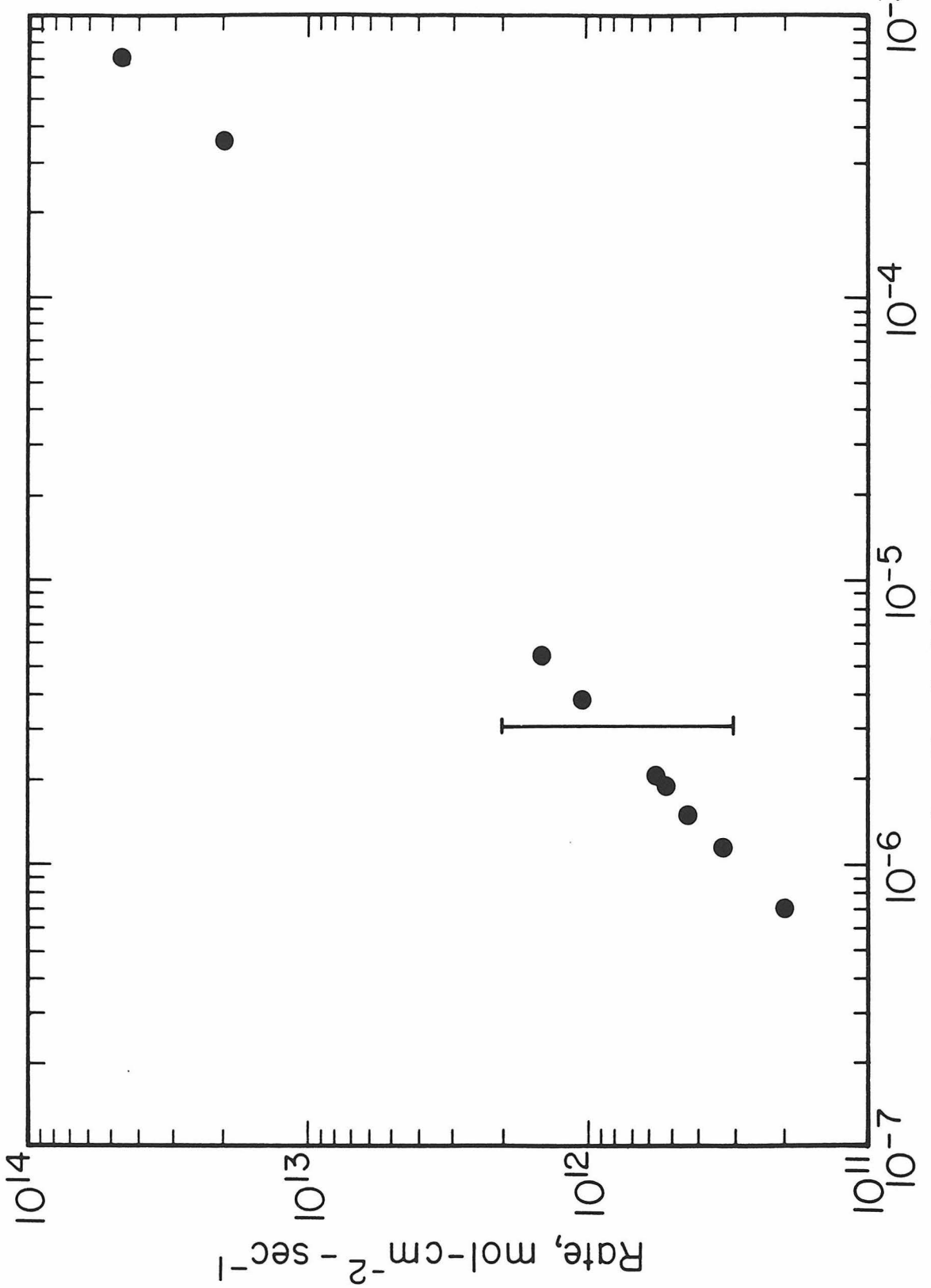
Acetic Acid Dehydration at 675 K
Rate, mol-cm$^{-2}$-sec$^{-1}$
$10^{14}$
$10^{13}$
$10^{12}$
$10^{11}$
$10^{-7}$
$10^{-6}$
$10^{-5}$
$10^{-4}$
$10^{-3}$
Acetic Acid Pressure, Torr

Figure 3.

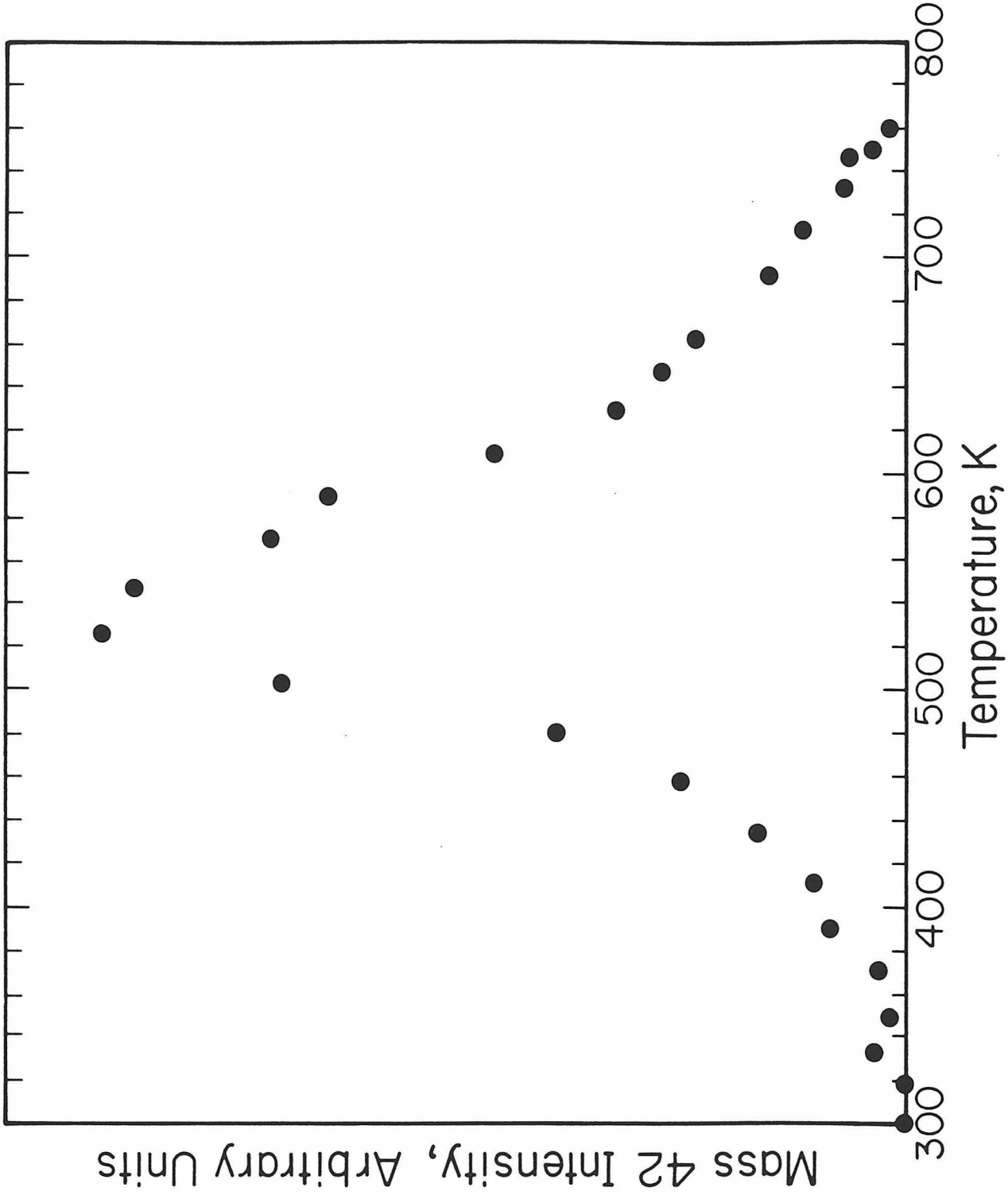
Mass 42 Intensity, Arbitrary Units
300
400
500
600
700
800
Temperature, K

Figure 4

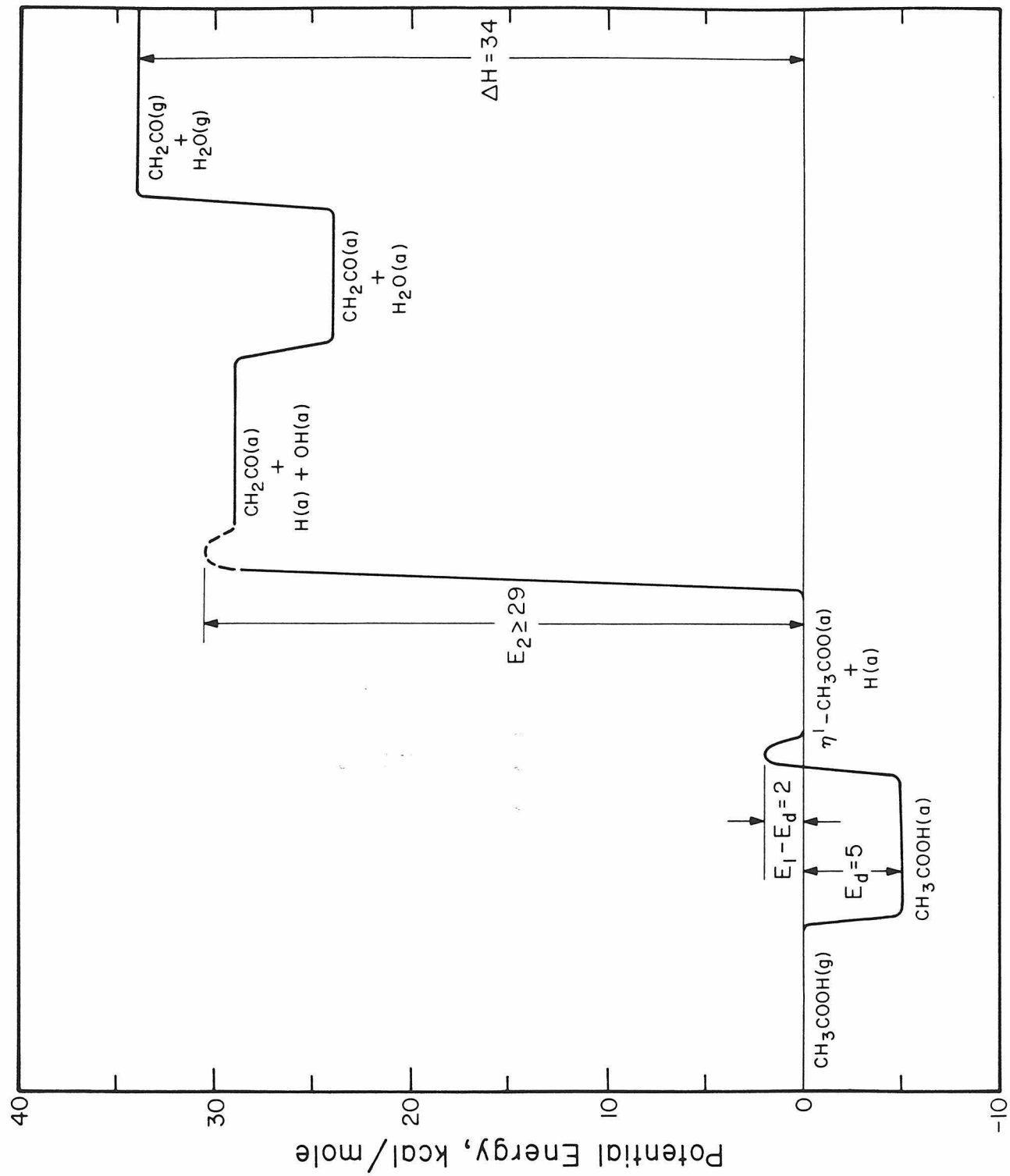
Potential Energy, kcal/mole
40
30
20
10
0
-10
$CH_3COOH(g)$
$CH_3COOH(a)$
$E_d=5$
$E_1-E_d=2$
$\eta^1-CH_3COO(a)$
+
H(a)
$E_2 \geq 29$
$CH_2CO(a)$
+
H(a) + OH(a)
$CH_2CO(a)$
+
$H_2O(a)$
$CH_2CO(g)$
+
$H_2O(g)$
$\Delta H = 34$

Figure 5

# Chapter 7.

# Conclusions

The principal conclusions of the research presented in this thesis may be summarized as follows:

*Chapters 3 and 4*

1. The steady-state kinetics of ammonia decomposition on both a polycrystalline platinum surface and the single crystalline Pt(110)-(1x2) surface is qualitatively similar.

2. Under conditions where the reaction rate is linearly dependent on ammonia pressure (at relatively lower pressures and/or higher temperatures), the rate of decomposition is controlled by a competition between the surface reaction that cleaves an N-H bond and the desorption of molecularly chemisorbed ammonia.

3. When the rate of ammonia decomposition is independent of ammonia pressure (at relatively higher pressures and/or lower temperatures), the surface is saturated with nitrogen adatoms, and the recombinative desorption of these nitrogen adatoms determines the rate of reaction.

4. Steady-state kinetic data obtained over a wide range of experimental conditions have been both analyzed and unified successfully into a microscopic mechanistic model using kinetic parameters determined independently from ultrahigh vacuum measurements.

*Chapters 5 and 6*

1. On an initially clean polycrystalline platinum surface, $^{13}CO$, CO, $^{13}CO_2$, $H_2$ and adsorbed carbon-12 are the major reaction products of the decomposition of $CH_3{}^{13}COOH$.

2. The decomposition of acetic acid on platinum produces a graphitic overlayer on which the steady-state catalytic dehydration of acetic acid to ketene and water occurs.

3. The catalytic dehydration of acetic acid on the graphitized platinum surface proceeds via an irreversibly adsorbed intermediate which is formed by the dissociative chemisorption of acetic acid.

# Appendix.

## Inhibition by Hydrogen of the Heterogeneous Decomposition of Ammonia on Platinum

[This Appendix consists of an article coauthored with W. Tsai and W. H. Weinberg, which appeared in the *Journal of Physical Chemistry* **89**, 4926 (1985).]

Reprinted from The Journal of Physical Chemistry, 1985, 89, 4926.


# Inhibition by Hydrogen of the Heterogeneous Decomposition of Ammonia on Platinum

**W. Tsai, J. J. Vajo, and W. H. Weinberg***

*Division of Chemistry and Chemical Engineering, California Institute of Technology, Pasadena, California 91125 (Received: May 28, 1985)*

Absolute reaction rates have been measured in a continuous flow microreactor for the inhibition by hydrogen of the heterogeneous decomposition of ammonia over a polycrystalline platinum wire at pressures between $10^{-3}$ and 0.6 torr, with ammonia to hydrogen partial pressure ratios varying from 1:1 to 1:4 and temperatures between 400 and 1200 K. Inhibition of the decomposition is observed at relatively high total pressures (0.2–0.6 torr) for all temperatures studied. The reaction orders with respect to hydrogen and ammonia are −1.5 and 1.0, respectively, with an apparent activation energy of 38 kcal/mol. For relatively low total pressures ($10^{-3}$–$5 \times 10^{-3}$ torr), inhibition is only observed at temperatures below 650 K, where the activation energy varies from 33 to 55 kcal/mol and the reaction order with respect to hydrogen approaches −1.5 at low temperatures. The decomposition becomes uninhibited at high temperatures and the activation energy is 4.5 kcal/mol. The kinetics of this reaction as well as previous results for the $NH_3 + D_2$ exchange reaction are described quantitatively by a mechanistic model employing independently measured adsorption–desorption parameters of $NH_3$, $N_2$, and $H_2$, where the rate coefficient for hydrogen desorption is a function of the fractional surface coverage of nitrogen adatoms. The hydrogenation of $NH_2(a)$ to produce molecularly adsorbed ammonia is predicted to be the dominant factor in the inhibition of the ammonia decomposition.

## 1. Introduction

The catalytic synthesis of ammonia is one of the most important heterogeneous processes ever developed. There have been numerous studies and reviews regarding the mechanism of ammonia synthesis, the kinetics of the reaction, and the characterization of the catalytic surface.[1-9] The catalytic decomposition of ammonia on transition metals has also been investigated extensively, presumably due both to its (apparent) simplicity and its relevance to the synthesis of ammonia. Although the decomposition has been studied widely on platinum,[10-13] a complete mechanism, which describes the reaction over a wide range of experimental conditions in terms of elementary steps, has not been available until recently.[14] In conjunction with the decomposition of pure ammonia, the inhibition by hydrogen of the decomposition reaction has also been examined frequently.[13,15-17] Classical kinetic studies of ammonia decomposition on platinum filaments and evaporated films have been investigated in batch reactors with large excesses of hydrogen in the feed stream ($P_{H_2}/P_{NH_3}$ varying from 3 to 6) at atmospheric pressure and temperatures between 600 and 1000 K. The reaction order with respect to hydrogen under these conditions was reported to vary from −1.3 to −1.83 in different experiments,[15-17] and the apparent activation energy was found to vary over a wide range from 30.1 to 59 kcal/mol.

Loffler and Schmidt studied the inhibition of ammonia decomposition by hydrogen on a platinum wire in a flow reactor at ammonia partial pressures from 0.05 to 0.65 torr and partial pressures of hydrogen from 0.15 to 0.68 torr in the temperature range between 600 and 1600 K.[13] Using a Langmuir–Hinshelwood (L-H) rate expression, they determined that the reaction order with respect to hydrogen was $-1.5 \pm 0.3$ and that the activation energy approaches 32 kcal/mol asymptotically at low temperatures. They were able to fit the L-H rate expression to within 20% of their experimental data over the complete range of temperatures and pressures that they studied. While the Langmuir–Hinshelwood rate expression provides a consistent framework for discussion of a heterogeneous reaction, it gives no microscopic information concerning the energetics and the mechanistic details of the reaction, and the lack of kinetic parameters for the adsorption and desorption of $NH_3$, $H_2$, and $N_2$ precluded a critical evaluation of particular kinetic models.

The presence of hydrogen in the reactant stream can influence the decomposition of ammonia in the following two ways: (1) adsorbed hydrogen may react chemically, by hydrogenating intermediates generated during the decomposition; and (2) chemisorbed hydrogen may block surface sites that are necessary for ammonia adsorption. Each of these inhibition mechanisms has been observed previously.[18-21] Apel'baum and Temkin determined from their kinetic measurements at low temperatures and 0.01 torr total pressure that during ammonia decomposition on a platinum wire, the surface coverage of nitrogen decreases with an increase in the partial pressure of hydrogen.[18] This observation is consistent with both a hydrogenation reaction and a site blocking mechanism. However in a recent review, Grunze, considering the results of Loffler and Schmidt,[13] attributed the inhibition of the decomposition of ammonia by hydrogen to the reverse reaction, the hydrogenation reaction to reform ammonia.[19] In addition, using laser-induced fluorescence,[20] Selwyn and Lin showed that the addition of hydrogen (≤0.15 torr) to 0.1 torr of ammonia at 1200–1400 K enhances the yield of NH radicals desorbing from a polycrystalline platinum wire. They suggested that this is due to a surface reaction that converts N(a) to NH(a). Thermal desorption mass spectrometry experiments showed that the amount of ammonia adsorbed on a ruthenium (0001) surface previously saturated with hydrogen is diminished when compared to ammonia

(1) Boudart, M. *Catal. Rev.-Sci. Eng.* **1981**, *23*, 1.
(2) Grunze, M.; Bonzo, F.; Ertl, G. "Proceedings of the 7th International Vacuum Congress, Vienna, 1977"; Dobrozemsky: Vienna, 1977; p 1137.
(3) Boudart, M. In "Physical Chemistry: An Advanced Treatise"; Eyring, H.; Ed.; Academic Press: New York, 1975; p 1.
(4) Ertl, G. *Catal. Rev.-Sci. Eng.* **1980**, *21*, 201.
(5) Emmett, P. H.; Brunauer, S. J. *J. Am. Chem. Soc.* **1934**, *56*, 35.
(6) Emmett, P. H. In "The Physical Basis for Heterogeneous Catalysis"; Draughs, E., Jaffee, R. I., Eds.; Plenum Press: New York, 1975; pp 3–34.
(7) Boudart, M. In "Proceedings of the 6th International Congress on Catalysis, London, 1976"; Royal Society of Chemistry: Letchworth, U.K., 1977; Vol. 1.
(8) Love, K. S.; Emmett, P. H. *J. Am. Chem. Soc.* **1941**, *63*, 3297.
(9) Emmett, P. H.; Kummer, J. T. *Ind. Eng. Chem.* **1943**, *35*, 677.
(10) Melton, C. E.; Emmett, P. H. *J. Phys. Chem.* **1964**, *68*, 3318.
(11) Gland, J. L.; Kollin, E. B. *Surf. Sci* **1981**, *104*, 478.
(12) Loffler, D. G.; Schmidt, L. D. *Surf. Sci.* **1976**, *59*, 195.
(13) Loffler, D. G.; Schmidt, L. D. *J. Catal.* **1976**, *41*, 440.
(14) Vajo, J. J.; Tsai, W.; Weinberg, W. H. *J. Phys. Chem.* **1985**, *89*, 3243.
(15) Dixon, J. K. *J. Am. Chem. Soc.* **1931**, *53*, 2071.
(16) Logan, S. R.; Kemball, C. *Trans. Faraday Soc.* **1960**, *56*, 144.
(17) Robertson, A. J. B.; Willhoft, E. M. A. *Trans. Faraday Soc.* **1967**, *63*, 476.
(18) Apel'baum, L. O.; Temkin, M. I. *Russ. J. Phys. Chem.* **1959**, *33*, 585.
(19) Grunze, M. In "The Chemical Physics of Solid Surfaces and Heterogeneous Catalysis"; King, D. A., Woodruff, D. P., Eds.; Elsevier: Amsterdam, 1982; Vol. 4, p 150.
(20) Selwyn, G. S.; Lin, M. C. *Chem. Phys.* **1982**, *67*, 213.
(21) Danielson, L. R.; Dresser, M. J.; Donaldson, E. E.; Dickinson, J. T. *Surf. Sci.* **1978**, *71*, 599.

0022-3654/85/2089-4926$01.50/0 

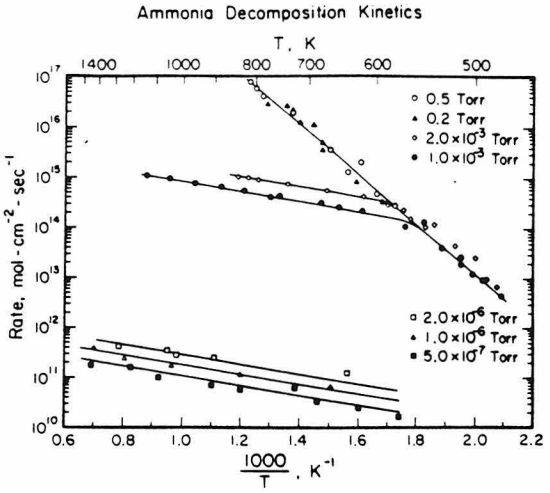


**Figure 1.** Arrhenius plots of the rate of ammonia decomposition on platinum for ammonia pressures of 0.5, 0.2, $2 \times 10^{-3}$, $1 \times 10^{-3}$, $2 \times 10^{-6}$, $1 \times 10^{-6}$, and $5 \times 10^{-7}$ torr. Lines have been drawn through the data points as a visual aid.

adsorption on the clean surface, although no detailed calibration was made to determine the reduction quantitatively.[21] Similar qualitative results were obtained by preadsorbing deuterium on a Pt(111) surface.[11] Apparently, hydrogen adatoms either block the surface sites necessary for ammonia adsorption or indirectly affect the nature of the ammonia adsorption sites, thereby reducing the amount adsorbed.

In a recent study in our laboratory of the steady-state decomposition of $NH_3$ and $ND_3$ over polycrystalline platinum at pressures between $5 \times 10^{-7}$ and 0.5 torr and temperatures between 400 and 1200 K, the energetics of the reaction mechanism were clarified by employing a steady-state nonequilibrium model to describe the experimental results in terms of elementary surface reactions.[14] It was found that ammonia decomposes with zero-order kinetics at low temperatures and/or high pressures. Under these conditions the reaction rate is controlled by the desorption of the product nitrogen. A first-order dependence on ammonia pressure was observed at high temperatures and/or low pressures, where the rate of decomposition is controlled by a surface reaction involving the cleavage of an N–H bond. These data are summarized in the form of an Arrhenius plot in Figure 1. In addition, the isotopic exchange reaction, $NH_3 + D_2$, produced all three exchange products through a mechanism involving dissociative adsorption of both $NH_3$ and $D_2$. In particular, reasonable agreement with the experimental data was obtained from model calculations by assuming that $ND_3$ results from the deuteration of nitrogen adatoms. Furthermore, during the course of a $NH_3 + D_2$ exchange experiment at a total pressure of $1.2 \times 10^{-3}$ torr, inhibition of the decomposition reaction was observed at low temperatures.[14]

The various reaction steps included in the model to describe the decomposition and the isotopic exchange reaction are the following:

1. The adsorption and desorption of the reactants, $NH_3$ and $D_2$, and the desorption of the products $N_2$, $H_2$, HD, $NH_2D$, and $ND_3$ from the surface. (Note that in order to simplify the calculation of the steady-state reaction rates, the surface species NH(a) and ND(a) were omitted from the model. Consequently, the production of $NHD_2$, which would have resulted from deuteration of NH(a), is not included.)

2. The surface reaction of deuterium adatoms with $NH_2(a)$ and $ND_2(a)$ to form $NH_2D(a)$ and $ND_3(a)$.

3. The surface reaction of nitrogen with deuterium adatoms to form the intermediate $ND_2(a)$. Hydrogenation of the intermediates N(a) and $NH_2(a)$ was omitted because the rate of hydrogenation was found to be an order of magnitude lower than the rate of deuteration under our experimental conditions.

By formulating the model in terms of elementary surface reactions, no assumption was made concerning any chemisorption equilibrium on the catalytic surface, as is implicit in the L-H approach. Moreover, it should be emphasized that all the kinetic parameters used in the model are coverage-independent, and the success of the model in predicting absolute decomposition rates indicates the relative insensitivity of the rate parameters to surface coverages. This can be understood as follows. At high temperatures, where the surface coverage of all species is low, the model is sensitive only to the kinetic parameters for the surface reaction and ammonia desorption, although in this case the nitrogen desorption parameters approach the low coverage limiting values. Similarly, at low temperatures, where the surface coverage of nitrogen approaches unity, the model is sensitive only to the nitrogen desorption parameters. However, thermal desorption studies of nitrogen desorption from a polycrystalline platinum wire indicate that the activation energy as well as the preexponential factor of the nitrogen desorption rate coefficient are rather constant over a range of surface coverage from 0.1 to 0.9.[22] On the other hand, the variation with surface coverage of the desorption rate coefficient of hydrogen is irrelevant since the backward surface reaction is negligible during the decomposition of pure ammonia under differential conditions.

In the work described here, we have studied the inhibition of ammonia decomposition by hydrogen over polycrystalline platinum at total pressures from $10^{-3}$ to 0.6 torr with ammonia to hydrogen partial pressure ratios varying from 1:1 to 1:4, and at temperatures between 400 and 1200 K. On the basis of our measured absolute rates, we have extended our previous mechanistic model to describe accurately the inhibition reaction over the full range of experimental conditions studied and to improve the agreement between the model calculations and the exchange data.

The organization of this paper is the following. Experimental details are described in section 2, and the experimental data are presented in section 3. A refined mechanistic model is developed in section 4 and discussed in section 5. Finally, the results are summarized in section 6.

## 2. Experimental Procedures

The experiments were performed over a range of total pressures from $10^{-3}$ to 0.6 torr in a steady-state flow microreactor that has been described previously.[14,23] The catalyst was a 20-cm length of 0.0125-cm-diameter high purity (99.99%) polycrystalline platinum wire. Ammonia (99.99%, anhydrous grade) and hydrogen (99.995%, research grade) were initially mixed in a manifold system in the various partial pressure ratios. The reaction products, which leaked through a capillary tube from the main chamber of the reactor, were monitored continuously by an EAI 1200 quadrupole mass spectrometer in a high vacuum section with a base pressure of approximately $10^{-8}$ torr. The reactor is shown schematically in Figure 2. Calibration of the mass spectrometer was achieved by adding different pressures of nitrogen to the feed (ammonia + hydrogen) representing conversions of less than 10% and monitoring the product nitrogen signal. The average residence time in the reactor was established via experiments that determined the absolute pumping speed for various mixtures of ammonia and hydrogen. Absolute reaction rates were then obtained by using the continuous stirred tank reactor (CSTR) equation. The reactor was well characterized as a CSTR from a series of step-response experiments.[23]

Prior to the decomposition experiments, the platinum wire was heated in $10^{-3}$–0.1 torr of oxygen (99.99%) at 1100 K for 4 h and then reduced in $10^{-3}$–0.1 torr of hydrogen (99.995%) under the same conditions. The actual pressures corresponded to the pressure at which the decomposition of ammonia was carried out subsequently. This treatment led to reproducible decomposition rates of ammonia.

(22) Wilf, M.; Dawson, P. T. *Surf. Sci.* **1976**, *60*, 561.
(23) Vajo, J. J.; Tsai, W.; Weinberg, W. H. *Rev. Sci. Instrum.*, in press.

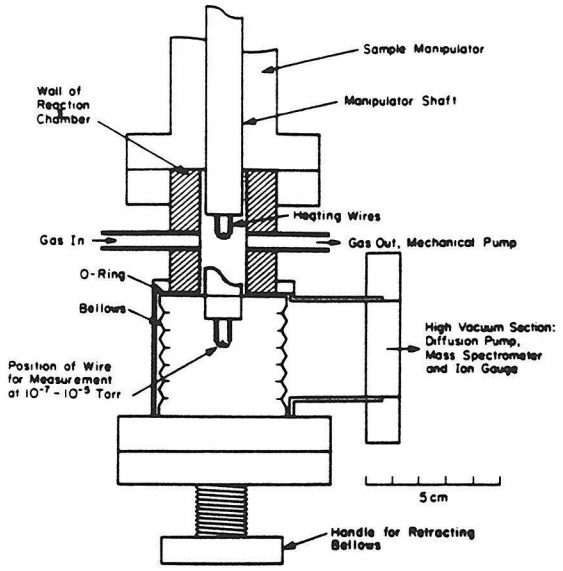


**Figure 2.** Cross section of microreactor body showing the wire in position for experiments at both $10^{-3}$–1 and $10^{-7}$–$10^{-5}$ torr. Ports for pressure measurement and the leak to the high-vacuum section, which are orthogonal to the inlet and outlet flow ports, are not shown. The volume of the baratron and the access ports together with the shaded region is the reactor volume, 30 $cm^3$. The sample manipulator is described in detail elsewhere.[23]

## 3. Experimental Results

Absolute reaction rates for the decomposition of ammonia with hydrogen inhibition are shown in Figures 3 and 4 as a function of reciprocal temperature for total pressures from $10^{-3}$ to 0.6 torr with ammonia to hydrogen partial pressure ratios varying from 1:1 to 1:4. (The curves in Figures 3 and 4 designate results of model calculations which will be discussed in the next section.) Pronounced inhibition of ammonia decomposition is observed for total pressures between 0.3 torr ($P_{H_2}/P_{NH_3}$ = 2) and 0.6 torr ($P_{H_2}/P_{NH_3}$ = 2) over the whole range of temperatures studied, as may be seen in Figure 3 parts a and b. Inhibition was observed at low temperatures, below approximately 650 K, for pressures between $2 \times 10^{-3}$ torr ($P_{H_2}/P_{NH_3}$ = 1) and $5 \times 10^{-3}$ torr ($P_{H_2}/P_{NH_3}$ = 4), as may be seen in Figure 4. The degree of inhibition is indicated by the magnitude of the difference in reaction rates between pure ammonia and an ammonia–hydrogen mixture with the same partial pressure of ammonia (Figure 3 and 4). The reaction order with respect to hydrogen between 0.3 and 0.6 torr total pressure is −1.5 ± 0.3 (Figure 3a) and that with respect to ammonia is 1.0 ± 0.2 (Figure 3b). These results are in agreement with earlier results of Loffler and Schmidt for similar conditions.[13] Between $2 \times 10^{-3}$ and $5 \times 10^{-3}$ torr total pressure, the reaction order with respect to hydrogen also approaches −1.5 at low temperatures (Figure 4). The apparent activation energy is 38 ± 2 kcal/mol at pressures between 0.3 and 0.6 torr, and varies from 33 ± 3 kcal/mol for $2 \times 10^{-3}$ torr ($P_{H_2}/P_{NH_3}$ = 1) to 55 ± 4 kcal/mol for $5 \times 10^{-3}$ torr ($P_{H_2}/P_{NH_3}$ = 4) total pressures. For high temperatures, between $2 \times 10^{-3}$ and $5 \times 10^{-3}$ torr, the decomposition becomes uninhibited, and the kinetic order with respect to hydrogen increases continuously to zero. The absolute rates in this limit agree quantitatively with our previous data for the decomposition of pure ammonia,[14] as is shown explicitly in Figure 4. The apparent activation energy is 4.5 ± 0.2 kcal/mol under these conditions.

## 4. Mechanistic Modeling

In our previous work, a mechanistic model based on elementary reactions was developed to describe the kinetics of ammonia decomposition and the isotopic exchange reaction with deuterium

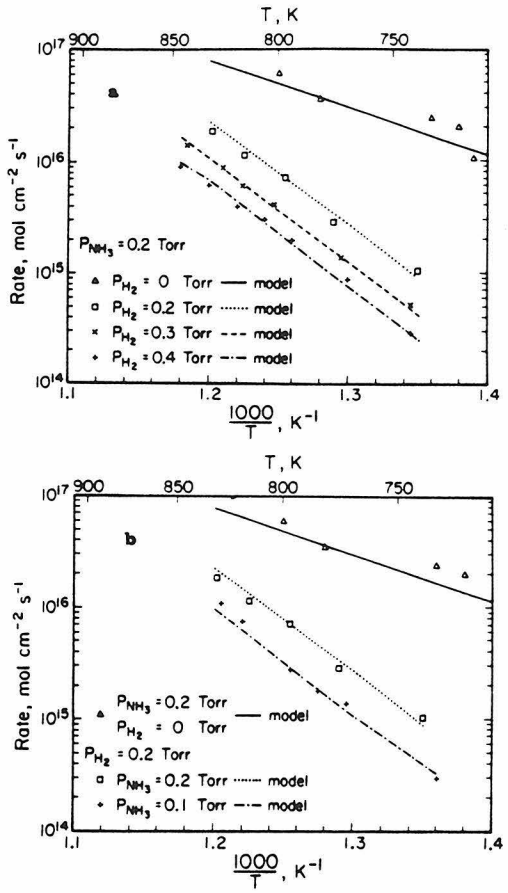


**Figure 3.** Arrhenius plots of the rate of ammonia decomposition with hydrogen inhibition on platinum and the comparison of calculations based on the mechanistic model described in the text with the experimental data. (a) $P_{NH_3}$ = 0.2 torr, $P_{H_2}$ = 0, 0.2, 0.3, and 0.4 torr. (b) $P_{NH_3}$ = 0.2 torr, $P_{H_2}$ = 0, 0.2 torr, and $P_{NH_3}$ = 0.1 torr, $P_{H_2}$ = 0.2 torr.

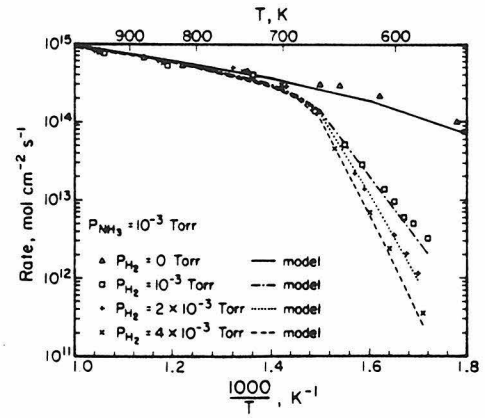


**Figure 4.** Arrhenius plots of the rate of ammonia decomposition with hydrogen inhibition on platinum and the comparison of model calculations with the experimental data. $P_{NH_3}$ = $10^{-3}$ torr, $P_{H_2}$ = 0, $10^{-3}$, 2 × $10^{-3}$, and 4 × $10^{-3}$ torr.

to produce $NH_2D$ and $ND_3$. The reaction mechanism is formulated as follows:

$$NH_3(g) \underset{k^0_{d,NH_3}\theta_{d,NH_3}}{\overset{S_{NH_3}F_{NH_3}}{\rightleftharpoons}} NH_3(a) \qquad (1)$$

$$NH_3(a) \underset{k^0_{-1},E_{-1}}{\overset{k^0_1,E_1}{\rightleftharpoons}} NH_2(a) + H(a) \quad (2)$$

$$NH_2(a) \underset{k^0_{-2},E_{-2}}{\overset{k^0_2,E_2}{\rightleftharpoons}} N(a) + 2H(a) \quad (3)$$

$$H_2(g) \underset{k^0_{d,H_2}E_{d,H_2}}{\overset{S_{H_2}F_{H_2}}{\rightleftharpoons}} 2H(a) \quad (4)$$

$$2N(a) \xrightarrow{k^0_{d,N_2}E_{d,N_2}} N_2(g) \quad (5)$$

The steady-state mass balance equations for the reactants and the products were solved by employing an iterative scheme. Since independently measured rate parameters were used to describe the adsorption and desorption of ammonia, nitrogen, and hydrogen on the platinum surface, the only adjustable parameters introduced were the activation energies and preexponential factors for the surface reactions, eq 2 and 3. These were varied within reasonable limits in order to obtain the best agreement between the calculations and the experimental results. To model the inhibition kinetics, the same mechanism with the same set of kinetic parameters was found to predict the observed kinetics reasonably well between $2 \times 10^{-3}$ and $5 \times 10^{-3}$ torr total pressure. However, the calculated rates between 0.3 and 0.6 torr are approximately 2 orders of magnitude lower than the measured rates, and the predicted reaction order with respect to hydrogen is −3, compared to −1.5 observed experimentally (cf. section 3).

In the previous modeling of the exchange reaction, which also exhibited inhibition of the decomposition reaction for a total pressure of $1.2 \times 10^{-3}$ torr ($P_{D_2}/P_{NH_3} = 0.2$), it was suggested that the deviations between the model predictions and the experimental results (the calculated values for the rate of formation of $NH_2D$ and $ND_3$ are shifted to higher temperatures with respect to the data) indicate that it may be necessary to allow a variation of certain kinetic parameters with surface coverages in the model.[14] Hence, in view of the failure of the model to predict inhibition rates between 0.3 and 0.6 torr, one immediately suspects a possible variation in one or more of the kinetic parameters with the surface coverages of ammonia, hydrogen and/or nitrogen.

The effect of $\theta_{NH_3}$, the fractional surface coverage of ammonia, on any rate parameters will be small because the maximum ammonia coverage on the platinum surface under the reaction conditions employed is found to be $10^{-3}$,[14] and the influence of hydrogen adatoms is also small since the fractional coverage of hydrogen adatoms under reaction conditions is estimated to be less than $8 \times 10^{-3}$. However, the fractional surface coverage of nitrogen adatoms, which is on the order of 0.1 to unity,[14] may be important in modifying the various kinetic parameters present in the model. An initial adjustment of the model has been made for the desorption rate coefficient of hydrogen. This rate coefficient is particularly important during the inhibition reaction since the backward hydrogenation step is not negligible when hydrogen is present in the reactant feed, although it is not important in the decomposition of pure ammonia. In general, the activation energy and the preexponential factor of any heterogenous reaction rate coefficient may be a function of surface coverage. In particular, there are many examples in the literature where the activation energy and the preexponential factor of the hydrogen desorption rate coefficient decrease as a function of surface coverage (see the discussion below and ref 24–30). Consequently, the rate of desorption of hydrogen may be represented as

$$R_{d,H_2} = 2k^0_{d,H_2}(\theta)(n_s\theta_H)^2 \exp[-E_d(\theta)/kT] \quad (6a)$$

where

$$k^0_{d,H_2}(\theta) = k^0_{d,H_2} \exp(-\alpha\theta) \quad (6b)$$

$$E_d(\theta) = E_d - \beta\theta \quad (6c)$$

In this case $\theta$, the fractional surface coverage, is given essentially by $\theta_N$, the fractional surface coverage of nitrogen. *Here $\alpha$ and $\beta$ are allowed to vary such that a physically reasonable range of rate parameters for hydrogen desorption is obtained. Note that the model is modified to accommodate the change of only these two parameters, while retaining the same set of parameters successfully used previously in all other cases.* These parameters are summarized in Table I.

**TABLE I: Model Parameters for the Decomposition Reactions of Ammonia on Platinum**

| | parameter | value | ref |
|---|---|---|---|
| $k^0_{d,NH_3}$ | ammonia desorption preexponential | $1 \times 10^{14}$ s$^{-1}$ | 11, 35 |
| $E_{d,NH_3}$ | ammonia desorption energy | 12 kcal/mol | 11, 35 |
| $S^0_{NH_3}$ | ammonia probability of adsorption | 1 | 11, 35 |
| $k^0_{d,N_2}$ | nitrogen desorption preexponential | $4 \times 10^{-6}$ cm$^2$ s$^{-1}$ | 22 |
| $E_{d,N_2}$ | nitrogen desorption energy | 22 kcal/mol | 22 |
| $k^0_{d,H_2}$ | hydrogen desorption preexponential | 0.01 cm$^2$ s$^{-1}$ | 36, 37 |
| $E_{d,H_2}$ | hydrogen desorption energy | 19 kcal/mol | 36, 37 |
| 36, 37 | hydrogen probability of adsorption | 0.1 | 36, 37 |
| $k^0_1$, $k^0_2$ | surface reaction preexponentials | $1.5 \times 10^{12}$ s$^{-1}$ | |
| $E_1$ | surface reaction activation energy | 16 kcal/mol | |
| $k^0_{-2}$ | hydrogenation reaction preexponential | $3 \times 10^{-17}$ cm$^4$ s$^{-1}$ | |
| $E_{-2}$ | surface hydrogenation activation energy | 28 kcal/mol | |
| $k^0_{-1}$ | exchange reaction preexponential | 0.05 cm$^2$ s$^{-1}$ | |
| $E_{eff}$ | $E_2 - E_{-1}$ | 4 kcal/mol | |
| $n_s$ | surface atom density | $1 \times 10^{15}$ cm$^{-2}$ | |
| $\alpha$ | parameter for hydrogen desorption | 5 | |
| $\beta$ | parameter for hydrogen desorption | 14 kcal/mol | |

The model results indicate that values of $\alpha$ and $\beta$ which are able to describe the inhibition data are not unique. For instance, for both sets of parameters $\alpha = 5$, $\beta = 14$ kcal/mol and $\alpha = 6$, $\beta = 8$ kcal/mol, there is close agreement between the model calculations and the observed experimental values. In order to discriminate between these and other sets of $\alpha$ and $\beta$ which accurately describe the inhibition data, Equation 6 was used to calculate rates of production of $NH_2D$ and $ND_3$ for a partial pressure ratio of deuterium to ammonia of 1:5 with a total pressure of $1.2 \times 10^{-3}$ torr. Comparison of these calculations with the previous experimental results[14] indicates that not all of the sets $\alpha$ and $\beta$ which describe the inhibition results can also describe the exchange results. Indeed, $\alpha$ and $\beta$ are unique within experimental uncertainties, and their values are found to be $\alpha = 5$ and $\beta = 14$ kcal/mol. A sensitivity analysis of the model with respect to $\alpha$ and $\beta$ indicates that the agreement with the measured values degrades considerably if $\alpha$ and $\beta$ are varied by more than ±0.5. For $\alpha = 5$ and $\beta = 14$ kcal/mol, the variation in the activation energy and preexponential factor for hydrogen desorption is from 19 to 10.6 kcal/mol and $10^{-2}$ to $5 \times 10^{-4}$ cm$^2$ s$^{-1}$, for nitrogen coverages from zero to 0.6, respectively. (The maximum fractional surface coverage of nitrogen under reaction conditions is calculated to be 0.6.)

The calculated results based on these parameters are shown in Figures 3 and 4. The correct reaction orders, −1.5 for hydrogen and 1.0 for ammonia, are predicted under the conditions where these values are observed experimentally. Each of the calculated activation energies of the reaction also agree to within ±2 kcal/mol with the experimental values. In general, the inhibition decreases as the temperature increases and the hydrogen coverage decreases. The model calculations agree perfectly with the data near 690 K between $2 \times 10^{-3}$ and $5 \times 10^{-3}$ torr, where the rate of decomposition approaches the rate characteristic of pure ammonia. Furthermore, the measured rates, which are also in qualitative agreement with the model between 0.3 and 0.6 torr total pressure, do not approach the noninhibited rate due to an insufficiently high temperature in this case. However, our data and model (which predicts that the inhibition should become negligible near 1090 K) are both consistent with previous results of Loffler and Schmidt[13] which indicate that the inhibition does indeed become negligible under these high-pressure conditions between 1000 and 1100 K.

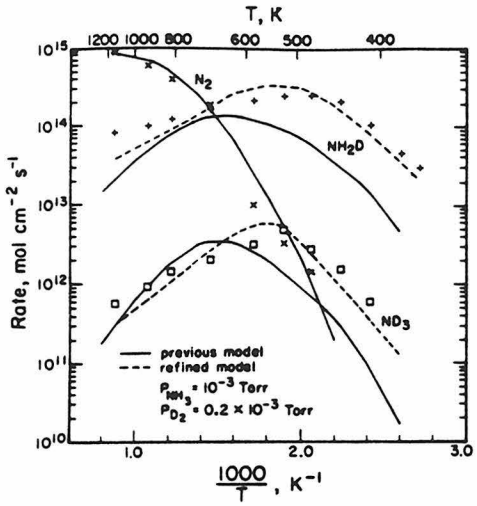


**Figure 5.** Comparison of model calculations with the experimental exchange data for $N_2$, $NH_2D$, and $ND_3$ for $P_{NH_3} = 10^{-3}$ and $P_{D_2} = 0.2 \times 10^{-3}$ torr. Previous model calculations are also shown to indicate the improvement of the model prediction.

In addition, as may be seen in Figure 5, there is improved agreement between the model calculations and the exchange data when compared with the previously calculated results using a constant rate coefficient for hydrogen desorption.[14] Specifically, the maxima in the absolute rates of production of $NH_2D$ and $ND_3$ are shifted to lower temperatures in qualitative agreement with experiment. In addition, the low-temperature apparent activation energy for the production of $NH_2D$ is calculated to be 8.7 kcal/mol compared to the experimental value of 8.4 ± 0.4 kcal/mol, while it was estimated to be 10.1 kcal/mol previously.[14] The high-temperature activation energy is determined to be 3.9 kcal/mol compared to measured value of 2.2 ± 0.1 kcal/mol (formerly estimated to be 5.1 kcal/mol). For the production of $ND_3$, the low-temperature apparent activation energy is calculated to be 4.4 kcal/mol compared to the observed value of 4.0 ± 0.4 kcal/mol (previously calculated to be 5.9 kcal/mol), and the high-temperature activation energy is calculated to be 8.9 kcal/mol compared to the experimental value of 8.7 ± 0.6 kcal/mol (formerly calculated to be 9.5 kcal/mol).

As discussed previously, the model results are relatively insensitive to a variation in the nitrogen desorption rate coefficient with coverage. This insensitivity arises at high temperatures because the rate of decomposition of ammonia with and without hydrogen present in the feed is controlled by the surface reaction and desorption of ammonia. Under these conditions the nitrogen desorption parameters approach the low coverage limiting values. Since there is experimental evidence that the desorption parameters of nitrogen do not vary appreciably over a wide range of surface coverages,[22] a single coverage-independent set of nitrogen desorption parameters is expected to suffice, even for low temperatures where the reaction rates are sensitive to the rate of desorption of nitrogen. This has been confirmed by the quantitative agreement between calculated and measured values for the decomposition of ammonia at low temperatures.[14] Although it appears that the nitrogen desorption parameters are coverage-independent, they have been varied as well as the surface reaction parameters for eq 2 and 3, with a functional form similar to eq 6. It was found that none of these parameters, when varied, could give an accurate description of both the inhibition and the exchange chemistry, compared to varying the hydrogen desorption rate parameters with coverage.

## 5. Discussion

The model results indicate that $\theta_N$ varies from 0.2 to 0.6 between 0.3 and 0.6 torr total pressure and from 0.02 to 0.15 between $2 \times 10^{-3}$ and $5 \times 10^{-3}$ torr. Obviously, varying the hydrogen desorption parameters with $\theta_N$ in eq 6 has a more pronounced effect for pressures between 0.3 and 0.6 torr where the nitrogen coverage is relatively high, than for pressures near $10^{-3}$ torr where the nitrogen coverage is low. For the same reason, it is clear why the original set of coverage-independent parameters is capable of predicting reaction rates near $10^{-3}$ torr while failing between 0.3 and 0.6 torr total pressure. Furthermore, the variation of the nitrogen coverage with temperature between 0.3 and 0.6 torr total pressure is rather constant for all partial pressure ratios of hydrogen and ammonia studied. For example $\theta_N$ varies from 0.58 to 0.32 for $P_{H_2}/P_{NH_3} = 1$ between 740 and 833 K, and from 0.34 to 0.18 for $P_{H_2}/P_{NH_3} = 2$ within the same temperature range. This is manifest by the relatively constant apparent activation energy of 38 kcal/mol for the inhibited decomposition. Since the rate of decomposition of ammonia is given by

$$R_{NH_3} = 2k^0_{d,N_2}(n_s\theta_N)^2 \exp(-E_{d,N_2}/kT) \quad (7)$$

a constant change in $\theta_N$ with temperature will result in a constant apparent activation energy. In contrast, the variation of nitrogen coverage within the temperature range studied at pressures between $2 \times 10^{-3}$ and $5 \times 10^{-3}$ torr is relatively large compared to the variation at higher pressures, and, in addition, it is strongly dependent on the partial pressure of hydrogen. For example, $\theta_N$ varies from 0.15 to 0.06 for $P_{H_2}/P_{NH_3} = 1$ between 580 and 720 K, while it changes from 0.15 to 0.015 for $P_{H_2}/P_{NH_3} = 4$. This results in an increase in the apparent activation energy from 33 to 55 kcal/mol as the partial pressure ratio of hydrogen to ammonia increases from 1 to 4.

Two possible pathways of inhibition were suggested in the introduction, namely, hydrogenation of surface intermediates to re-form ammonia and blocking of ammonia adsorption sites by dissociatively adsorbed hydrogen. An analysis of the reaction model will provide insight concerning the contributions from each of these mechanisms. Although preadsorbed hydrogen is known to block the adsorption of ammonia at low surface temperatures,[11,21] the contribution from this inhibition mechanism is minor in our work because the maximum fractional coverage of hydrogen on the surface under the reaction conditions studied is approximately $8 \times 10^{-3}$. Thus the hydrogenation of surface intermediates is predicted to be the primary mechanism for the inhibition of ammonia decomposition. A detailed understanding regarding the nature of the backward (hydrogenation) reactions may be obtained by considering the exchange reactions between ammonia and deuterium. From our proposed dissociative exchange mechanism,[14] $NH_2D$ is produced from a reaction between $NH_2(a)$ and deuterium adatoms, and $ND_3$ is produced from the successive deuteration of nitrogen adatoms. Similarly, $NHD_2$ is believed to be produced by reaction of deuterium adatoms with NH(a), although this reaction is not included in the model. Therefore, a comparison of the measured relative rates of production of $NH_2D$, $NHD_2$, and $ND_3$ indicates directly the contribution from hydrogenation of $NH_2(a)$, NH(a), and nitrogen adatoms to the inhibition of ammonia decomposition.

Previously it was determined that for a partial pressure ratio of deuterium to ammonia of 1:5 with a total pressure of $1.2 \times 10^{-3}$ torr, the ratio of the rates of production of $NH_2D$, $NHD_2$, and $ND_3$, measured at the temperature corresponding to the maximum value of the rates, is 1:0.17:0.02, respectively.[14] For a total pressure of $2 \times 10^{-3}$ torr ($P_{D_2}/P_{NH_3} = 1$), the ratio of the maximum rates is 1:0.5:0.07 for $NH_2D$, $NHD_2$, and $ND_3$, respectively. Clearly, an increase in the deuterium partial pressure enhances the rate of hydrogenation of surface nitrogen relative to the rate of hydrogenation of $NH_2(a)$. However, at these pressures, hydrogenation of $NH_2(a)$ remains the dominant pathway of inhibition compared to the hydrogenation of NH(a) and nitrogen adatoms, which form $NHD_2$ and $ND_3$, respectively. This experimental result is supported by the model calculations which predict the ratio of the maximum rates of production of $NH_2D$ and $ND_3$ to be 1:0.09 for $P_{D_2}/P_{NH_3} = 1$ at $2 \times 10^{-3}$ torr and 1:0.17 for $P_{D_2}/P_{NH_3} = 4$ at $5 \times 10^{-3}$ torr total pressure. Thus the calculated ratio agrees to within 20% with the observed ratio at $2 \times 10^{-3}$ torr, the highest pressure at which the exchange

experiment was conducted. Furthermore, an extrapolation of this calculation for the exchange reaction to 0.4 torr total pressure ($P_{D_2}/P_{NH_3} = 1$) indicates that the ratio of the rates is 1:0.23 for $NH_2D$ and $ND_3$ production, respectively. Hence, ratios of the calculated rates, together with the experimetally observed values, indicate that the hydrogenation of $NH_2(a)$ is the predominant inhibition pathway over the whole range of pressures studied. To summarize, the inhibition of ammonia decomposition is believed to occur predominantly through the hydrogenation of $NH_2(a)$ to produce molecularly adsorbed ammonia. This results in a reduction of nitrogen adatom coverage on the surface and consequently the observed inhibition.

The functional form given by eq 6, which describes the desorption of hydrogen, is an example of the so-called compensation effect. Hence, the activation energy and the preexponential factor vary in sympathy with coverage, reducing the observed change in the value of the desorption rate. With $\alpha = 5$ and $\beta = 14$ kcal/mol in eq 6, the value of the preexponential factor of the hydrogen desorption rate coefficient at zero nitrogen coverage is $k^0_{d,H_2}(\theta) = 10^{-2}$ cm$^2$ s$^{-1}$, and $E_d(\theta) = 19$ kcal/mol; while the values at high coverage ($\theta_N = 0.6$) are $k^0_{d,H_2}(\theta) = 5 \times 10^{-4}$ cm$^2$ s$^{-1}$ and $E_d(\theta) = 10.6$ kcal/mol. This variation appears physically reasonable since similar variations have been found experimentally for the desorption rate coefficients of hydrogen as a function of coverage.[24-30] For example, studies of the adsorption and desorption of hydrogen from Ni(100), Ni(100)-p(2×2)S, and Ni(100)-c(2×2)S surfaces[24] indicate that the presence of sulfur reduces the values of the desorption rate parameters which characterize hydrogen recombination. The activation energy of desorption of 21.3 kcal/mol and the preexponential factor of $5 \times 10^{-2}$ cm$^2$ s$^{-1}$ on clean Ni(100) are reduced to 17.4 kcal/mol and $4 \times 10^{-4}$ cm$^2$ s$^{-1}$ on the p(2×2)S surface, and to 10 kcal/mol and $3 \times 10^{-6}$ cm$^2$ s$^{-1}$ on the c(2×2)S surface. The low value for $k^0_{d,H_2}$ on the surface with half a monolayer of sulfur present, which gives rise to the compensation effect, was suggested to originate from severe steric hindrance to hydrogen recombination.[24] The same effect occurs except to a lesser extent in the case of a quarter monolayer of sulfur. A similar change in hydrogen desorption kinetics was observed when carbon was present on the Ni(100) surface.[25] For the Ni(100) surface with 0.25 monolayer carbon, the activation energy for hydrogen desorption was 9.5 kcal/mol with a preexponential factor of $10^{-6}$ cm$^2$ s$^{-1}$ in contrast to the clean surface values of 21.3 kcal/mol and $5 \times 10^{-2}$ cm$^2$ s$^{-1}$. In addition, the compensation effect has also been observed for hydrogen desorption from Rh(111),[26] where the activation energy of hydrogen desorption was observed to decrease linearly by almost 10 kcal/mol, while the preexponential factor was found to decrease by 5 orders of magnitude for hydrogen coverages varying from 0 to 0.5. This variation was attributed to the involvement of a mobile precursor state of molecular hydrogen during desorption, as described by Gorte and Schmidt.[31] A similar precursor state for hydrogen desorption, which occurs during ammonia decomposition with finite nitrogen coverages, is certainly reasonable.

Compensatory behavior has also been attributed to multiple adsorption states and to repulsive lateral interactions.[32,33] Evidence for these mechanisms may be obtained by analyzing thermal desorption measurements of hydrogen on platinum. A recent study of hydrogen desorption from the Pt(110)-(1×2) surface has revealed the existence of two dissociatively adsorbed states.[34] At low coverages, hydrogen desorbs from a single state with a peak temperature of approximately 360 K. This state becomes saturated at higher coverages and a second peak in the thermal desorption spectrum appears, initially with a peak temperature of approximately 260 K.[34] Although an analysis in terms of activation energies and preexponential factors has not been conducted, we can compare these data on Pt(110) with thermal desorption spectra generated for surfaces with different precoverages of nitrogen using eq 6b,c to obtain the kinetic parameters for the desorption of hydrogen. Thermal desorption spectra can be calculated by integrating the rate equation describing the desorption reaction, i.e.

$$R_{d,H_2} = n_s(d\theta_H/dt) = 2k^0_{d,H_2}(n_s\theta_H)^2 \exp(-E_{d,H_2}/kT)$$

where $k^0_{d,H_2}$ and $E_{d,H_2}$ are the preexponential factor and the activation energy appropriate for a given nitrogen coverage. Thermal desorption spectra were calculated for two surfaces, both with a small fractional coverage ($\theta_H = 0.01$) of hydrogen: a surface with no nitrogen coverage, $\theta_N = 0$, and a surface with $\theta_N = 0.6$. For $\theta_N = 0$ ($k^0_{d,H_2} = 0.01$ cm$^2$ s$^{-1}$ and $E_{d,H_2} = 19$ kcal/mol), the calculated hydrogen desorption peak temperature is 370 K, while for $\theta_N = 0.6$ ($k^0_{d,H_2} = 5 \times 10^{-4}$ cm$^2$ s$^{-1}$ and $E_{d,H_2} = 10.6$ kcal/mol), the peak temperature is 250 K. The agreement of these results with the thermal desorption measurements on Pt(110)[34] is consistent with both multiple adsorption states and repulsive lateral interactions. In the former case, adsorbed nitrogen blocks the adsite for hydrogen which desorbs at 360 K. Therefore, as the nitrogen coverage increases, the fraction of hydrogen adsorbed in the high-temperature adstate decreases, while the fraction in the low-temperature adstate increases. In the latter case, repulsive interactions between nitrogen and hydrogen adatoms reduce the hydrogen desorption energy, which mimicks population of the low-temperature hydrogen adstate and the depopulation of the high-temperature adstate. In addition, our calculations are consistent with thermal desorption measurements of hydrogen from Pt(111),[30] which indicate two adsorption states with peak temperatures of approximately 380 and 270 K. Since compensatory behavior may be attributed to many different mechanisms, further work is being conducted in our laboratory to characterize the mechanism of hydrogen desorption from nitrogen-covered platinum surfaces.

In summary, the mechanistic model given by eq 1–5 together with eq 6 is able to describe quantitatively the decomposition of ammonia, the isotopic exchange reaction of ammonia with deuterium, and the inhibition of the decomposition of ammonia by hydrogen over a pressure range which spans 7 orders of magnitude and over a temperature range of 800 K. The success of the model attests to the general utility of analyzing kinetic data obtained over a wide range of experimental conditions by using kinetic parameters determined independently from UHV measurements. Finally, an accurate description of the interaction of ammonia with platinum up to a pressure of approximately 1 torr has been obtained without hypothesizing any mechanistic steps or processes which cannot be directly investigated at pressures amenable to modern surface science techniques.

## 6. Conclusions

The results of this study can be summarized as follows:

1. Inhibition of ammonia decomposition is observed for total pressures between 0.3 torr ($P_{H_2}/P_{NH_3} = 2$) and 0.6 torr ($P_{H_2}/P_{NH_3} = 2$) and for temperatures between 740 and 850 K. Under these conditions, the apparent activation energy is 38 ± 2 kcal/mol, and the reaction orders with respect to hydrogen and ammonia are −1.5 ± 0.3 and 1.0 ± 0.2, respectively.

2. For total pressures between $2 \times 10^{-3}$ torr ($P_{H_2}/P_{NH_3} = 1$) and $5 \times 10^{-3}$ torr ($P_{H_2}/P_{NH_3} = 4$), inhibition is observed at temperatures below approximately 650 K, where the reaction order with respect to hydrogen approaches −1.5 ± 0.3 at low temper-

(24) Johnson, S.; Madix, R. J. *Surf. Sci.* **1981**, *108*, 77.
(25) Ko, E. I.; Madix, R. J. *Appl. Surf. Sci.* **1979**, *3*, 236.
(26) Yates, Jr., J. T.; Thiel, P. A.; Weinberg, W. H. *Surf. Sci.* **1979**, *84*, 427.
(27) Christmann, K.; Ertl, G.; Pignet. T. *Surf. Sci.* **1976**, *54*, 365.
(28) Ibbotson, D. E.; Wittrig, T. S.; Weinberg, W. H. *J. Chem. Phys.* **1980**, *72*, 4885.
(29) Engstrom, J. R.; Tsai, W.; Weinberg, W. H., in preparation.
(30) McCabe, R. W.; Schmidt, L. D. *Surf. Sci.* **1977**, *65*, 189.
(31) Gorte, R.; Schmidt, L. D. *Surf. Sci.* **1978**, *76*, 559.
(32) Galwey, A. K. *Adv. Catal.* **1977**, *26*, 247 and references therein.
(33) Goymour, C. G.; King, D. A. *J. Chem. Soc., Faraday Trans. 1* **1973**, *69*, 749.
(34) Szuromi, P. D.; Engstrom, J. R.; Weinberg, W. H. *J. Phys. Chem.* **1985**, *89*, 2497.
(35) Gland, J. L. *Surf. Sci.* **1978**, *71*, 327.
(36) Poelsema, B.; Mechtersheimer, G.; Comsa, G. *Surf. Sci.* **1981**, *111*, 519.
(37) Poelsema, B.; Mechtersheimer, G.; Comsa, G. *Surf. Sci.* **1981**, *111*, L728.

atures. The activation energy varies from 33 ± 3 kcal/mol for $2 \times 10^{-3}$ torr to 55 ± 4 kcal/mol for $5 \times 10^{-3}$ torr total pressure. The decomposition becomes uninhibited at high temperatures, and the apparent activation energy is 4.5 ± 0.2 kcal/mol.

3. The observed kinetics for the reaction of ammonia and hydrogen on platinum are described quantitatively by a model employing elementary surface reactions, where the rate coefficient for hydrogen desorption is a function of the fractional surface coverage of nitrogen adatoms.

4. The hydrogenation of $NH_2(a)$ to produce molecularly adsorbed ammonia is the dominant factor in the inhibition of ammonia decomposition.

*Acknowledgment.* We gratefully acknowledge the financial support of the Army Research Office under Grant No. DAAG29-83-K-0094, and the Central Research and Development Department of E.I. du Pont de Nemours and Co.

**Registry No.** $NH_3$, 7664-41-7; $H_2$, 1333-74-0; Pt, 7440-06-4.